IDŐJÁRÁS

QUARTERLY JOURNAL OF THE HUNGAROMET
HUNGARIAN METEOROLOGICAL SERVICE

CONTENTS

Special issue:

11th Seminar for Homogenization and Quality Control in Climatological Databases and 6th Interpolation Conference jointly organized with the 14th EUMETNET Data Management Workshop

Guest Editor: Mónika Lakatos

VOL. 128 * NO. 2 * APRIL – JUNE 2024

IDŐJÁRÁS

Quarterly Journal of the HungaroMet Hungarian Meteorological Service

Editorial Office: Kitaibel P.u. 1, H-1024 Budapest, Hungary
P.O. Box 38, H-1525 Budapest, Hungary
E-mail: journal.idojaras@met.hu

Indexed and abstracted in Science Citation Index Expanded™ and Journal Citation Reports/Science Edition
Covered in the abstract and citation database SCOPUS®
Included in EBSCO's database

Subscription by mail:
IDŐJÁRÁS, P.O. Box 38, H-1525 Budapest, Hungary
E-mail: journal.idojaras@met.hu

Editorial

Special Issue: 11th Seminar for Homogenization and Quality Control in Climatological Databases and 6th Interpolation Conference jointly organized with the 14th EUMETNET Data Management Workshop

The 11th Seminar for Homogenization and Quality Control in Climatological Databases and 6th Interpolation Conference were jointly organized with the 14th EUMETNET Data Management Workshop on 9–11 May, 2023 at the headquarters of the Hungarian Meteorological Service, Budapest, Hungary. The following topics were announced and some of them discussed in more depth in this Special Issue, that are crucial for effective climate data management and analysis.

- Data Management and Rescue: Includes cataloguing, digitization, and archiving processes necessary for salvaging and organizing historical climate records.
- Climate Observations and Standards: Encompasses standards, best practices, and metadata frameworks like the WMO Information System (WIS), INSPIRE, and climate network rating to maintain data integrity.
- Quality Control: Covers automatic/manual techniques for assessing reliability to ensure data accuracy.
- Homogenization Techniques: Focuses on methods for homogenizing climate time-series data from monthly to sub-daily scales, addressing exploration of inhomogeneities and applying benchmarking methods.
- Temporal Scales and Interpolation: Explores temporal scales from synoptic situations to climatological mean values and interpolation formulas tailored to spatial probability distributions of climate variables.
- Statistical Estimation and Modeling: Discusses estimation and modeling of statistical parameters (e.g., spatial trend, covariance) for interpolation formulas using spatiotemporal samples and auxiliary model variables.
- Auxiliary Data Integration: Considers the use of auxiliary co-variables and background information (e.g., dynamical model results, satellite, radar data) for spatial interpolation, including data assimilation and reanalysis techniques.
- Applications of Interpolation Methods: Examines various interpolation methods for meteorological and climatological fields, highlighting experiences with different variables.

- Gridded Databases and Monitoring Products: Showcases gridded databases, climate monitoring products, digital climate atlases, and climate normals for diverse applications in climate research and monitoring.

This Special Issue of Időjárás is already the second issue of this journal dedicated to this topic, and we hope in the continuation.

Mónika Lakatos
Guest Editor

DOI:10.28974/idojaras.2024.2.1

IDŐJÁRÁS

Quarterly Journal of the HungaroMet Hungarian Meteorological Service
Vol. 128, No. 2, April – June, 2024, pp. 143–154

Statistical modeling of the present climate by the interpolation method MISH – theoretical considerations

Tamás Szentimrey

Varimax Limited Partnership, Budapest, Hungary

Author E-mail: szentimrey.t@gmail.com

(Manuscript received in final form October 31, 2023)

Abstract— Our method MISH (Meteorological Interpolation based on Surface Homogenized Data Basis; *Szentimrey* and *Bihari*) was developed for spatial interpolation of meteorological elements. According to mathematical theorems, the optimal interpolation parameters are known functions of certain climate statistical parameters, which fact means we could interpolate optimally if we knew the climate. Furthermore, the data assimilation methods also need to know the climate if Bayesian estimation theory is to be correctly applied. Therefore, we have developed the MISH system also to model the climate statistical parameters, i.e. present climate, by using long data series. It is a nonsense that we try to model the future climate but we do not know the present climate.

Key-words: climate modeling, climate statistical parameters, data series, spatial interpolation, data assimilation, MISH, MASH

1. Introduction

In the statistical climatology, the climate can be formulated as the probability distribution of the meteorological events or variables. The purpose of the statistical climatology is to estimate or model the climate probability distribution or equivalently the climate statistical parameters. Furthermore, the meteorological data series make possible to estimate or model the climate statistical parameters in accordance with the establishments of statistical climatology principles.

Our method MISH (Meteorological Interpolation based on Surface Homogenized Data Basis; *Szentimrey* and *Bihari*, 2007, 2014; *Szentimrey*, 2017, 2021, 2023c) was developed for spatial interpolation of meteorological elements. According to the mathematical theorems, the optimal interpolation parameters are known functions of certain climate statistical parameters, which fact means we could interpolate optimally if we knew the climate. Consequently, according to the principles of climatology, the modeling part of software MISH is based on long meteorological data series. The main difference between MISH and the geostatistical interpolation methods built in GIS (Geographic Information System) is that the sample for modeling at GIS methods is only the predictors, which is a single realization in time, while at the MISH method we use spatiotemporal data for modeling, which form a sample in time and space alike.

We focus on the methodology of the modeling subsystem built in MISH. This subsystem was developed to model the following climate statistical parameters for half minutes grid: monthly, daily expected values, standard deviations, and the spatial and temporal correlations. Consequently, the modeling subsystem of MISH is completed for all the first two spatiotemporal moments. If the joint spatiotemporal probability distribution of a given meteorological element is normal (e.g., daily and monthly mean temperatures) then the spatiotemporal moments above uniquely determine this distribution, which is the mathematical model of the present climate for this meteorological element.

In our conception, the meteorological questions and topics cannot be treated separately. Therefore, we present a block diagram (*Fig. 1*) to illustrate the possible connection between various important meteorological topics. The software MISH (*Szentimrey* and *Bihari*, 2014) and MASH (Multiple Analysis of Series for Homogenization; *Szentimrey*, 2023a,b) were developed by us. These software were applied also in the CARPATCLIM project (*Szentimrey et al.*, 2012a,b; *Lakatos et al.*, 2013). The paper of *Izsák et al.* (2022) presents another application to create a representative database for Hungary.

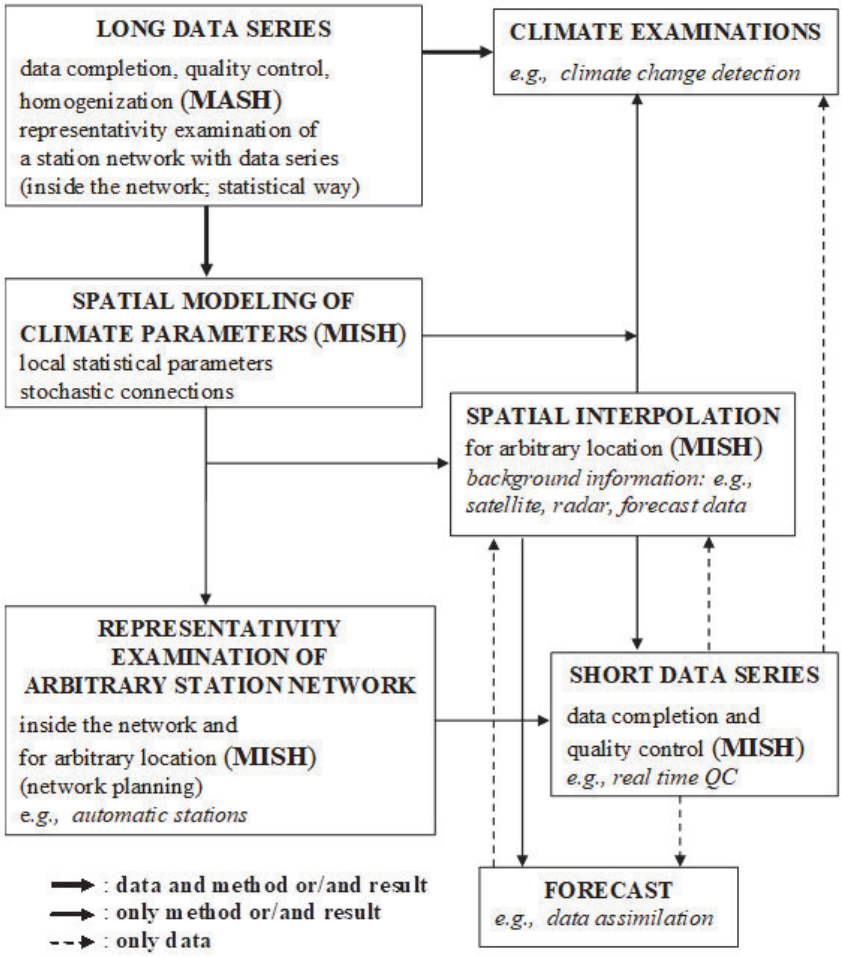

Fig. 1. Block diagram for the possible connection between various basic meteorological topics and systems.

2. Theoretical additive model of spatial interpolation

According to the interpolation problem for monthly or daily data, the unknown predictand $Z(\mathbf{s}_0, t)$ is estimated by use of the known predictors $Z(\mathbf{s}_i, t)$

$(i = 1, \ldots, M)$ where **s** is the location vector ($\mathbf{s} \in D$ spatialdomain) and t is the index of year. The type of the adequate interpolation formula depends on the probability distribution of the meteorological variable. Assuming normal distribution (e.g., temperature), the additive (linear) formula is adequate (*Szentimrey* and *Bihari*, 2007; *Szentimrey et al.*, 2011).

2.1. Climate statistical parameters

The expected values are
$\mathrm{E}\big(Z(\mathbf{s}_i, t)\big) = \mu(t) + E(\mathbf{s}_i)(i = 0, .., M)$,
where $\mu(t)$ is the temporal trend or the climate change signal and $E(\boldsymbol{s})$ is the spatial trend. The standard deviations $D(\mathbf{s}_i) = \mathrm{D}\big(Z(\mathbf{s}_i, t)\big)$ $(i = 0, \ldots, M)$ and the correlation system is as, **r** is the predictand-predictors correlation vector, **R** is the predictors-predictors correlation matrix.

2.2. Additive (linear) interpolation formula

Assuming the normal distribution of the variables and the above model of expected values, the appropriate additive meteorological interpolation formula is
$\hat{Z}(\mathbf{s}_0, t) = \lambda_0 + \sum_{i=1}^{M} \lambda_i \cdot Z(\mathbf{s}_i, t)$,
where $\sum_{i=1}^{M} \lambda_i = 1$ because of unknown $\mu(t)$. The quality of interpolation can be characterized by the root mean square error $RMSE(\mathbf{s}_0)$ and by the representativity value: $REP(\mathbf{s}_0) = 1 - \frac{RMSE(\mathbf{s}_0)}{D(\mathbf{s}_0)}$.

Remark: Multiplicative model of spatial interpolation

In this paper only the linear or additive model is described in detail, which is appropriate in case of normal probability distribution. However, perhaps it is worthwhile to remark that for case of a quasi lognormal distribution (e.g., precipitation sum), we deduced a mixed multiplicative additive formula which is used also in our MISH system, and it can be written in the following form:
$\hat{Z}(\mathbf{s}_0, t) = \vartheta \cdot \left(\prod_{q_i \cdot Z(\mathbf{s}_i, t) \geq \vartheta} \left(\frac{q_i \cdot Z(\mathbf{s}_i, t)}{\vartheta} \right)^{\lambda_i} \right) \cdot \left(\sum_{q_i \cdot Z(\mathbf{s}_i, t) \geq \vartheta} \lambda_i + \sum_{q_i \cdot Z(\mathbf{s}_i, t) < \vartheta} \lambda_i \cdot \left(\frac{q_i \cdot Z(\mathbf{s}_i, t)}{\vartheta} \right) \right)$,
where the interpolation parameters are $\lambda_i \geq 0$ $(i = 1, \ldots, M)$, $\sum_{i=1}^{M} \lambda_i = 1$, and $\vartheta = m(\mathbf{s}_0)$, $q_i = \frac{m(\mathbf{s}_0)}{m(\mathbf{s}_i)}$, where $m(\mathbf{s}_i)$ $(i = 0, \ldots, M)$ are the spatial median values.

2.3. The optimal interpolation

The optimal interpolation parameters λ_0, λ_i $(i = 1, \ldots, M)$ minimize the root mean square error $RMSE(\mathbf{s}_0)$, and these are known functions of the climate statistical parameters! The optimal interpolation is when we use the optimal parameters.

The optimal constant term is $\lambda_0 = \sum_{i=1}^{M} \lambda_i \big(E(\mathbf{s}_0) - E(\mathbf{s}_i)\big)$.
The vector of optimal weighting factors $\boldsymbol{\lambda} = [\lambda_1, .., \lambda_M]^T$ and the optimal representativity $REP(\mathbf{s}_0)$ can be written as function of the parameters: $D(\mathbf{s}_0)/D(\mathbf{s}_i)$ $(i = 1, \ldots, M)$, $\mathbf{r}$, $\mathbf{R}$. The expected values and these parameters are climate statistical parameters, consequently we could interpolate optimally if we knew the climate well. For example, let us see the next theorem.

Theorem 1

If $D(\mathbf{s}_0)/D(\mathbf{s}_i) = 1 \quad (i = 1, \ldots, M)$ then:

(i) The vector of optimal weighting factors: $\boldsymbol{\lambda} = \mathbf{R}^{-1}\left(\mathbf{r} + \frac{(1-\mathbf{1}^{\mathrm{T}}\mathbf{R}^{-1}\mathbf{r})}{\mathbf{1}^{\mathrm{T}}\mathbf{R}^{-1}\mathbf{1}}\mathbf{1}\right)$.

(ii) The optimal representativity is

$$REP(\mathbf{s}_0) = 1 - \sqrt{(1 - \mathbf{r}^{\mathrm{T}}\mathbf{R}^{-1}\mathbf{r}) + (1 - \mathbf{1}^{\mathrm{T}}\mathbf{R}^{-1}\mathbf{r})^2 \cdot \frac{1}{\mathbf{1}^{\mathrm{T}}\mathbf{R}^{-1}\mathbf{1}}}\,.$$

Consequently the unknown climate statistical parameters are $E(\mathbf{s}_0) - E(\mathbf{s}_i)$ $(i = 1, \ldots, M)$ (do not depend on temporal trend of climate change) and the correlations $\mathbf{r}$, $\mathbf{R}$.

3. Modeling of climate statistical parameters in MISH

The main difference between geostatistics and meteorology can be found in the amount of information being usable for modeling the statistical parameters. In geostatistics, the usable information or the sample for modeling is only the actual predictors $Z(\mathbf{s}_i, t)$ $(i = 1, \ldots, M)$ which belong to a fixed instant of time, that is a single realization in time (*Cressie*, 1991), while in meteorology we have spatiotemporal data, namely long data series which form a sample in time and space as well and make possible to model the climate statistical parameters in question. If the meteorological station location $\mathbf{S}_k$ $(k = 1, .., K)$ have long data series $Z(\mathbf{S}_k, t)(t = 1, .., n)$ then the climate statistical parameters can be estimated statistically for the stations (*Szentimrey et al*, 2011).

3.1. Modeling of monthly climate statistical parameters for a half minutes grid

3.1.1. First step of modeling by using model variables

The monthly climate statistical parameters belonging to the stations $\mathbf{S}_k$ $(k = 1, .., K)$ can be used for modeling the correlation structure as well as the spatial variability of local statistical parameters (*Szentimrey* and *Bihari*, 2014). The basic principle of this neighborhood modelling is as follows. Let $P(\mathbf{s}), Q(\mathbf{s}), r(\mathbf{s}_1, \mathbf{s}_2)(\mathbf{s}, \mathbf{s}_1, \mathbf{s}_2 \in D)$ be certain model functions depending on

different model variables with the following properties, within a neighborhood $\|\mathbf{S}_{j1} - \mathbf{S}_{j2}\| < d_0 \qquad (j_1, j_2 = 1,..,K)$:

(a) Modeling of correlations is $r(\mathbf{S}_{j1}, \mathbf{S}_{j2}) \approx \mathrm{corr}(Z(\mathbf{S}_{j1}, t), Z(\mathbf{S}_{j2}, t))$;

(b) Modeling of difference of means (E) is $P(\mathbf{S}_{j1}) - P(\mathbf{S}_{j2}) \approx E(\mathbf{S}_{j1}) - E(\mathbf{S}_{j2})$;

(c) Modeling of ratio of standard deviations (D) is $\frac{Q(\mathbf{S}_{j1})}{Q(\mathbf{S}_{j2})} \approx \frac{D(\mathbf{S}_{j1})}{D(\mathbf{S}_{j2})}$.

The model variables may be distance, height, topography.

3.1.2. Second step of modeling by interpolation

Predictand location is $\mathbf{s}_0$, predictor station locations are $\mathbf{S}_{0i}$ $(i = 1,\ldots,M)$. The weighting factors can be calculated according to *Theorem 1*, where $\mathbf{r}$, $\mathbf{R}$ contain the modeled predictand-predictors, predictors-predictors correlations based on Section 3.1.1 (a).

Modeling of means, expected values (E) by additive interpolation is

$$E(\mathbf{s_0}) = \sum_{i=1}^{M} \lambda_i \big(P(\mathbf{s_0}) - P(\mathbf{S_{0i}})\big) + \sum_{i=1}^{M} \lambda_i E(\mathbf{S_{0i}})$$

Modeling of standard deviations (D) by multiplicative interpolation is

$$D(\mathbf{s}_0) = \prod_{i=1}^{M} \left(\frac{Q(\mathbf{s}_0)}{Q(\mathbf{S}_{0i})} \cdot D(\mathbf{S}_{0i}) \right)^{\lambda_i}.$$

3.2. Relation of daily and monthly data interpolation

Theorem 2

Let us assume the following properties for the daily values within a month:

(i) Expected values and standard deviations are

$$E_d(\mathbf{s}_0) - E_d(\mathbf{s}_i) = E_{0i}, \quad \frac{D_d(\mathbf{s}_0)}{D_d(\mathbf{s}_i)} = D_{0i} \quad (i = 1,\ldots,M\,; \;\; d = 1,..,30)$$

(ii) Correlations

$$\mathrm{corr}\left(Z_{d_1}(\mathbf{s}_{i_1}, t),\; Z_{d_2}(\mathbf{s}_{i_2}, t)\right) = r^S_{i_1 i_2} \cdot r^T_{d_1 d_2}$$
$$(i_1, i_2 = 1,\ldots,M\,; \;\; d_1, d_2 = 1,..,30),$$

where $r^S_{i_1 i_2}$ is the correlation structure in space and $r^T_{d_1 d_2}$ is the correlation structure in time.

Then the optimum interpolation parameters for the daily values and the monthly mean are identical: $\lambda_{i,d} = \lambda_{i,month}$ $(i = 0,\ldots,M;\ \ d = 1,..,30)$.
Moreover, the representativity values for the daily values and the monthly mean are also identical: $REP_d(\mathbf{s}_0) = REP_{month}(\mathbf{s}_0)$ $(d = 1,..,30)$ in the case of optimal interpolation parameters.
Consequently, the monthly modeled climate statistical parameters and the modelling methodology can also be applied to model the daily climate statistical parameters.
Special modeling parts for daily data are modeling of temporal daily autocorrelations $\rho(\mathbf{s})$ and daily standard deviations $D_{daily}(\mathbf{s})$ per months. We assume that the daily data of a given month constitute an AR(1) process with common standard deviation $D_{daily}(\mathbf{s})$ and temporal first-order autocorrelation $\rho(\mathbf{s})$. Modeling of autocorrelation $\rho(\mathbf{s})$ by additive interpolation is

$\rho(\mathbf{s}_0) = \sum_{i=1}^{M} \lambda_i \rho(\mathbf{S}_{0i})$,

where autocorrelations $\rho(\mathbf{S}_{0i})$ belonging to the stations and the weighting factors are calculated according to Section 3.1.2. The daily standard deviation $D_{daily}(\mathbf{s})$ can be estimated by using the monthly standard deviation $D_{month}(\mathbf{s})$ and the first-order autocorrelation $\rho(\mathbf{s})$.
The *RMSE* can be calculated as follows: $RMSE(\mathbf{s}_0) = D(\mathbf{s}_0) \cdot (1 - REP(\mathbf{s}_0))$.

3.3. Modeled monthly and daily spatiotemporal climate statistical parameters in MISH

The necessary unknown climate statistical parameters can be modeled for a half minutes grid. These modeled monthly and daily spatiotemporal statistical parameters in MISH system are:

(i) spatial expected values (spatial trend) $E(\mathbf{s})$,

(ii) spatial standard deviations $D(\mathbf{s})$,

(iii) spatial correlations $r(\mathbf{s}_1, \mathbf{s}_2)$, and

(iv) temporal first-order autocorrelations $\rho(\mathbf{s})$.

Consequently, the first two spatiotemporal moments can be modeled for daily and monthly data by the MISH procedure! The normal distribution is uniquely determined by these moments. Some examples for the modeled climate statistical parameters are presented in *Fig. 2.*

Example
Mean temperature data in September for 10 arbitrary locations somewhere in Hungary.
Input: the location coordinates only without any temperature data.
Output: modelled climate statistical parameters

Location indices:

1	2	3	4	5	6	7	8	9	10

Monthly Expected Values:

14.59	14.99	14.95	15.06	15.16	15.16	15.13	15.08	15.01	15.05

Daily Expected Values:

14.59	14.99	14.95	15.06	15.16	15.16	15.13	15.08	15.01	15.05

Monthly Standard Deviations:

1.34	1.62	1.68	1.67	1.68	1.66	1.72	1.66	1.61	1.64

Daily Standard Deviations:

2.84	3.44	3.47	3.46	3.47	3.60	3.73	3.58	3.48	3.46

Temporal Daily Autocorrelations:

0.74	0.74	0.75	0.75	0.75	0.73	0.73	0.73	0.73	0.74

Matrix of Spatial Autocorrelations:

1.00	0.99	0.99	0.98	0.97	0.96	0.97	0.97	0.98	0.98
0.99	1.00	0.99	0.99	0.98	0.95	0.96	0.96	0.97	0.98
0.99	0.99	1.00	0.99	0.99	0.94	0.95	0.95	0.96	0.97
0.98	0.99	0.99	1.00	0.99	0.91	0.93	0.93	0.95	0.96
0.97	0.98	0.99	0.99	1.00	0.90	0.91	0.91	0.93	0.94
0.96	0.95	0.94	0.91	0.90	1.00	0.99	0.99	0.98	0.98
0.97	0.96	0.95	0.93	0.91	0.99	1.00	0.99	0.99	0.98
0.97	0.96	0.95	0.93	0.91	0.99	0.99	1.00	0.99	0.99
0.98	0.97	0.96	0.95	0.93	0.98	0.99	0.99	1.00	0.99
0.98	0.98	0.97	0.96	0.94	0.98	0.98	0.99	0.99	1.00

Fig. 2. Example for modeling of present climate by MISH.

4. The main features of software MISHv2.01

The new software version of MISH method (*Szentimrey* and *Bihari*, 2007, 2014; *Szentimrey*, 2017, 2021, 2023c) is under development, and it is consisting of two units that are the modeling and the interpolation systems. The interpolation system can be operated on the results of the modeling system. We summarize briefly the most important facts about these two units of the software.

Modeling subsystem for climate statistical (local and stochastic) parameters:

– Modeling of all the first two spatiotemporal moments for daily and monthly data (expected values, standard deviations, spatiotemporal correlations).

– Based on long homogenized data series and supplementary deterministic model variables. The model variables may be such as height, topography,

distance from the sea, etc. Neighborhood modeling, correlation model for each grid point, dense half minutes grid.

– Benchmark study, cross-validation test for interpolation error or representativity.
– Modeling procedure must be executed only once before the interpolation applications.

Totally different principle from the other methods!

Interpolation subsystem:

– Additive (e.g., temperature) or multiplicative (e.g., precipitation) model and interpolation formula can be used depending on the climate elements.
– Daily, monthly values and many years' means can be interpolated.
– Few predictors are also sufficient for the interpolation and no problem if the greater part of daily precipitation predictors is equal to 0.
– The expected interpolation error RMSE is modelled too, representativity examination of arbitrary station network is performed.
– Real time quality control for daily and monthly data (additive model).
– Capability for application of supplementary background information (stochastic variables), e.g., satellite, radar, forecast data. (with QC: data assimilation)
– Data series completion that is missing value interpolation, completion for monthly or daily station data series.
– Capability for interpolation, gridding of monthly or daily station data series, as grid-point and grid-box average datasets alike.

The elder versions of MISH-MASH software can be downloaded from:
http://www.met.hu/en/omsz/rendezvenyek/homogenization_and_interpolation/software/
We plan to share the new version MISHv2.01 next year (2025).

5. The relationship between MISH and data assimilation

The MISH system is capable of interpolation with background information and quality control (see *Fig. 1*), which is essentially a data assimilation procedure (*Szentimrey*, 2016).

5.1. Interpolation with background information in MISH

The background information, e.g., forecast, satellite, radar data can be efficiently used to decrease the interpolation error. In this paper only the interpolation based on additive model or normal distribution is presented. According to Section 2, let

us assume that, $Z(\mathbf{s}_0, t)$ is the predictand, $\hat{Z}(\mathbf{s}_0, t) = \lambda_0 + \sum_{i=1}^{M} \lambda_i Z(\mathbf{s}_i, t)$ is the interpolated predictand, moreover, there is given the $\mathbf{G} = \{G(\mathbf{s}, t) \mid \mathbf{s} \in D\}$ background information on a dense grid.
Then the principle of interpolation with background information is that the interpolated predictand given $\mathbf{G}$ can be expressed as follows:

$$\hat{Z}_G(\mathbf{s}_0, t) = \hat{Z}(\mathbf{s}_0, t) + E\left(Z(\mathbf{s}_0, t) - \hat{Z}(\mathbf{s}_0, t) \mid \mathbf{G}\right), \quad (1)$$

where $\mathrm{E}\left(Z(\mathbf{s}_0, t) - \hat{Z}(\mathbf{s}_0, t) \mid \mathbf{G}\right)$ is the conditional expectation of $Z(\mathbf{s}_0, t) - \hat{Z}(\mathbf{s}_0, t)$, given $\mathbf{G}$.

5.2. Data assimilation and reanalysis data

The forecast and the reanalysis data are based on the data assimilation which procedure is in strong relationship with the methodology of interpolation with background information. The Bayes estimation theory is the mathematical background of the data assimilation methods in meteorology. The purpose of data assimilation is to determine a best possible atmospheric state using observations and short range forecasts. The typical way applied in practice to estimate the true atmospheric state is the minimization of the following variational cost function:

$$J(\mathbf{z}) = (\mathbf{z} - \mathbf{g})^{\mathrm{T}} \mathbf{Q}^{-1} (\mathbf{z} - \mathbf{g}) + (\mathbf{y}_0 - \mathbf{F}\mathbf{z})^{\mathrm{T}} \mathbf{P}^{-1} (\mathbf{y}_0 - \mathbf{F}\mathbf{z}), \quad (2)$$

where $\mathbf{z}$ is the analysis field, predictand (grid), $\mathbf{g}$ is the given background field (forecast), $\mathbf{y}_0$ is the given observations, predictors; $\mathbf{F}\mathbf{z} = \mathrm{E}(\mathbf{y}_0|\mathbf{z})$, $\mathbf{Q}$ is the background error covariance matrix, and $\mathbf{P}$ is the observation error covariance matrix.
It can be proved that this procedure is essentially an interpolation with background information including a quality control part for the predictors. The cost function (Eq. (2)) is known and referred by the forecasting community, as it is based on the Bayesian estimation theory. However, there are some mathematical omissions and simplifications at this cost function (*Szentimrey*, 2016).
This mathematical derivation of the Bayesian cost function is not correct, therefore, the decision according to Eq. (2) is not a real Bayes decision. For example this formula includes implicitly the assumption that the conditional expectation of $\mathbf{z}$, given $\mathbf{g}$ is identical with $\mathbf{g}$, i.e., $\mathrm{E}(\mathbf{z}|\mathbf{g}) = \mathbf{g}$, that means the conditional expectation does not depend on climate, and the forecast is always optimal. Or the relation of the background error covariance matrix $\mathbf{Q}$ and the climate is absolutely not known by the forecasting community. Consequently, the necessary climate statistical parameters are also neglected at the data assimilation procedures applied in practice.

The data assimilation technique is used also to produce reanalysis data series in order to monitor the climate change based on past observation series. However, beside the inadequacies mentioned above there are further sources of errors for reanalysis data. One of them is the inhomogeneity of the used station data series i.e., these series are often affected by artificial shifts due to changes in the measurement conditions (relocations, instrumentation). Another problem may be the little spatial representativity, i.e., relatively few station data series are used for production of reanalysis data series as a consequence of the data policy between the countries (*Lakatos et al.*, 2021; *Bandhauer et al.*, 2022).

6. Conclusion

It is a nonsense that we try to model the future climate but we do not know the present climate. We should know the present climate well, if want an efficient methodology for spatial interpolation and data assimilation. For this purpose, special advanced mathematics is needed of course. Originally, we have developed the MISH system also to model the climate statistical parameters, i.e., climate, by using long station data series, since the optimal spatial interpolation needs modeled climate statistical parameters. But the question can be turned back. The climate modeling can be based on spatial interpolation of station climate statistical parameters.

References

Bandhauer, M., Isotta, F., Lakatos, M., Lussana, C., Båserud, L., Izsák, B., Szentes, O., Tveito, O.E., and *Frei, C.*, 2022: Evaluation of daily precipitation analyses in E-OBS (v19.0e) and ERA5 by comparison to regional high-resolution datasets in European regions. *Int. J. Climatol. 42*, 727–747. https://doi.org/10.1002/joc.7269

Cressie, N., 1991: Statistics for Spatial Data., Wiley, New York.

Izsák, B., Szentimrey, T., Lakatos, M., Pongrácz, R., and *Szentes, O.*, 2022: Creation of a representative climatological database for Hungary from 1870 to 2020. *Időjárás 126*, 1–26. https://doi.org.10.28974/idojaras.2022.1.1

Lakatos, M., Szentimrey, T., Bihari, Z., and *Szalai, S.*, 2013: Creation of a homogenized climate database for the Carpathian region by applying the MASH procedure and the preliminary analysis of the data. *Időjárás 117*, 143–158.

Lakatos, M., Szentimrey, T., Izsák, B., Szentes, O., Hoffmann, L., Kircsi, A., and *Bihari, Z.,* 2021: Comparative study of CARPATCLIM, E-OBS and ERA5 dataset, Proceedings of the 10th Seminar for Homogenization and Quality Control in Climatological Databases and 5th Conference on Spatial Interpolation Techniques in Climatology and Meteorology (Eds. *Lakatos M, Hoffmann L, Kircsi A, Szentimrey T*), Budapest, Hungary, 2020, WCDMP-No. 86, pp. 84-101

Szentimrey, T. and *Bihari, Z.*, 2007: Mathematical background of the spatial interpolation methods and the software MISH (Meteorological Interpolation based on Surface Homogenized Data Basis), Proceedings of the Conference on Spatial Interpolation in Climatology and Meteorology, Budapest, Hungary, 2004, COST Action 719, COST Office, 2007, 17–27

Szentimrey, T, Bihari, Z., Lakatos, M., and *Szalai, S*., 2011: Mathematical, methodological questions concerning the spatial interpolation of climate elements. Proceedings of the Second Conference on Spatial Interpolation in Climatology and Meteorology, Budapest, Hungary, 2009. *Időjárás 115*, 1–11.

Szentimrey T. et al., 2012a: Final report on quality control and data homogenization measures applied per country, including QC protocols and measures to determine the achieved increase in data quality. Carpatclim Project, Deliverable D1.12. http://www.carpatclim-eu.org/docs/deliverables/D1_12.pdf

Szentimrey T. et al., 2012b: Final report on the creation of national gridded datasets, per country. Carpatclim Project, Deliverable D2.9. http://www.carpatclim-eu.org/docs/deliverables/D2_9.pdf

Szentimrey, T. and *Bihari, Z.,* 2014: Manual of interpolation software MISHv1.03, Hungarian Meteorological Service.

Szentimrey, T., 2016: Analysis of the data assimilation methods from the mathematical point of view. (pp. 193-205), In (eds. *Bátkai, A., Csomós, P., Faragó, I., Horányi, A., Szépszó, G*.) Mathematical Problems in Meteorological Modelling. Springer International Publishing, Switzerland, 193–205, https://doi.org/10.1007/978-3-319-40157-7_10

Szentimrey, T., 2017: New developments of interpolation method MISH: modelling of interpolation error RMSE, automated real time quality control, Proceedings of the 9th Seminar for Homogenization and Quality Control in Climatological Databases and 4th Conference on Spatial Interpolation Techniques in Climatology and Meteorology (Eds. *Szentimrey T, Lakatos M, Hoffmann L*), Budapest, Hungary, 2017, WCDMP-No. 85, 115–124.

Szentimrey, T., 2021: Mathematical questions of spatial interpolation and summary of MISH, Proceedings of the 10**th** Seminar for Homogenization and Quality Control in Climatological Databases and **5**th Conference on Spatial Interpolation Techniques in Climatology and Meteorology (Eds. *Lakatos M, Hoffmann L, Kircsi A, Szentimrey T*), Budapest, Hungary, 2020, WCDMP-No. 86, 59–68.

Szentimrey, T., 2023a: Overview of mathematical background of homogenization, summary of method MASH and comments on benchmark validation. *Int. J. Climatol.43*, 6314–6329. https://doi.org/10.1002/joc.8207

Szentimrey, T., 2023b: Manual of homogenization software MASHv4.01, Varimax Limited Partnership.

Szentimrey, T., 2023c: Statistical modelling of the present climate by the interpolation method MISH – theoretical considerations, (extended abstract), Proceedings of the 11**th** Seminar for Homogenization and Quality Control in Climatological Databases and 6th Conference on Spatial Interpolation Techniques in Climatology and Meteorology (Eds. *Lakatos M, Puskás M, Szentimrey T*), Budapest, Hungary, 2023, WCDMP-No. 87, 45–50. https://library.wmo.int/idurl/4/68452

DOI:10.28974/idojaras.2024.2.2

IDŐJÁRÁS

Quarterly Journal of the HungaroMet Hungarian Meteorological Service
Vol. 128, No. 2, April – June, 2024, pp. 155–170

Operational homogenization of daily climate series in Spain: experiences with different variables

Belinda Lorenzo*, **José A. Guijarro**, **Andrés Chazarra**, **César Rodríguez-Ballesteros**, **José V. Moreno**, **Ramiro Romero-Fresneda**, **Maite Huarte**, and **Ana Morata**

Spanish State Meteorological Agency (AEMET)
Leonardo Prieto Castro 8, 28071 Madrid, Spain

**Corresponding author E-mail: blorenzom@aemet.es*

(Manuscript received in final form February 29, 2024)

Abstract— Calculation of the new climatological standard normals for the period 1991–2020 was a motivation to carry out the homogenization of the required climatic variables in the Spanish Meteorological Agency (AEMET).

The national observation network has undergone changes along its history that often introduce non-climatic interferences to the series. On the other hand, for the calculation of various parameters and climatic indices, it is essential to have complete daily series. With this in mind, homogenization of daily series of precipitation, maximum and minimum temperatures, sunshine hours, relative humidity, station level pressure, mean wind speed, and maximum wind gust was carried out.

This paper shows how the homogenization process was performed, covering the period 1975–2020 with carefully selected daily data sets from the national climatological database. The homogenization software Climatol v.4.0 was used for this process, and derived variables such as average temperature, sea level pressure, and vapor pressure were calculated from their related homogenized series.

The peculiarities and issues of each variable are explored and, finally, the homogenization results were used to readily calculate the 1991–2020 climatological standard normals with the dedicated software CLINO_tool v.1.5.

Key-words: standard normals, homogenization, Climatol, CLINO_tool, climatic variables, daily data

1. Introduction

Calculation of the new climatological standard normals for the period 1991–2020 (*WMO*, 2017) was a motivation to carry out the homogenization of all the daily series of the required climatic variables in the Spanish State Meteorological Agency (AEMET).

Having high-quality series which allow objective monitoring of the climatic behavior in a region is fundamental. Climatological series are subjected to changes of different nature. Some examples could be: instrumentation, location, changes in environment conditions near the station, different measurement methods, etc.

All these changes produce alterations in the data series which have no climatological or meteorological origin. Thus, in order to study possible changes in the climate or watch its behavior, time series long enough and without non-climatological alterations are necessary. These are homogenized series (*WMO*, 2020).

The land observation network of AEMET is made up of stations with specialist observers, volunteer observers, and automatic stations. The stations with professional workers are well distributed throughout the country, and usually do observations of many different variables. The stations with volunteers, complements the network throughout the entire territory. This selfless collaboration is very valuable. It provides measurements from areas that would otherwise lack information. Mostly, these stations measure precipitation and many also get temperature data. In recent times, the number of these collaborating stations has been reduced, but the number of automatic stations has increased. The automatic stations provide data for other variables in addition to temperature and precipitation.

All the data collected through these different methods is stored in the national climatological database.

This study focuses on the calculation of homogenized series of different climate variables.

To make this possible, the series were homogenized using a pre-release of the R package *Climatol* version 4 (*Guijarro*, 2023b). Given the computational requirements, the daily processing was computed in AEMET's HPC Cirrus.

Throughout the entire study period, the available data has different nature of origin but complements each other to perform the homogenization. Climatol responds well to short series, such as those obtained from recent automatic stations. Furthermore, series that no longer exist but that existed throughout the period can help to homogenize series that currently exist. All this variety of data series is very valuable for understanding the behavior of the variables in an area throughout the entire period considered.

When it was necessary to obtain the normals for the last reference period 1981–2010, the homogenized series of precipitation and temperature in that

period were calculated (*Botey et al.*,2013; *Chazarra et al.*, 2018). On that occasion, monthly data series were homogenized using an earlier version of homogenization software Climatol (*Guijarro*, 2014). These previous works were taken as a base and reference, being expanded with the calculation of homogenization of daily series and were included more variables such as: sunshine duration, relative humidity, station level pressure, mean wind speed, and maximum wind gust.

Working with daily series offers several advantages. For example, straightforward calculation of daily parameters and climatic indices, such as number of days over certain thresholds. However, it also brings certain disadvantages such as their high variability and the huge calculation capacity that is required.

When homogenized series were obtained, the derived variables, such as average temperature, sea level pressure, and vapor pressure were calculated from their related homogenized series.

Finally, once all the relevant series have been obtained, the 1991–2020 climatological standard normals were calculated automatically and written in the required format to be sent to WMO by means of the CLINO_tool (v.1.5) (*Guijarro*, 2023b).

2. Procedure

2.1. Data, regions and period selection

This study is carried out covering the period 1975-2020. Although the purpose was to obtain the 1991–2020 standard climatological normals, the period 1975–2020 was chosen to allow the recalculation of the 1981–2010 normals, adding 6 years backwards to improve the detection of inhomogeneities in the early 80s.

A large amount of daily data for the period 1975–2020 are available in the AEMET Climatological Database, especially when it comes to precipitation and temperature. For the other variables, considerably less daily data are stored.

This is because the collaborator stations mainly measure precipitation and to a lesser extent temperature, as it was mentioned above. Their data is of a daily nature. The remaining variables are measured at the main stations of the official AEMET network. Their number has increased in recent times due to the introduction of automatic stations that provide ten-minute data. This type of data has been stored in the climatological database since last years of the 2000s. In the main network stations, the nature of the data can be hourly, for example if it is manual, or ten-minute if it is automatic. Therefore, there are three types of data according to their measurement: daily, hourly, and ten-minute. All of them are computed to obtain the corresponding daily data and stored in the climatological database.

In a first step, only data series with a minimum of 5 years of daily data are accepted. Except in the case of precipitation, where only series with a minimum of 10 years are taken into consideration, due to their high number and the irregularity of their data.

When two or more variables have a functional dependency, those observed have been selected (extreme temperatures, relative humidity, station level pressure), leaving the others (mean temperature, water vapor partial pressure, sea level pressure) for a posterior calculation.

For precipitation and temperature, the study area is divided into 12 regions: mainland Spain (divided in turn into ten regions with similar climatic conditions and coinciding with the main hydrographic basins), the Balearic Islands, and the Canary Islands, due to their spatial and climatic differentiation.

For the rest of variables except precipitation and temperature, the study area is divided into three regions: mainland Spain (including autonomous cities of Ceuta and Melilla), the Balearic Islands, and the Canary Islands, due to their spatial and climatic differentiation. Mainland is divided into fewer regions mainly due to lack of data that makes its performing difficult.

2.2. General steps using Climatol

To perform the homogenization of the daily series of all the variables, a pre-release of the R package Climatol v4.0 was used. This software is very flexible, it allows to homogenize different climatic variables and in different time scales (*Guijarro*, 2023b).

Daily data have a high variability over time that makes it difficult to detect changes in their mean. The basic process with Climatol consists of obtaining monthly series from the daily data and homogenizing them. The daily series are divided with the breakpoints obtained in this monthly homogenization. Finally, all the series can be reconstructed from their homogeneous sub-periods in a final stage by estimating all their missing data.

The schematic general steps used in this work with Climatol are:

1. Preparation of the series in the required input format. To do this, the function *csv2climatol* from the Climatol package is used, set to each variable.
2. Only for precipitation: replace trace values by zeros and dissaggregate values accumulated during a few days. The distribution of accumulated is calculated with the *homogen* function using the *cumc* = -4 parameter.
3. First exploratory analysis of the daily series to control their quality (*homogen* function).
4. Obtain the monthly series from the daily data. The daily data is grouped into monthly series with the idea of obtaining the breakpoints. The *dd2m* function is used.

5. Homogenization of the monthly aggregates. The monthly homogenization is carried out to obtain the breakpoints, using the *homogen* function, with the appropriate parameters in each case (*Table 1*).
6. Careful manual review of these results by service specialists, identifying bad quality issues, deleting anomalous periods or whole series where needed, and repeating step 5.
7. Daily homogenization. Taking advantage of the breakpoints offered by the previous steps, it proceeds to the homogenization of the daily data. The parameter metad = TRUE is used in the *homogen* function.
8. Calculation of the daily series of variables considered derived from the corresponding homogenized ones.

Finally, with the homogenized series, the CLINO files required with the climatological normals for the standard period 1991–2020 can be straightforward obtained. CLINO_tool v.1.5 software is used.

In the homogenizations carried out, the following parameters (Table 1) have been used in the *homogen* function, following the recommendations of the documentation (*Guijarro*, 2023a):

- *dz.max* sets the thresholds for rejecting anomalous data or warning about suspicious data,
- *inht* is the inhomogeneity threshold, that is, the value of the homogeneity test above which the series will be split,
- *std* is the type of normalization applied to the data (e.g., default: std=3 means subtract the mean and divide by the standard deviation; with std=2 the data will be divided by its mean value; std=1 only centers the data by subtracting its mean value),
- *nref* is the maximum number of nearby data to use to estimate those of the problem series,
- *vmin* and *vmax* serve to limit the possible values that the data can take, and
- *gp* is the graphics parameter e.g., gp = 4 indicates moving annual sums instead of average values in final graphics.

Table 1. Parameters used in *homogen* function

	monthly		daily		both			
	dz.max	***inht***	***dz.max***	***nref***	***std***	***vmin***	***vmax***	***gp***
Precipitation	15	20	25	1	2	-	-	4
Temperature	6	-	15	-	-	-	-	-
Sunshine hours	6	-	12	-	1	0	-	-
Relative humidity	6	-	15	-	-	0	100	-
Station level pressure	6	-	15	-	-	0	-	-
Mean wind speed and max. wind gust	6	-	15	-	2	-	-	-

The peculiarities of the process for each variable are described below.

2.3. Precipitation

Firstly, the input data is selected. From the information stored in the climatological database, those stations with precipitation series of at least 10 years of daily data are selected resulting in a total of 6293 initial stations distributed throughout the entire territory (*Fig. 1*). Due to the huge amount of data, to facilitate its computation, the territory is divided into the 12 regions mentioned above.

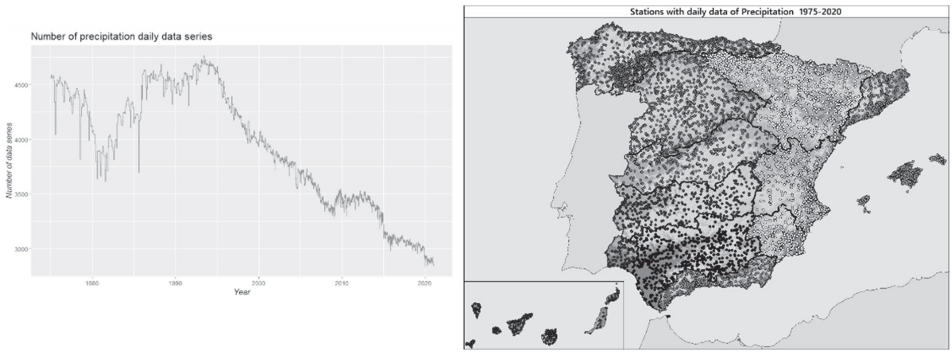

Fig. 1. Number of daily data series for precipitation (left) and distribution of precipitation stations (right).

In this variable, when the precipitation is negligible (<0.1 mm), the data is stored in the database with a value of -3. This values are changed to 0, to avoid small errors in aggregate data.

When the measurement of the amount of precipitation of the day cannot be carried out, it is marked as "accumulated". On the day when the observation can already be made, the total precipitation accumulated in the previous days is recorded. This situation occurs mostly in manual measurements, mainly in collaborator stations. But this can also happen with automatic stations, for example, when snow freezes in rain gauge without a heater. Before proceeding with homogenization, these accumulations must be distributed over the days without measurements. Climatol version 4.0 allows this process to be done using the *cumc* = -4 parameter in the *homogen* function.

The data is then grouped into monthly values, using the *dd2m* function from the Climatol package. It must be taken into account that in this case the monthly values are totals and not average values, so to indicate this, the value of the *valm* parameter must be changed to 1.

With the parameters indicated (*Table 1*), the monthly homogenization is made.

Subsequently, the results are carefully manually reviewed by specialist personnel. Among other criteria used, this review is also based on metadata when possible. As a result of this review, 30 series are rejected throughout the entire territory. To avoid the influences of these rejected stations on nearby stations, the entire process is redone.

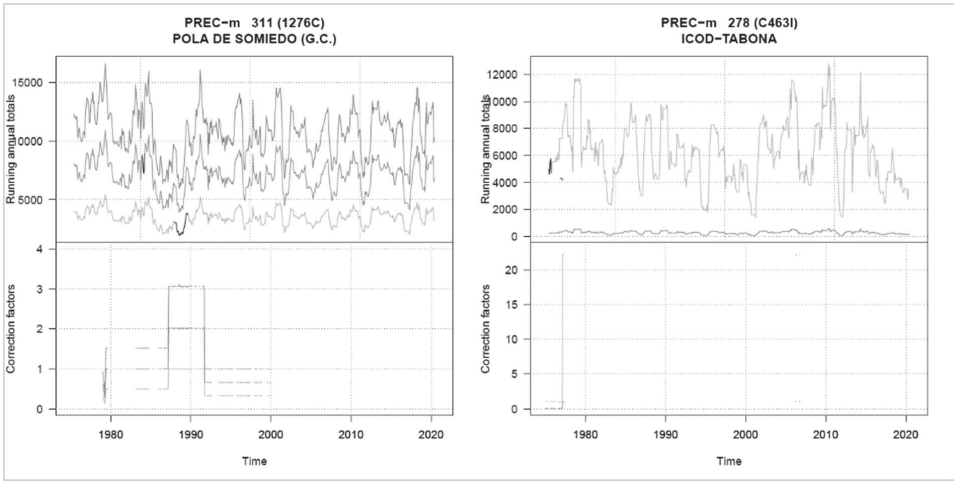

Fig. 2. Examples of series rejected after monthly homogenization.

An example of this is shown in *Fig. 2*. The running annual totals of the reconstructed monthly precipitation series of two rejected stations are shown. In this case, upper graphs show the running annual totals of the reconstructed monthly precipitation series (parameter *gp*=4, *Table 1*). The original series are drawn darker. The other lines represent the reconstructed series from the different homogeneous fragments. Lower graphs show the correction factors applied to the original data in the reconstruction of the series.

In both figures it can be seen that there are few data, especially in the one on the right. Both series are rejected due to their lack of quality data, and none of the reconstructed series offers conclusive or representative information.

The breakpoints obtained in the monthly homogenization are used to calculate the daily homogenization.

2.4. Maximum and minimum temperature

Regarding temperature, the homogenized variables are the maximum and minimum daily temperature. The daily series of average temperature from the homogenized series of maximum and minimum temperatures are obtained in a derivative way. In this case, from the series stored in the climatological database, those with a minimum of five years of data are selected resulting in a total of 3704 selected stations for the entire territory, which is divided into 12 regions (*Fig. 3*).

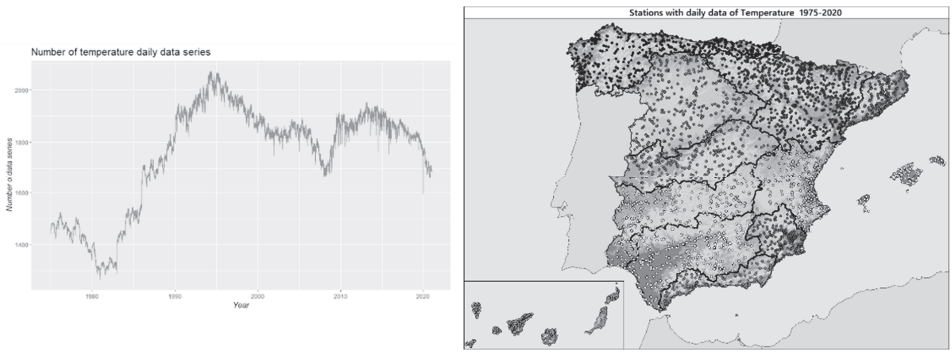

Fig. 3. Number of daily data series for temperature and distribution of temperature stations.

The entire process described above is carried out, but in this case the distribution of accumulated values is no longer necessary, and the grouping into monthly values is done by calculating daily averages.

After homogenizing the grouped monthly data, results are manually reviewed, and 34 series are rejected. The whole process is recalculated to obtain the homogenized daily series.

2.5. Sunshine duration

In this case, a total of 238 series are selected throughout the territory, which is divided into 3 different climatic regions (*Fig. 4*) corresponding to mainland Spain, the Balearic Islands, and the Canary Islands. The increase in the number of stations observed at the beginning of the 2010s is due to the installation of automatic measurement equipment.

After the monthly homogenization, a total of 12 series are rejected after manual review, and all process is redone. After the daily homogenization, the total hours of sunshine can exceed the theoretical number of hours that a certain place should have. So to fix this if necessary, an auxiliary function *fix.sunshine* is used.

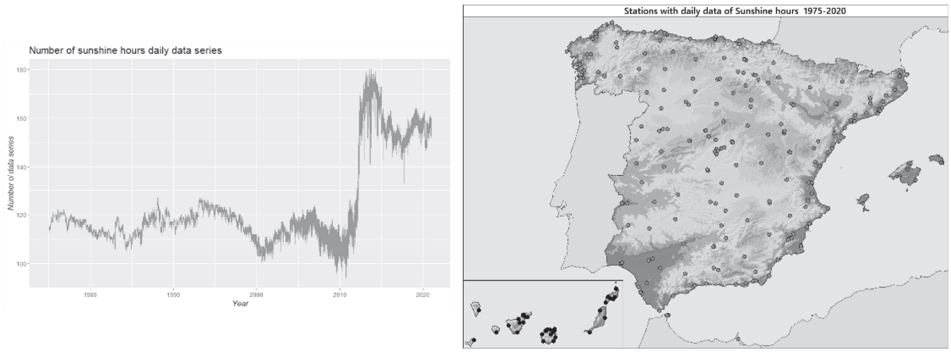

Fig. 4. Number of daily data series and distribution of stations for sunshine hours.

2.6. Relative humidity

Vapor pressure is the main variable required for the calculation of the climatic normal. However, it is a variable calculated from other observed variables. Considering the consistency with the observation, it was decided to homogenize the relative humidity. Vapor pressure is obtained then from the resulting data series and the corresponding average temperature series.

As at least 5 years of daily data are required, we have a total of 914 data series available for calculation. Processing is divided into three climatic regions

(*Fig. 5*) corresponding to mainland Spain, the Balearic Islands, and the Canary Islands.

In this variable, there is also a considerable increase in the number of available stations around 2010. This is attributed to the installation of a large number of automatic stations during that period. Nevertheless, the daily mean value of this variable is calculated using data from 07, 13, and 18 UTC hours to maintain consistency with historical data. Before 1996, only information at these specified hours was recorded.

After the monthly homogenization, about 15 stations are eliminated from the calculation.

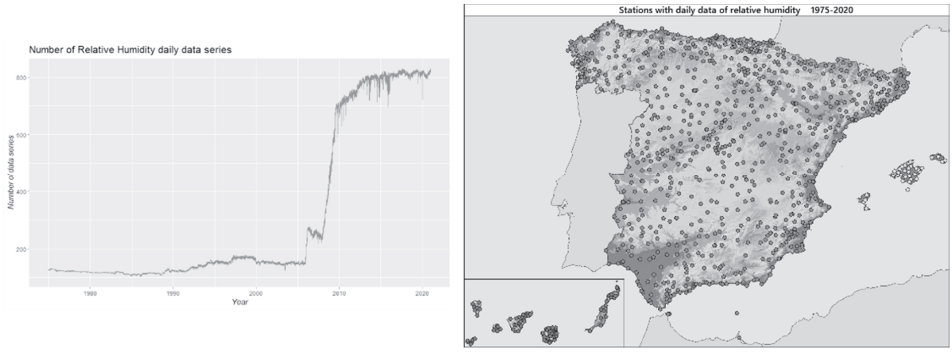

Fig. 5. Number of daily data series for relative humidity and distribution of its stations.

2.7. Station level pressure

In this case, the main variable required in the climatological normals is the pressure at sea level. However, it is a variable derived from the pressure at the station level, which is the one observed. For consistency with the observation/record method, it was decided to homogenize the observed variable and from the results, to obtain the homogenized daily series of pressure at sea level.

Similar to what happens with relative humidity, the daily mean value of this variable is obtained from the values at 07, 13, and 18 UTC hours.

After discarding those series with less than 5 years of data, a total of 274 stations are available (*Fig. 6*), of which 13 are rejected after evaluating their quality.

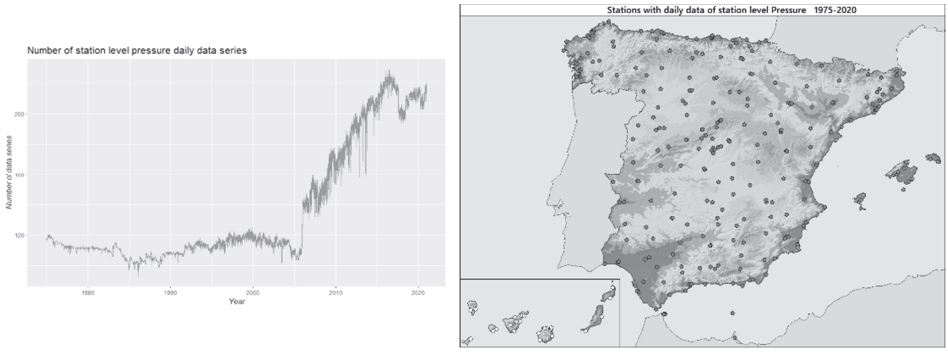

Fig. 6. Number of daily data series for station level pressure and distribution of its stations.

2.8. Mean wind speed and maximum wind gust

The maximum wind gust is treated as a secondary variable to report normal climatological values. Taking advantage of this calculation, the average wind speed has also been homogenized.

Similar to the previous variables, the daily mean value of this variable continues to be calculated from the data at 07, 13, and 18 UTC hours, even though the majority of measurement stations are automatic.

In both variables, after rejecting those series with less than five years of daily data, near 900 series are gathered (*Fig. 7*), of which 11 are rejected after a quality review after the monthly homogenization.

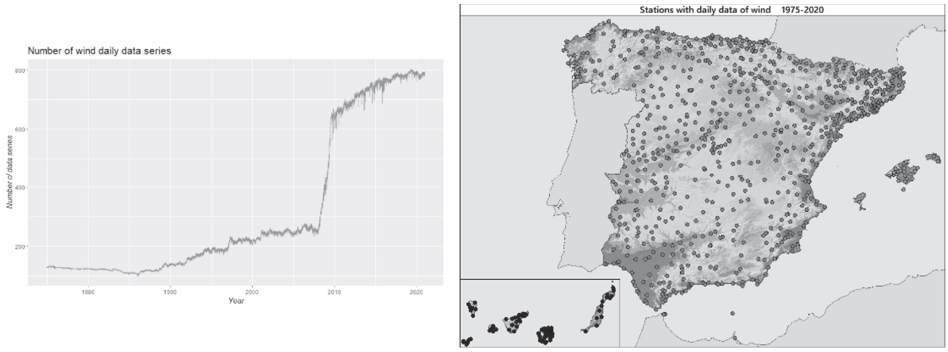

Fig. 7. Number of daily data series for wind and distribution of its stations.

2.9. Derivate values

As previously mentioned, the series of derived variables are calculated from the homogenized daily series of the variables from which they are derived.

The average temperature is calculated from the series of daily maximum and minimum temperature. The vapor pressure is obtained from the series of relative humidity and average temperature. Likewise, the pressure at sea level is derived from the pressure at the station level.

2.10. Normal values

Once all the relevant series have been obtained, the CLINO files can be calculated straightforward using the software CLINO_tool v.1.5. This CLINO files are requested with a specific structure. With CLINO_tool, these files are automatically generated from the Climatol output after the daily homogenizations (*Fig. 8*).

```
World Meteorological Organization Climate Normals for 1991-2020,,,,,,,,,,,,,,,,
Single Station Data Sheet For All Climatological Surface Parameters,,,,,,,,,,,,,,,,
,,,,,,,,,,,,,,,,
Station Header Record,,,,,,,,,,,,,,,,
,,,,,,,,,,,,,,,,
Country_Name,Spain,,,,,,,,,,,,,,,
Station_Name,A CORUÑA,,,,,,,,,,,,,,,
,,,,,,,,,,,,,,,,
WMO_Number,Latitude,Longitude,Station_Height,,,,,,,,,,,,,
8001,43|21|57|N,008|25|17|W,58.000000,,,,,,,,,,,,,
,,,,,,,,,,,,,,,,
WMO Integrated Global Observing System (WIGOS) Station Identifier (if available)
0-20000-0-08001,,,,,,,,,,,,,,,,
,,,,,,,,,,,,,,,,
,,,,,,,,,,,,,,,,
Principal Climatological Surface Parameters,,,,,,,,,,,,,,,,
,,,,,,,,,,,,,,,,
,,,,,,,,,,,,,,,,
Parameter_Code,Parameter_Name,Units,,,,,,,,,,,,,,
1,Precipitation_Total,mm,,,,,,,,,,,,,,
,,,,,,,,,,,,,,,,
WMO_Number,Parameter_Code,Calculation_Name,Calculation_Code,January,February,March,April
,May,June,July,August,September,October,November,December,Annual
8001,1,Sum,4,120.8,88.5,87.6,86.9,66.3,45.7,31.2,40.7,57.0,120.7,149.9,122.3,1017.6
```

Fig. 8. Example of the CLINO file heading.

It must be taken into account that the CLINO_tool only calculates normals from series having the required minimum of 80% of data in the reference period 1991–2020.

3. Results

The main results are the homogenized data series of the variables involved. Some particular cases about the relationship between changes involved in stations and breaks detected are discussed below.

3.1. Summary of breaks

Table 2 shows a summary of number of series and breaks detected by variable.

Table 2. Summary of the breaks by variable

Climatological variable	Number of series	Number of break-points	Average break-points/series
Precipitation	6293	1759	0.28
Maximum temperature	3704	5630	1.52
Minimum temperature	3704	5577	1.51
Sunshine hours	238	126	0.52
Relative humidity	914	601	0.66
Station level air pressure	274	353	1.29
Mean wind speed	900	586	0.65
Maximum wind gust	883	495	0.56

It highlights the low value of average breaks-points/series for precipitation. High number of series and irregularity of their data are observed. Fewer jumps in the average are detected. Moreover, the review of the test histograms and anomaly graphs suggested a lowering of the default value of parameter *inht*, which is 25, to 20 (*Table 1*). Variability is inherent to this variable. It is of interest to increase the value of the parameter *dz.max,* so that fewer anomalous data points are rejected.

The same does not happen with temperature. After observing the anomaly graphs, the threshold value *inht* = 25, is appropriate for monthly values of temperature. Although in a little conservative way, we are trying not to detect false jumps in the average at the cost of letting the minor ones pass.

3.2. Change in location

Fig. 9 shows a graph with the running annual means of hours of sunshine at the Tenerife Sur airport located in the Canary Islands. In this case, a break was detected for November 2014. According the stored metadata, it has been verified that in November 2014, the location station at the airport was changed, thus giving a possible explanation for this break. In this case, this break produces a split in two series, where the last period undergoes an additional correction of more than 0.5 hours in the data prior to the break.

We can find another example in *Fig. 10*, that shows a graph with the running annual totals of precipitation at Llinars del Vallès (mainland). Here the Climatol has detected a break in 1995. According to the registered metadata it is described, that in the middle of the decade there was a change of location from a garden to an interior terrace at 250 m apart.

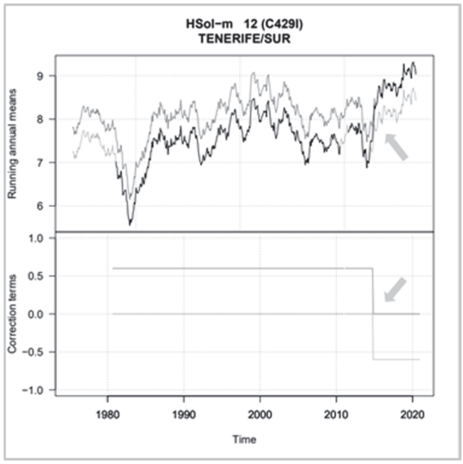

Fig 10. Running annual means for sunshine in Tenerife Sur with a break in November 2014.

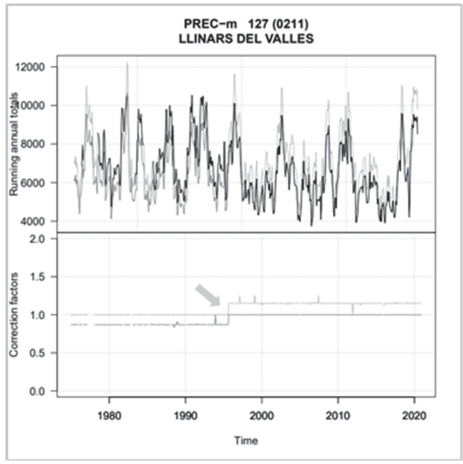

Fig. 9. Running annual totals for precipitation with a break in 1995.

3.3. Change in shelter

Fig. 11 shows a graph with the running annual means of maximum temperature at Hervás (mainland) with a break detected in 2018. It is a THIES-type automatic station that started operating in 2008. According to the records, in 2018, a change of shelter was carried out with a change of height.

3.4. Change in instrumentation

Fig. 12 shows how a change of instrumentation could affect the measurements of wind. In this case, a break was detected in the late 2000s. It is a SEAC-type automatic station that at the end of the decade was replaced by a THIES-type station. On this occasion, the series prior to the break see their values clearly increased.

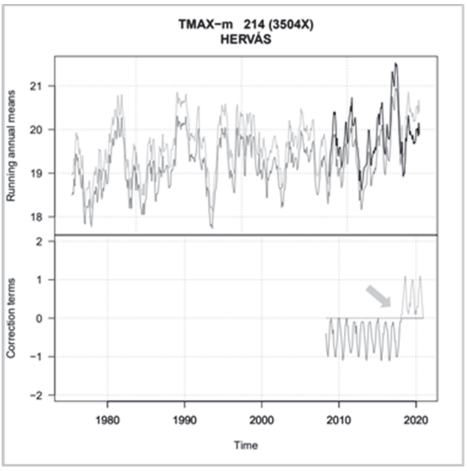

Fig. 11. Running annual means for maximum temperature with a break in 2018.

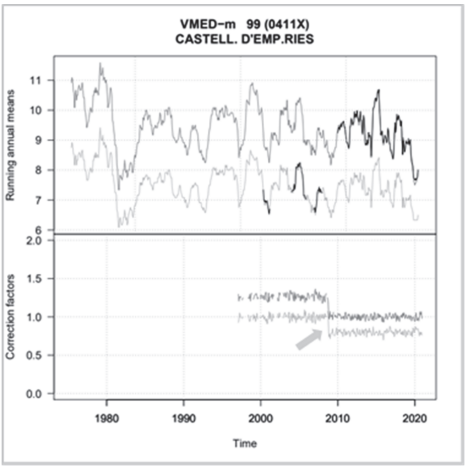

Fig. 12. Running annual means for mean wind speed.

3.5. Change in calculation/measurement methods

The following example (*Fig. 13*) shows a graph with the running annual means for the station level pressure. In this case, a break was detected in 1996. According to metadata, after 1996, the barometric reference was changed to reduce the pressure calculation. There is no further recorded metadata that could explain the other break detected in 2008.

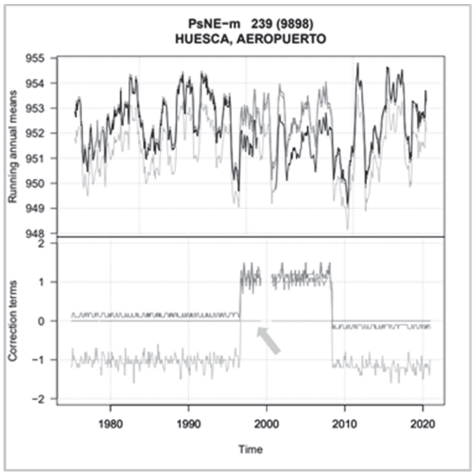

Fig. 13. Running annual means for station pressure.

4. Conclusions

Due to the large amount of data and simultaneously running threads, the calculation involves a computationally heavy load. It became necessary to resort to processing in the homogenization process HPC, especially thinking about the calculation time.

Climatol has responded well to detecting jumps whose origin appears to be related to non-climatological changes recorded in the metadata.

Obtaining the normal values from the homogenized series using CLINO_tool has been straightforward.

As a continuation, the maps corresponding to the climatological normals for the period 1991–2020 will be obtained.

An interesting perspective for the future could be obtaining daily data grids and maps of variables such as precipitation and temperature from the homogenized data. They could be compared with non-homogenized grids but validated by automatic methods.

References

Botey, R., Guijarro, J.A. and *Jiménez, A*., 2013: Valores normales de precipitación mensual 1981-2010. Agencia Estatal de Meteorología.

Chazarra, A., Flórez, E., Peraza, B., Tohá, T., Lorenzo, B., Criado, E., Moreno, J.V., Romero, R. and *Botey, R.*, 2018. Mapas Climáticos de España (1981–2010) y ETo (1996–2016); AEMET.

Guijarro, J.A., 2014: User's guide of the *climatol* R Package (version 2.2).

Guijarro, J.A., 2023a: CLINO tool. https://climatol.eu/pub/CLINO_tool.tgz

Guijarro, J.A., 2023b: User's guide of the *climatol* R Package (version 4). https://climatol.eu/climatol4-en.pdf

WMO, 2017: Guidelines on the Calculation of Climate Normals. WMO-No. 1203. https://library.wmo.int/idurl/4/55797

WMO, 2020: Guidelines on Homogenization. WMO-No. 1245, 54 pp, Geneva, Switzerland.

DOI:10.28974/idojaras.2024.2.3

IDŐJÁRÁS

Quarterly Journal of the HungaroMet Hungarian Meteorological Service
Vol. 128, No. 2, April – June, 2024, pp. 171–193

Precipitation conditions in Hungary from 1854 to 2022

Olivér Szentes[1,2,*], **Mónika Lakatos**[1], and **Rita Pongrácz**[3]

[1] *National Laboratory for Water Science and Water Safety,*
HungaroMet Hungarian Meteorological Service,
Kitaibel Pál u.1, Budapest 1024, Hungary

[2]*ELTE Faculty of Science*
Doctoral School of Earth Sciences, Budapest, Hungary

[3]*ELTE Department of Meteorology,*
Pázmány Péter st. 1/A, Budapest 1117, Hungary

**Corresponding author E-mail: szentes.o@met.hu*

(Manuscript received in final form January 12, 2024)

Abstract— In Hungary, the regular precipitation measurements began in the 1850s under the direction of the then Austrian Meteorological Institute based in Vienna, and from 1870 onwards continued under the Budapest-based "Meteorológiai és Földdelejességi Magyar Királyi Központi Intézet", now HungaroMet Hungarian Meteorological Service. Over the decades, the measurements have undergone many changes, including changes in instrumentation and relocation of stations, which cause inhomogeneities in the data series. In addition, the number of stations and the density of the station network have also changed significantly. As a result, the data series need to be homogenized and interpolated to a uniform grid in order to study the climate and its changes over the long term. In this paper, we present the methods used, discuss the station systems used for precipitation homogenization and interpolation in different periods, analyze the main verification statistics of homogenization and also the results of interpolation, and examine the annual, seasonal, and monthly precipitation data series and their extremes for the period 1854–2022.

Key-words: climate data, precipitation changes in Hungary, homogenization, interpolation, MASH, MISH, verification statistics, gridded data series

1. Introduction

To better understand the climate system and its changes, we need to analyze long data series with high quality. Precipitation is a highly variable element in space and time, so long time series and many more stations are needed to describe the spatial characteristics of precipitation compared to, for example, temperature. Climate research and studies on precipitation conditions in Hungary, based on precipitation measurements, can typically be found from the beginning of the 20th century. There are few analyses dating back to the 19th century (*Izsák et al.*, 2022). Most of the precipitation data are digitized from the mid-20th century, from 1951 onwards. Precipitation measurements from the earlier period are mostly available on precipitation data sheets and in climatological books. It is, therefore, important to collect these data series, which have not yet been digitized, in order to have as accurate knowledge as possible of precipitation conditions and their changes.

The data series contain inhomogeneities due to, for example, station relocations, instrument changes, or changes in the environment, and therefore, homogenization is necessary. Several methods and software have been developed in recent decades to homogenize meteorological elements (*Venema et al.*, 2012, 2020). These include, for example, the MASH (*Szentimrey*, 1999, 2017, 2023), the standard normal homogeneity test (SNHT) (*Alexandersson*, 1986; *Alexandersson* and *Moberg*, 1997), the HOMER (*Mestre et al.*, 2013; *Joelsson et al.*, 2021), and the ACMANT (*Domonkos*, 2015) methods.

For homogenization of data series, quality control, and filling in the missing values, we use the MASH (Multiple Analysis of Series for Homogenization) procedure at the Climate Department of the Hungarian Meteorological Service (OMSZ) (*Szentimrey*, 1999, 2008a, 2017). By applying the MASHv3.03 software, homogenized and quality-controlled data series become available without missing data for further analysis. The MASH method is based on hypothesis testing. To homogenize the precipitation series, we used a multiplicative model with a significance level of 0.01. Inhomogeneities are estimated from the monthly data series. The monthly, seasonal, and annual inhomogeneities are harmonized in all MASH systems (considering different station networks).

There are several interpolation methods that are used to produce gridded climate data series (*Sluiter*, 2009). For the spatial interpolation of precipitation, the MISH (Meteorological Interpolation based on Surface Homogenized Data Basis) method, specifically developed for the interpolation of meteorological elements, is used at the Hungarian Meteorological Service (*Szentimrey* and *Bihari*, 2007, 2014).

2. Applied methods

For homogenization of data series, quality control and filling in the missing data, we use the MASH (*Szentimrey*, 1999, 2008b, 2017) procedure at the Climate Department of HungaroMet Hungarian Meteorological Service. By applying the MASHv3.03 software we have missing data filled, homogenized, and quality-controlled data series.

2.1. The main properties of MASH procedure

The homogenization of monthly series includes:

- a relative homogeneity test procedure,
- a step-by-step iteration procedure,
- additive (e.g., temperature) or multiplicative (e.g., precipitation) models that can be selected,
- quality control and missing data completion,
- homogenization of seasonal and annual series,
- metadata (probable dates of breakpoints) that can be used automatically,
- automatically generated verification files.

The homogenization of daily series is:

- based on the detected monthly inhomogeneities,
- quality controlled and containing the completion of missing data for each day.

If the data series are lognormally distributed (e.g., precipitation), then the multiplicative model can be used (*Szentimrey*, 2008a). In the case of relative methods, a general form of multiplicative model for additional monthly series belonging to the same month in a small climate region can be expressed as follows:

$$X_j^*(t) = C^*(t) \cdot IH_j^*(t) \cdot \varepsilon_j^*(t) \quad (j = 1,2,\dots,N;\ t = 1,2,\dots,n), \qquad (1)$$

where X^* indicates the candidate series, C^* is the climate change, IH^* is the inhomogeneity, ε^* is the noise, N is the number of stations, and n is the total number of time steps.
Logarithmization for additive model gives the following equation:

$$X_j(t) = C(t) + IH_j(t) + \varepsilon_j(t) \quad (j = 1,2,\dots,N;\ t = 1,2,\dots,n), \qquad (2)$$

where

$$X_j(t) = \ln X_j^*(t) \quad , \quad C(t) = \ln C(t),$$

$$IH_j(t) = \ln IH_j^*(t) \quad , \quad \varepsilon_j(t) = \ln \varepsilon_j^*(t).$$

A problem occurs if $X_j^*(t)$ values are near or equal to 0. This problem can be solved by a transformation procedure that slightly increases the small values. Consequently, the multiplicative model can be transformed into the additive model (*Szentimrey*, 1999, 2017). Once homogenization is complete, the data series are retransformed.

2.2. The main properties of MISH method

By using the MISHv1.03 software (*Szentimrey* and *Bihari*, 2007, 2014), spatially representative data series are obtained. MISH consists of a modeling and an interpolation subsystem.

The main features of the modeling subsystem for climate statistical (local and stochastic) are as follows:

- it is based on long term homogenized data series and supplementary deterministic model variables (height, topography, distance from the sea etc.),
- additive (e.g., temperature) or multiplicative (e.g., precipitation) models can be selected,
- the modeling procedure should be executed only once before the interpolation applications,
- it uses a high resolution grid (e.g., 0.5'×0.5').

The main characteristics of the interpolation subsystem are as follows:

- use of the modeled parameters for the interpolation of the meteorological elements to any point or grid,
- use of background information (e.g., satellite, radar, forecast data),
- data series completion (missing value interpolation for daily or monthly station data) during the interpolation process,
- capability for interpolation, gridding of monthly or daily station data series.

In practice, many kinds of interpolation methods exist (e.g., inverse distance weighting (IDW), kriging, spline interpolation), therefore the question is the difference between them (*Szentimrey et al.*, 2011). According to the interpolation problem, the unknown predictand $Z(\mathbf{s}_0, t)$ is estimated by use of the known predictors $Z(\mathbf{s}_i, t)$ $(i = 1, \dots, M)$, where the location vectors $\mathbf{s}$ are the elements of the given space domain, M is the total number of predictors, and t is the time. The type of the adequate interpolation formula depends on the probability distribution of the meteorological element.

In the case of precipitation, a multiplicative model can be applied for a quasi-lognormal distribution:

$$\hat{Z}(s_0,t) = \vartheta \cdot \left(\prod_{q_i \cdot Z(s_i,t) \geq \vartheta} \left(\frac{q_i \cdot Z(s_i,t)}{\vartheta} \right)^{\lambda_i} \right) \cdot \left(\sum_{q_i \cdot Z(s_i,t) \geq \vartheta} \lambda_i + \sum_{q_i \cdot Z(s_i,t) < \vartheta} \lambda_i \cdot \left(\frac{q_i \cdot Z(s_i,t)}{\vartheta} \right) \right), \quad (3)$$

where $\vartheta > 0$, $q_i > 0$, $\sum_{i=1}^{M} \lambda_i = 1$, and $\lambda_i \geq 0$ $(i = 1, \dots, M)$, q_i, λ_i $(i = 1, \dots, M)$ are the interpolation parameters (*Szentimrey* and *Bihari*, 2014).

The root mean squared interpolation error (RMSE) is defined as follows:

$$RMSE(s_0) = \sqrt{E\left(\left(Z(s_0,t) - \hat{Z}(s_0,t) \right)^2 \right)}, \quad (4)$$

and the representativity of the station network can be defined as follows:

$$REP(s_0) = 1 - \frac{RMSE(s_0)}{D(s_0)}, \quad (5)$$

where E is the expected value and $D(s_0)$ is the standard deviation of the predictand.

2.3. ANOVA (analysis of variance)

To compare gridded data sets interpolated from different numbers of data series, ANOVA is performed to examine the estimated spatiotemporal variances (*Szentimrey* and *Bihari*, 2014; *Izsák et al.*, 2022).

Notations:

$\mathrm{Z}(\mathrm{s_j}, \mathrm{t})$ $(\mathrm{j} = 1, \dots, \mathrm{N}; \mathrm{t} = 1, \dots, \mathrm{n})$ – gridded data series $(\mathrm{s_j}: \mathrm{location}, \mathrm{t}: \mathrm{time})$,

$\widehat{\mathrm{E}}(\mathrm{s_j}) = \frac{1}{\mathrm{n}} \sum_{\mathrm{t}=1}^{\mathrm{n}} \mathrm{Z}(\mathrm{s_j}, \mathrm{t})$ (j=1,…,N) – temporal mean at location s_j,

$\widehat{\mathrm{D}}(\mathrm{s_j}) = \sqrt{\frac{1}{\mathrm{n}} \sum_{\mathrm{t}=1}^{\mathrm{n}} (\mathrm{Z}(\mathrm{s_j}, \mathrm{t}) - \widehat{\mathrm{E}}(\mathrm{s_j}))^2}$ (j=1,…,N) – temporal standard deviation at location s_j,

$\widehat{\mathrm{E}}(\mathrm{t}) = \frac{1}{\mathrm{N}} \sum_{\mathrm{j}=1}^{\mathrm{N}} \mathrm{Z}(\mathrm{s_j}, \mathrm{t})$ (t=1,…,n) – spatial mean at moment *t*,

$\widehat{\mathrm{D}}(\mathrm{t}) = \sqrt{\frac{1}{\mathrm{N}} \sum_{\mathrm{j}=1}^{\mathrm{N}} (\mathrm{Z}(\mathrm{s_j}, \mathrm{t}) - \widehat{\mathrm{E}}(\mathrm{t}))^2}$ (t=1,…,n) – spatial standard deviation at moment *t*,

$\widehat{\mathrm{E}} = \frac{1}{\mathrm{N} \cdot \mathrm{n}} \sum_{\mathrm{j}=1}^{\mathrm{N}} \sum_{\mathrm{t}=1}^{\mathrm{n}} \mathrm{Z}(\mathrm{s_j}, \mathrm{t}) = \frac{1}{\mathrm{N}} \sum_{\mathrm{j}=1}^{\mathrm{N}} \widehat{\mathrm{E}}(\mathrm{s_j}) = \frac{1}{\mathrm{n}} \sum_{\mathrm{t}=1}^{\mathrm{n}} \widehat{\mathrm{E}}(\mathrm{t})$ – total mean,

$\widehat{\mathrm{D}}^2 = \frac{1}{\mathrm{N} \cdot \mathrm{n}} \sum_{\mathrm{j}=1}^{\mathrm{N}} \sum_{\mathrm{t}=1}^{\mathrm{n}} (\mathrm{Z}(\mathrm{s_j}, \mathrm{t}) - \widehat{\mathrm{E}})^2$ – total variance.

Partitioning of Total Variance (Theorem):

$$\widehat{D}^2 = \frac{1}{N}\sum_{j=1}^{N}(\widehat{E}(s_j) - \widehat{E})^2 + \frac{1}{N}\sum_{j=1}^{N}\widehat{D}^2(s_j) = \frac{1}{n}\sum_{t=1}^{n}(\widehat{E}(t) - \widehat{E})^2 + \frac{1}{n}\sum_{t=1}^{n}\widehat{D}^2(t).$$

The analysis of these terms is recommended to characterize the spatiotemporal variability.

Spatial terms:

spatial variance of temporal means: $\frac{1}{N}\sum_{j=1}^{N}(\widehat{E}(s_j) - \widehat{E})^2$,

and temporal mean of spatial variances: $\frac{1}{n}\sum_{t=1}^{n}\widehat{D}^2(t)$.

Temporal terms:

spatial mean of temporal variances: $\frac{1}{N}\sum_{j=1}^{N}\widehat{D}^2(s_j)$,

and temporal variance of spatial means $\frac{1}{n}\sum_{t=1}^{n}(\widehat{E}(t) - \widehat{E})^2$.

We do not show the variances but the standard deviations instead, to make the values easier to interpret, especially in the case of precipitation:

total standard deviation: $\widehat{D} = \sqrt{\frac{1}{N\cdot n}\sum_{j=1}^{N}\sum_{t=1}^{n}(Z(s_j,t) - \widehat{E})^2}$,

spatial standard deviation of temporal means: $\sqrt{\frac{1}{N}\sum_{j=1}^{N}(\widehat{E}(s_j) - \widehat{E})^2}$,

root spatial mean of temporal variances: $\sqrt{\frac{1}{N}\sum_{j=1}^{N}\widehat{D}^2(s_j)}$,

temporal standard deviation of spatial means: $\sqrt{\frac{1}{n}\sum_{t=1}^{n}(\widehat{E}(t) - \widehat{E})^2}$,

root temporal mean of spatial variances: $\sqrt{\frac{1}{n}\sum_{t=1}^{n}\widehat{D}^2(t)}$.

3. Data

The meteorological measurements in Hungary are stored in the climate database of the HungaroMet. Today, meteorological measurements from automatic meteorological stations are continuously entered into the database. Records of older, pre-automation times are contained in climatological books and precipitation data sheets. The digitization of old data into the climate database is still ongoing. Most of the precipitation data from the 1950s are available in digital form also, whereas most of the precipitation data from earlier decades are still available only on paper. Recently, all monthly precipitation data from the beginning of the measurements in

Hungary have been collected, and these precipitation data can now be used also to create a homogenized and gridded climate database.

Before including data that has not yet been digitized, the existing daily precipitation database was renewed, and a study was published about this (*Szentes et al.*, 2023). That paper describes the changes in the station systems used and the main results of the homogenization. The renewal of the station networks was necessary because of the increasing lack of data, especially for the long series (due to the closure of stations), and therefore, the main objectives were (i) to minimize the missing data and (ii) to keep the old data series with long measurements by creating new merged station series. There is no significant change in the data set consisting of 131 stations used in the first half of the 20th century, the old and new systems are almost identical. However, in the last 10–20 years, several stations were discontinued and, in several cases, new station series were merged with nearby stations to have more data in years close to the present. In the shorter period (from 1951) we use 500 stations instead of the 461 stations previously used. From the previously used 461 stations, ~20 stations were deleted due to too much missing value and ~60 new stations, previously not used during the homogenization were added. The 500 data series for the shorter period (from 1951) includes the 131 data series which are available for the long period. The amount of missing data is not zero in the present either, because we use data from areas with higher spatial variability of precipitation (mountainous areas), where we have found stations that have been in operation for several decades then have stopped and there are no other stations in the vicinity to merge with.

3.1. Expansion of the station system before 1951

As shown above, the Hungarian precipitation climate database is currently based on two station systems: 131 stations from 1901, and 500 stations from 1951 (marked as different MASH systems later). The large jump in the number of data series from 1951 is explained by the fact that the majority of data series in the database were digitized from the mid-20th century. Extensive precipitation measurements in Hungary began in the 1850s. Recently, as a new achievement, all the monthly precipitation data have been collected from the beginning of measurements to 1950 (*Fig. 1*), which have not yet been digitized. This allowed a significant expansion of the station systems used for homogenization of data from the first half of the 20th century and the second half of the 19th century. In the last year, the monthly precipitation totals of all precipitation stations in Hungary were collected and digitized since the beginning of the measurements. Following this, new station systems were established, homogenized, and interpolated, which provided the first insight into the precipitation conditions in Hungary since the beginning of the measurements. *Figs. 2* and *3* show the number of available precipitation data series for the first half of the 20th century and the second half of the 19th century.

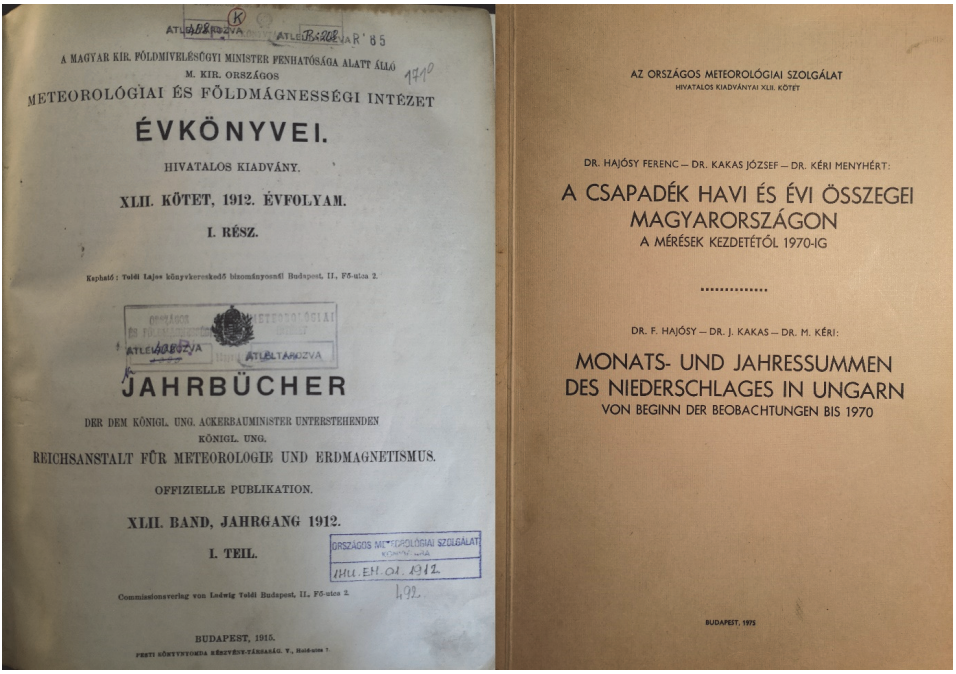
A MAGYAR KIR. FÖLDMIVELÉSÜGYI MINISTER FENHATÓSÁGA ALATT ÁLLÓ
M. KIR. ORSZÁGOS
METEOROLÓGIAI ÉS FÖLDMÁGNESSÉGI INTÉZET
ÉVKÖNYVEI.
HIVATALOS KIADVÁNY.
XLII. KÖTET, 1912. ÉVFOLYAM.
I. RÉSZ.
JAHRBÜCHER
DER DEM KÖNIGL. UNG. ACKERBAUMINISTER UNTERSTEHENDEN
KÖNIGL. UNG.
REICHSANSTALT FÜR METEOROLOGIE UND ERDMAGNETISMUS.
OFFIZIELLE PUBLIKATION.
XLII. BAND, JAHRGANG 1912.
I. TEIL.
BUDAPEST, 1915.
AZ ORSZÁGOS METEOROLÓGIAI SZOLGÁLAT
HIVATALOS KIADVÁNYAI XLII. KÖTET
DR. HAJÓSY FERENC — DR. KAKAS JÓZSEF — DR. KÉRI MENYHÉRT:
A CSAPADÉK HAVI ÉS ÉVI ÖSSZEGEI
MAGYARORSZÁGON
A MÉRÉSEK KEZDETÉTŐL 1970-IG
DR. F. HAJÓSY — DR. J. KAKAS — DR. M. KÉRI:
MONATS- UND JAHRESSUMMEN
DES NIEDERSCHLAGES IN UNGARN
VON BEGINN DER BEOBACHTUNGEN BIS 1970
BUDAPEST, 1975

Fig. 1. Example for climatological books containing monthly precipitation data for Hungary.

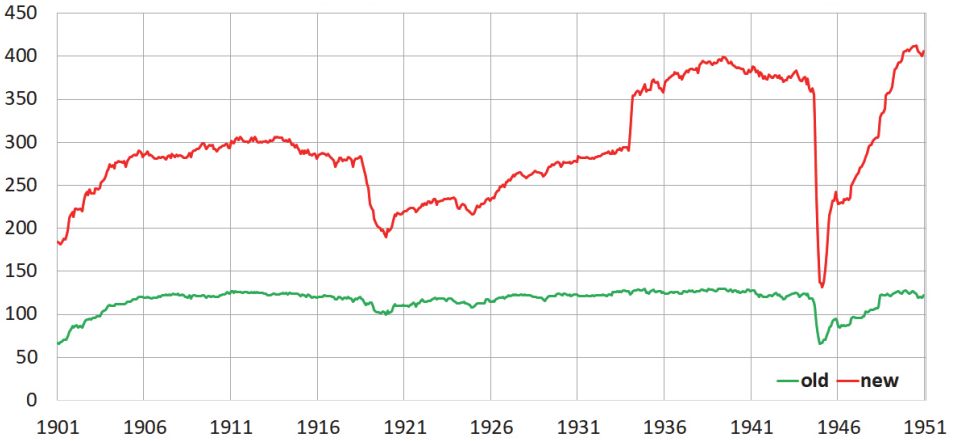

Fig. 2. Number of monthly precipitation station data series in Hungary (within today's border) during the first half of the 20th century.

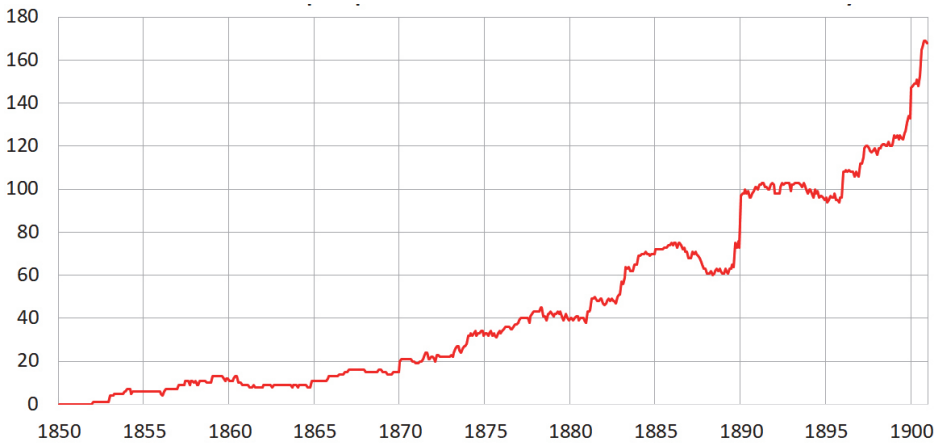

Fig. 3. Number of monthly precipitation station data series in Hungary (within today's border) during the second half of the 19th century.

Major station network expansions took place in the early 20th century and in the 1930s, so that the previous homogenization from 1901 onwards in one step was replaced by a two-step homogenization in the first half of the 20th century. The devastation of World War II is reflected in the temporary cessation of measurements at about 70% of the precipitation stations by 1945.

In the second half of the 1800s, the expansion of the network of stations was relatively continuous with an accelerating trend from the 1870s onwards. Regular measurements in different parts of the country started in 1854, under the control of the then Austrian Meteorological Institute (now GeoSphere Austria), so that 1854 can be considered as the beginning of precipitation measurements in Hungary. For the second half of the 19th century, the homogenization took place in three steps.

So, in total, there are six steps in the homogenization of precipitation, from 1854 to the present: from 1854 30, from 1870 50, from 1881 124, from 1901 318, from 1931 402, and from 1951 500 station data series (*Fig. 4*) are homogenized, any missing data is completed, and the overall resulting time series are quality controlled.

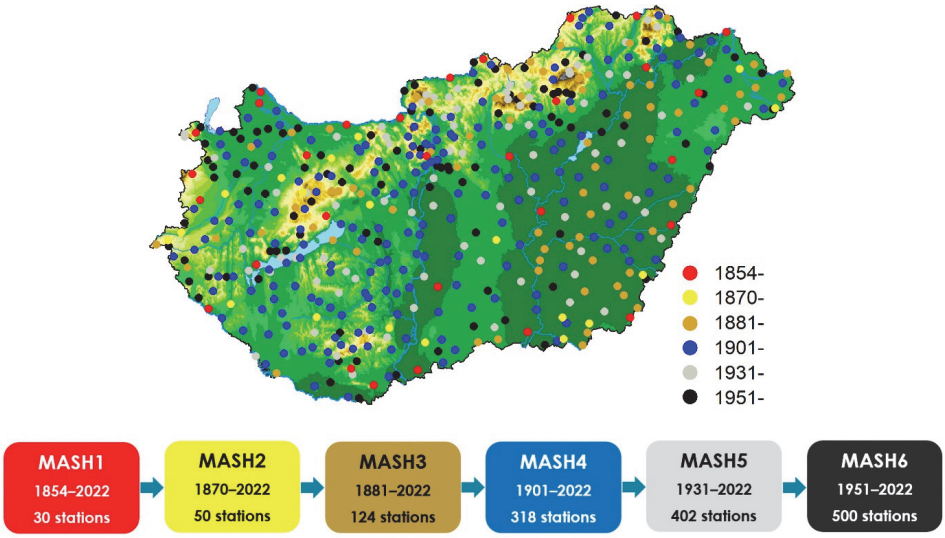

Fig. 4. The six MASH systems and the location of the precipitation stations used within them.

4. Results

4.1. Results of homogenization

The homogenization is carried out in a total of six separate station systems, where the inhomogeneities (monthly, seasonal, and annual) detected in each station system are harmonized during the homogenization procedure. Of course, MASH systems with shorter periods include the stations with longer data series (e.g., MASH2 system includes MASH1 data series from 1870). *Table 1* presents a summary of the main verification statistics for the annual precipitation sum for each station system.

Table 1. Main verification statistics of homogenization for annual precipitation sum

	MASH1	**MASH2**	**MASH3**	**MASH4**	**MASH5**	**MASH6**
Number of series	30	50	124	318	402	500
Critical value (significance level: 0.01)	28.00	28.00	28.00	28.00	29.00	29.00
Test statistics before homogenization	87.62	87.57	122.67	73.19	53.17	46.27
Test statistics after homogenization	28.42	28.16	30.74	29.11	25.58	25.18
Relative modification of series	0.30	0.28	0.25	0.19	0.15	0.12
Representativity of station network	0.55	0.56	0.61	0.67	0.69	0.70

Before homogenization, the average test statistics for all station systems is well above the critical value, while the test statistics after homogenization are close to or below the critical value, so the precipitation database can be considered homogeneous at the end. The modification of the data series is of course greater for longer data series, as longer data series contain more inhomogeneities, for example due to the more instrument changes and relocations.

The inhomogeneities due to relocations are illustrated well by the annual precipitation data of Budapest belterület (inner city) station (*Fig. 5*). This station is located at the headquarters of the HungaroMet. The largest breaks at this station were caused by relocations. Precipitation is currently measured on the roof of the meteorological observation tower, where the precipitation gauge was installed in 1985. The current location is much windier than before, which caused a reduction of about 6% in the annual precipitation.

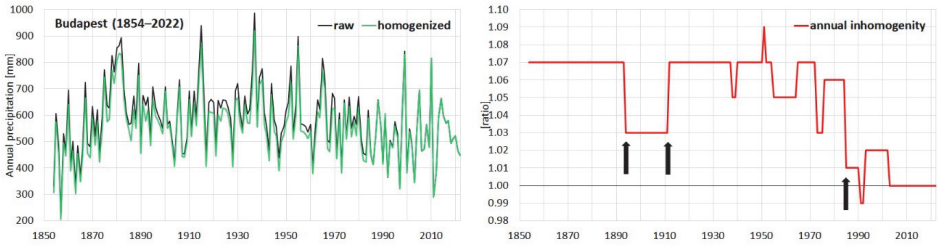

Fig. 5. Raw and homogenized annual precipitation sum (left) and annual inhomogeneities (right) of Budapest from 1854 to 2022, black arrows indicate the relocations.

4.2. Results of interpolation

After homogenization, the data series were interpolated with the MISHv1.03 software to a grid of 0.1°. The average of the grid points means the country average.

The question arises, how similar are the gridded data sets produced from different numbers of data series? We aim to produce a gridded precipitation database, where gridded data series interpolated from 30 stations (MISH1) and 500 stations (MISH6) show similar spatiotemporal characteristics. An ANOVA was carried out on the gridded datasets interpolated from six different station systems for the period 1951–2022 for all MISH systems. *Table 2* shows the main ANOVA results for the annual precipitation.

Table 2. The most important ANOVA results for the gridded annual precipitation series for the different station systems in the time period 1951–2022

	MISH1	MISH2	MISH3	MISH4	MISH5	MISH6
Total mean	597.87	598.40	600.30	601.46	601.19	602.05
Total standard deviation	131.72	131.73	133.14	135.20	135.19	135.72
Spatial standard deviation of temporal means	66.54	68.17	67.95	68.69	67.96	68.38
Root spatial mean of temporal variances	113.17	112.02	113.99	115.79	116.23	116.58
Temporal standard deviation of spatial means	97.50	96.53	97.55	98.80	99.04	99.11
Root temporal mean of spatial variances	85.94	87.20	88.21	89.65	89.49	90.15

The ANOVA results show that the total (spatial) mean for all MISH systems is around 600 mm, and the deviations are within 1%. The spatial standard deviations of temporal means and the temporal standard deviations of spatial means are also very similar.

Regarding the spatial standard deviation series of temporal means and the temporal standard deviations series of spatial means for the years 1951–2022 (*Fig. 6*), the interpolation results do not show significant differences from year to year. The ANOVA results are also very similar for the drier and wetter years.

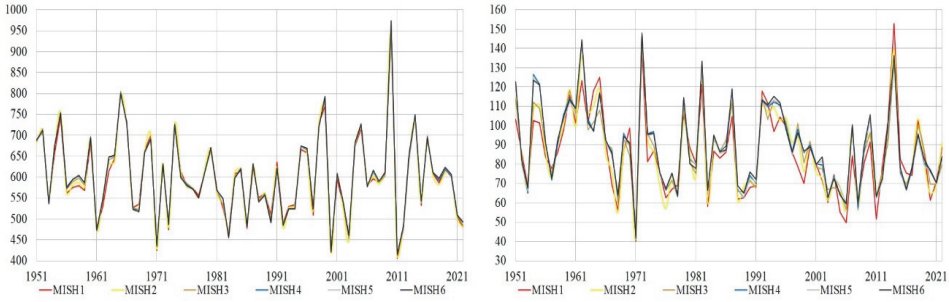

Fig. 6. Spatial mean series (left) and spatial standard deviation series (right) of annual precipitation (in mm) for the different MISH systems (indicated by different colors) from 1951 to 2022.

Comparing the grid point data series produced from fewer stations with the densest grid using 500 stations, we find that the absolute values of the mean errors (ME) for the spatial means are below 1 mm for all months in the period 1951–2022, and furthermore, the RMSE values are below 5 mm (*Fig. 7*). Therefore, also the spatial mean (country average) produced from a small number of station data sets can be considered representative for Hungary. These small deviations are due to the very good MISH-modeled climate statistical parameters, which are used in the interpolation procedure. In summer, much of the precipitation is convective, and therefore, there is much more spatial variability, which explains the slightly higher values in summer.

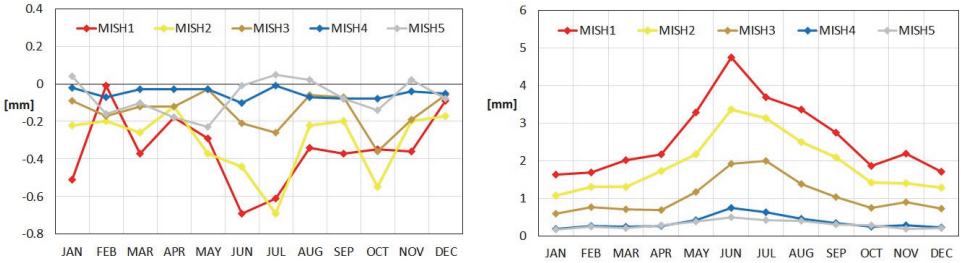

Fig. 7. Monthly mean errors (left) and Root Mean square errors (right) in spatial means of precipitation for the period 1951–2022 compared to interpolation from 500 stations in different MISH systems.

4.3. Annual precipitation

Before the seasonal and monthly precipitation, we first analyze the annual precipitation sum. *Fig. 8* shows the spatial means of annual precipitation for Hungary from 1854 to 2022.

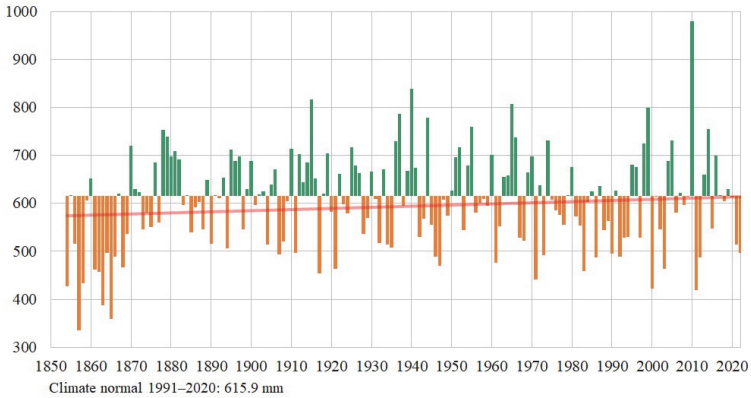

Fig. 8. Spatial means of annual precipitation in Hungary from 1854 to 2022, with the fitted exponential trend.

As a result of this work, precipitation conditions in Hungary can be analyzed from the beginning of precipitation measurements to the present day for the first time, including the very dry period around the 1860s. The year 2011 was the driest year since 1901, however, starting from 1854, there were three drier years around the 1860s: 1857, 1863, and 1865. In the period 1861–1866, rainfall was below 500 mm on average for the country in each year. This drought is also illustrated by the fact that Lake Fertő, for example, last dried up in the 1860s. The wettest year in Hungary since 1854 was 2010, while the wettest consecutive period of several years occurred around 1880, between 1878 and 1882. Over the whole period, the annual precipitation shows a slight increase of 6.9%, but this change is not significant at the 0.1 significance level.

Climate normals

The mean annual precipitation in Hungary is close to 600 mm as a countrywide average. However, there are larger variations in different parts of the country, but independent from the chosen climate normal period, a similar pattern of spatial distribution of precipitation is obtained (*Fig. 9*). The wettest areas of Hungary are the mountainous regions and the western and southwestern counties. These areas also receive mean annual precipitation of more than 700–750 mm. The driest part of the country is the central region of the Great Hungarian Plain, furthest from the mountains. In the central part of the Great Hungarian Plain, the least mean annual precipitation is below 550 mm for all climate normal periods, with variable spatial extent (*Szentes*, 2023).

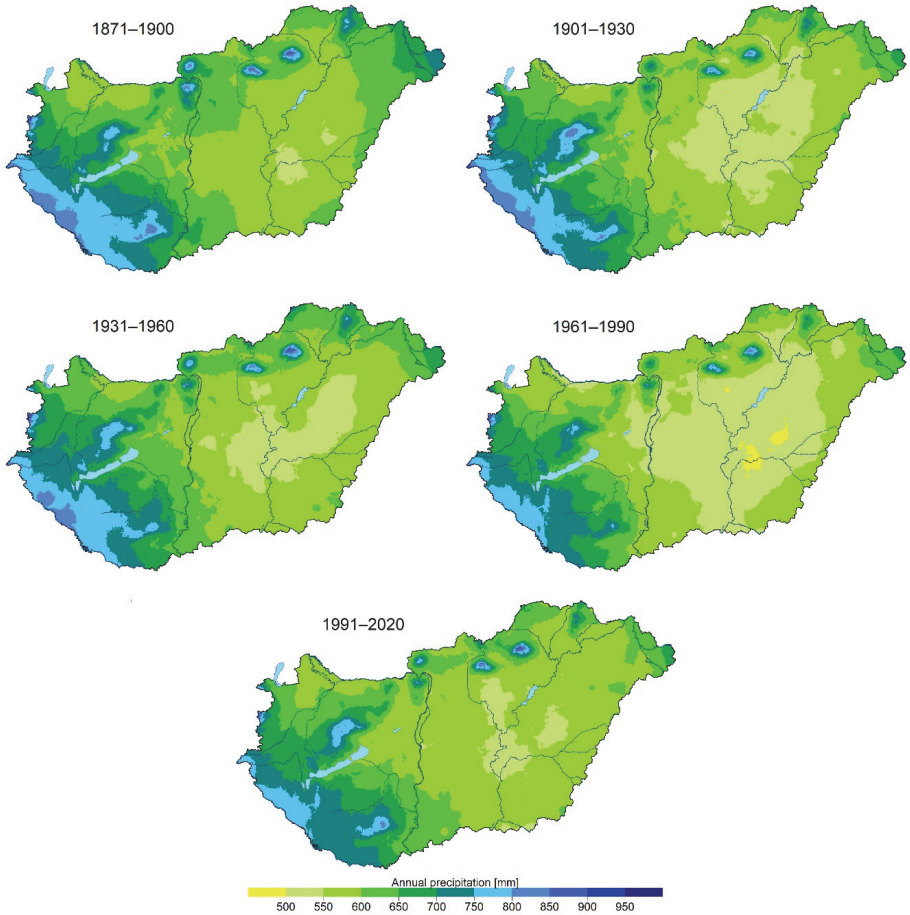

Fig. 9. Distribution of mean annual precipitation in Hungary in different climate normal periods.

4.4. Seasonal and monthly precipitation

Winter

In Hungary, the driest season is winter. The temporal mean of the spatial mean precipitation for the period 1991–2020 is 115.2 mm. Of all the seasons, only winter shows a significant change in precipitation, with an increase of 31.3% over the whole period. In the second half of the 19th century, extreme dry winters were common, with a few years of winter precipitation below 70 mm, while only a few wet winters occurred (*Fig. 10*). The wettest winters (above 150 mm) occurred in the 1950s, 1960s, and the last decade.

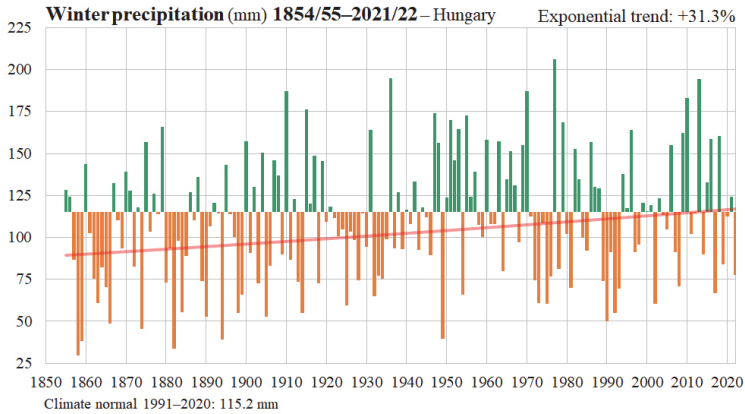

Fig. 10. Spatial means of winter precipitation in Hungary from 1854/1855 to 2021/2022, with the fitted exponential trend.

Regarding the precipitation for the winter months (*Fig. 11*), all three winter months show an increase, from which the change is significant only in February. Overall, the driest winter month is January, the wettest is December, but all three months remain below 50 mm on average.

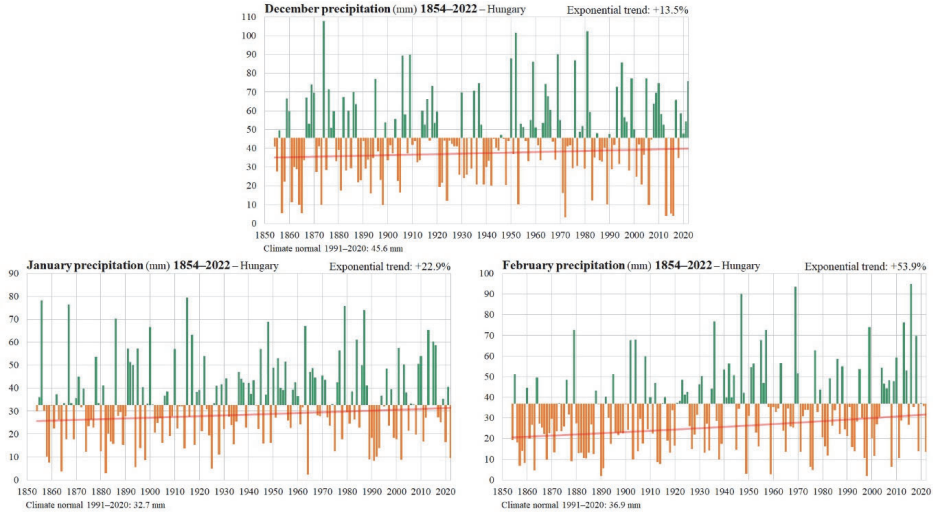

Fig. 11. Spatial means of precipitation in the winter months in Hungary from 1854 to 2022, with the fitted exponential trends.

Spring

The temporal mean of the spatial mean precipitation for the period 1991-2020 is 139.1 mm in spring. Over the whole period, spring precipitation shows a decrease, but this change is not significant. Several very dry springs occurred until the mid-1870s, as well as lately, since the 1990s (*Fig. 12*). In addition, dry springs were more frequent in the 1940s. However, from the late 1870s to the early 1940s, springs were mostly wetter than in the present day.

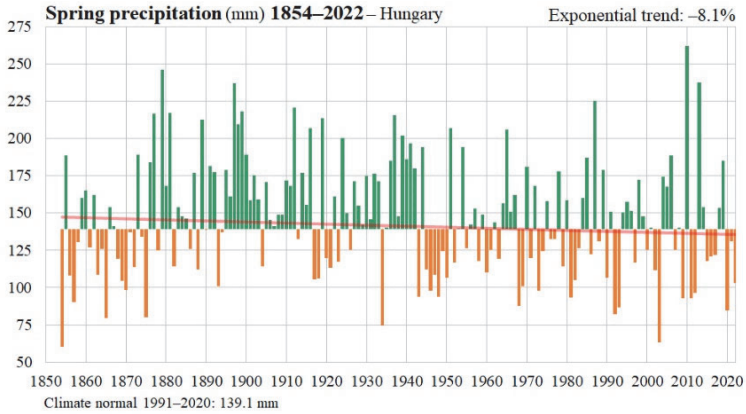

Fig. 12. Spatial means of spring precipitation in Hungary from 1854 to 2022, with the fitted exponential trend.

Among the spring months, there is a decrease in March and April and a slight increase in May. The decrease in March precipitation is significant. In average, March is the driest and May is the wettest spring month in Hungary, but April was drier than March several times in the last 15 years (*Fig. 13*).

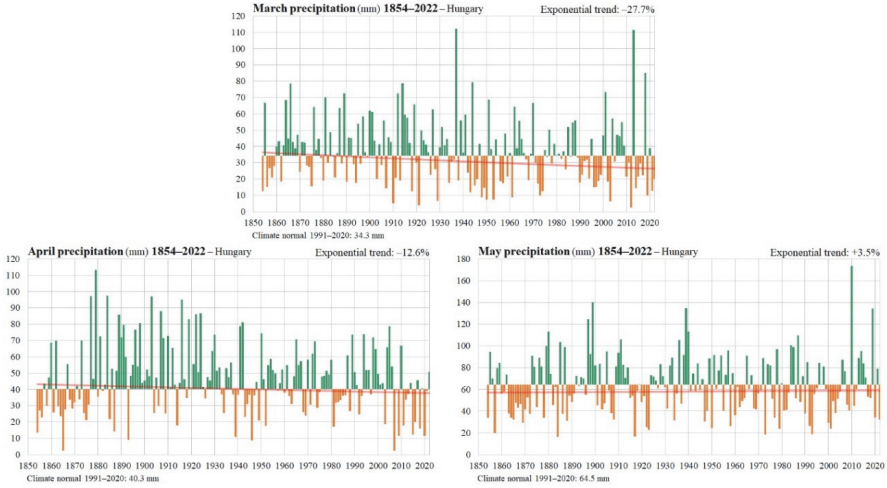

Fig. 13. Spatial means of precipitation in the spring months in Hungary from 1854 to 2022, with the fitted exponential trends.

Summer

In all climate normal periods in Hungary, summer is the wettest season. The temporal mean of the spatial mean precipitation for the latest climate normal period (1991–2020) is 203.1 mm in summer. A slight increase in summer precipitation is detected between 1854 and 2022, however, this is not significant. Dry summers were frequent during the dry period of the 1850s and 1860s, but extreme dry summers occur in Hungary in all decades (*Fig. 14*). In the wettest summers, the spatial means exceeds 250 mm, less frequently even 300 mm.

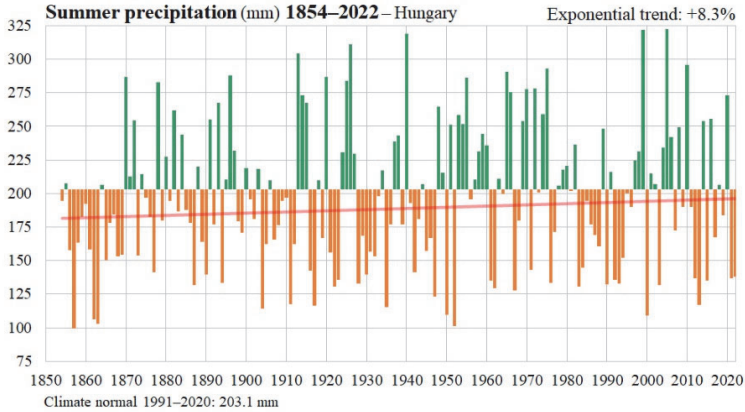

Fig. 14. Spatial means of summer precipitation in Hungary from 1854 to 2022, with the fitted exponential trend.

There is no significant change in precipitation for the summer months, with June and August showing near zero changes and July showing a slight increasing trend (*Fig. 15*). Previously, June was clearly the wettest month in Hungary, but the slightly higher increase in July precipitation resulted in the 1991-2020 averages for June and July being the same.

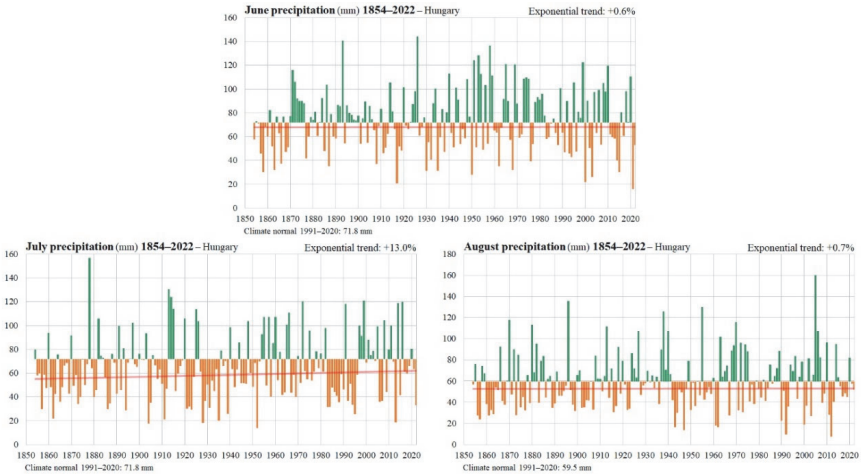

Fig. 15. Spatial means of precipitation in the summer months in Hungary from 1854 to 2022, with the fitted exponential trends.

Autumn

The temporal mean of the spatial mean precipitation for the period 1991-2020 is 158.5 mm in autumn. No significant trend in autumn precipitation amounts is detected over the whole period. Dry autumns were common in the 1850s, 1860s, 1970s, and 1980s. In spatial mean, autumns with higher precipitation (above 200 mm) occurred more frequently around 1880 and in the first half of the 20th century (*Fig. 16*).

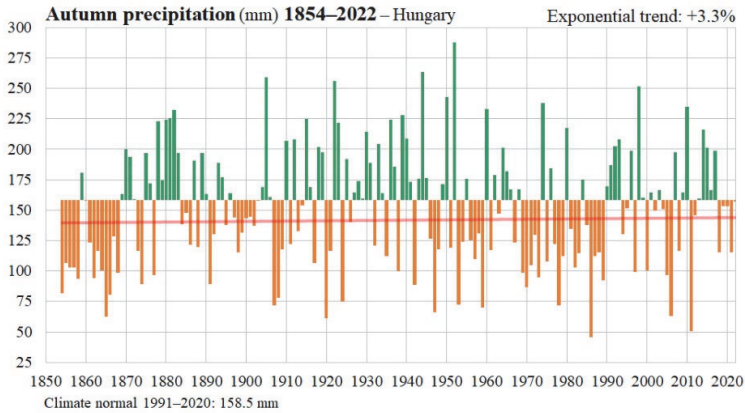

Fig. 16. Spatial means of autumn precipitation in Hungary from 1854 to 2022, with the fitted exponential trend.

The wettest autumn month in average is September in Hungary, while the driest is November. There is a slight increase in precipitation in September and November, but these are not significant changes. However, in October, there is a significant decrease in precipitation from 1854 to 2022 (*Fig. 17*).

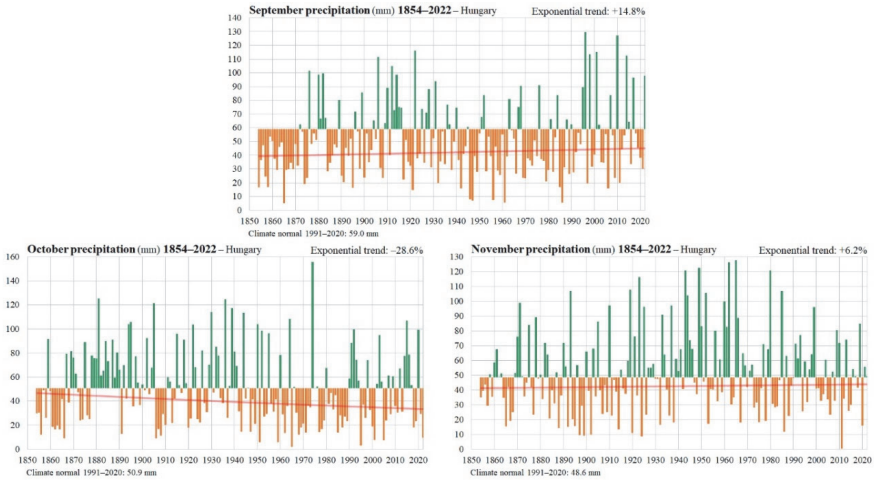

Fig. 17. Spatial means of precipitation in the autumn months in Hungary from 1854 to 2022, with the fitted exponential trends.

Fig. 18 summarizes the monthly, seasonal, and annual exponential trend estimates for the period 1854–2022. In most cases, non-significant precipitation increases are detected. Significant precipitation increases are detected only for February and winter, while significant precipitation decreases can be seen in March and October.

The driest month in Hungary since the beginning of precipitation measurements was November 2011 (0.3 mm). From October to April, the monthly minimum precipitations are below 5 mm and only in May, June, and July are above 10 mm (*Table 3*).

Overall, May 2010 was the wettest month since 1854 (the country mean is 173.8 mm). Moreover, July 1878, October 1974, and August 2005 also had over 150 mm in spatial mean precipitation. The only two months without any spatial mean above 100 mm, are January and February. The driest season between 1854 and 2022 was the winter of 1857/1858, while the wettest was the summer of 2005. The driest year since the beginning of precipitation measurements in Hungary occurred in 1857, and the wettest in 2010.

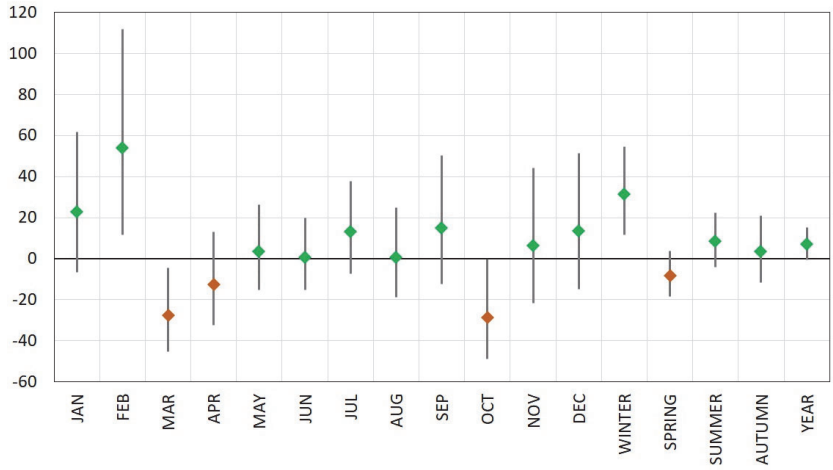

Fig. 18. Exponential trend estimation in % for the spatial means of monthly, seasonal and annual precipitation, over the total period of 1954–2022 in Hungary, with α=0.9 confidence level estimation.

Table 3. The monthly, seasonal, and annual extremes in spatial means from 1854 to 2022 with their year of occurrence, the means for the period 1991–2020, and the fitted exponential trends over the total period

Month/ Season	**Driest**		**Wettest**		**1991–2020 means** [mm]	**Exponential trend** [%] (and α=0.9 confidence level interval)
	mm	year	mm	year		
Jan	2.2	1964	79.6	1915	32.7	22.9 (–6.7 - 61.7)
Feb	1.8	1890	94.9	2016	36.9	53.9 (11.8 - 111.9)
Mar	2.4	2012	112.2	1937	34.3	–27.7 (–45.3 - –4.5)
Apr	2.4	1865	113.4	1879	40.3	–12.6 (–32.3 – 13.0)
May	16.3	1884	173.8	2010	64.5	3.5 (–15.2 - 26.3)
Jun	16.1	2021	144.3	1926	71.8	0.6 (–15.4 - 19.7)
Jul	13.8	1952	156.8	1878	71.8	13.0 (–7.4 - 37.8)
Aug	7.6	2012	160.0	2005	59.5	0.7 (–18.8 - 24.8)
Sep	5.2	1865	129.5	1996	59.0	14.8 (–12.4 - 50.4)
Oct	1.8	1965	155.9	1974	50.9	–28.6 (–48.8 - –0.2)
Nov	0.3	2011	127.8	1965	48.6	6.2 (–21.7 - 44.2)
Dec	3.4	1972	107.8	1874	45.6	13.5 (–15.0 - 51.5)
Winter	29.7	1857/1858	206.2	1976/1977	115.2	31.3 (11.6 - 54.4)
Spring	60.3	1854	262.1	2010	139.1	–8.1 (–18.6 - 3.7)
Summer	99.3	1857	322.6	2005	203.1	8.3 (–4.2 - 22.3)
Autumn	45.6	1986	287.6	1952	158.5	3.3 (–11.7 - 20.8)
Year	335.0	1857	980.4	2010	615.9	6.9 (–0.6 - 15.1)

5. Summary

Recently, significant changes have been made in the availability of the homogenized and gridded climate precipitation database produced by the Climate Department of the HungaroMet Hungarian Meteorological Service. The daily precipitation database was renewed, and all monthly precipitation data from the period before 1951 up to the beginning of the precipitation measurements were collected and used together with the existing station systems in the homogenization and interpolation procedure.

The MASH homogenization procedure of precipitation consists of six major steps from 1854 to the present: from 1854 30, from 1870 50, from 1881 124, from 1901 318, from 1931 402, and from 1951 500 station data series were homogenized, the missing data were completed, and the series were quality controlled.

After homogenization, the data series were interpolated with the MISH method to a 0.1° resolution grid. The average of the grid points gives the country average. Comparing the grid point data series produced from fewer stations with the densest grid using 500 stations, we found that the absolute values of the mean errors (ME) for the spatial means are below 1 mm for all months in the period 1951–2022, and furthermore, the RMSE values are below 5 mm. Therefore, also the spatial mean (country average) produced from a small number of station data sets can be considered representative for Hungary. These small deviations are due to the very good MISH-modeled climate statistical parameters, which were used in the interpolation procedure.

In this study, we also analyzed the spatial means of annual, seasonal, and monthly precipitation amounts for Hungary in the period 1854-2022, moreover, the extreme values and the detected precipitation trends were also calculated and shown.

With this new development of the Hungarian climatological precipitation database, a much more information-rich gridded precipitation dataset is available for climate studies, even for the first half of the 20th century. Finally, the most important result of this study is that we obtained a first insight into the precipitation conditions in Hungary from the very beginning of the precipitation measurements (i.e., from 1854) up to the present.

Acknowledgement: This paper was supported by the Sustainable Development and Technologies National Programme of the Hungarian Academy of Sciences (FFT NP FTA 2022-II-8/2022), the framework of the Széchenyi Fund Plus program with the support of the RRF-2.3.1-21-2022-00014 National Multidisciplinary Laboratory for Climate Change project, and the RRF-2.3.1-21-2022-00008 project.

References

Alexandersson, H., 1986: A homogeneity test applied to precipitation data. *Int. J. Climatol. 6*, 661–675. https://doi.org/10.1002/joc.3370060607

Alexandersson, H. and *Moberg, A.*, 1997: Homogenization of swedish temperature data. Part i: homogeneity test for linear trends. *Int. J. Climatol. 17*, 25–34. https://doi.org/10.1002/(SICI)1097-0088(199701)17:1<25:AID-JOC103>3.0.CO;2-J

Domonkos, P., 2015: Homogenization of precipitation time series with ACMANT. *Theor. Appl. Climatol. 122*, 303–314. https://doi.org/10.1007/s00704-014-1298-5

Izsák, B., Szentimrey, T., Lakatos, M., Pongrácz, R., and *Szentes, O.*, 2022: Creation of a representative climatological database for Hungary from 1870 to 2020. *Időjárás 126*, 1–26. https://doi.org/10.28974/idojaras.2022.1.1

Joelsson, M., Sturm, C., Södling, J., Engström, E., and *Kjellström, E.*, 2021: Automation and evaluation of the interactive homogenization tool HOMER. *Int. J. Climatol. 42,* 2861–2880. https://doi.org/10.1002/joc.7394

Mestre, O., Domonkos, P., Picard, F., Auer, I., Robin, S., Lebarbier, E., Böhm, R., Aguilar, E., Guijarro, J., Vertachnik, G., Klancar, M., Dubuisson, B., and *Stepanek, P.*, 2013: HOMER: A homogenization software – Methods and applications. *Időjárás 117*, 47–67.

Sluiter, R., 2009: Interpolation methods for climate data, KNMI.

Szentes, O., 2023: Szárazság Magyarországon 2022-ben és a múltban, *Légkör 68*, 9–19. (In Hungarian)

Szentes, O., Lakatos, M., and *Pongrácz, R.,* 2023: New homogenized precipitation database for Hungary from 1901. *Int. J. Climatol.43*, 4457–4471. https://doi.org/10.1002/joc.8097

Szentimrey T., 1999: Multiple Analysis of Series for Homogenization (MASH). Paper presented at the Proceedings of the Second Seminar for Homogenization of Surface Climatological Data, Budapest, Hungary, WMO WCDMP-No. 41: 27–46. Retrieved from https://library.wmo.int/index.php?lvl=notice_display&id=11624#.X48Glu28qUk

Szentimrey, T., 2008a: An overview on the main methodological questions of homogenization. In: Lakatos, M., Szentimrey, T., Bihari, Z., Szalai, S. (eds.) Proceedings of the Fifth Seminar for Homogenization and Quality Control in Climatological Databases. Seminar for Homogenization and Quality Control in Climatological Databases 5th session (29 May–2 June 2006; Budapest, Hungary). WMO/TD-No. 1493; WCDMP-No. 71, pp. 1–6. World Meteorological Organization.

Szentimrey T., 2008b: Development of MASH Homogenization Procedure for Daily Data. In: Lakatos, M., Szentimrey, T., Bihari, Z., Szalai, S. (eds.) Proceedings of the Fifth Seminar for Homogenization and Quality Control in Climatological Databases. Seminar for Homogenization and Quality Control in Climatological Databases 5th session (29 May–2 June 2006; Budapest, Hungary). WMO/TD-No. 1493; WCDMP-No. 71, pp. 123–130. World Meteorological Organization (WMO)

Szentimrey, T., 2017: Manual of homogenization software MASHv3.03, Hungarian Meteorological Service.

Szentimrey, T., 2023: Overview of mathematical background of homogenization, summary of method MASH and comments on benchmark validation. *Int. J. Climatol. 43*, 6314–6329. https://doi.org/10.1002/joc.8207

Szentimrey, T. and *Bihari, Z.,* 2007: Mathematical background of the spatial interpolation methods and the software MISH (Meteorological Interpolation based on Surface Homogeni-zed Data Basis). In: Proceedings from the Conference on Spatial Interpolation in Climatology and Meteorology, Budapest, Hungary, 2004, COST Action 719, COST Office, 17–27.

Szentimrey, T. and *Bihari, Z.*, 2014: Manual of interpolation software MISHv1.03, Hungarian Meteorological Service.

Szentimrey, T., Bihari, Z., Lakatos, M., Szalai, S., 2011: Mathematical, methodological questions concerning the spatial interpolation of climate elements. Proceedings of the Second Conference on Spatial Interpolation in Climatology and Meteorology, Budapest, Hungary, 2009, *Időjárás 115*, 1–11.

Venema et al., 2012: Benchmarking monthly homogenization algorithms. *Climate Past 8*, 89–115.

Venema, V., Trewin, B., Wang, X., Szentimrey, T., Lakatos, M., Aguilar, E., Auer, I., Guijarro, J., Menne, M., Oria, C., Louamba, W., and *Rasul, G.*, 2020: Guidelines on Homogenization, 2020 Edition, Geneva: World Meteorological Organization.

DOI:10.28974/idojaras.2024.2.4

IDŐJÁRÁS

Quarterly Journal of the HungaroMet Hungarian Meteorological Service
Vol. 128, No. 2, April – June, 2024, pp. 195–218

Comparison of historical and modern precipitation measurement techniques in Sweden

L. Magnus T. Joelsson*, **Johan Södling**, **Erik Kjellström**, and **Weine Josefsson**

Swedish Meteorological and Hydrological Institute (SMHI)
Folkborgsvägen 17, SE – 601 76 Norrköping, Sweden

**Corresponding author E-mail:* magnus.joelsson@smhi.se

(Manuscript received in final form January 29, 2024)

Abstract— Precipitation gauges used for observations in the 19th century are reconstructed and pairs of gauges are installed at two, climatologically different, regular weather observation sites (Norrköping and Katterjåkk). Norrköping is a quite well sheltered site with a low degree of frozen precipitation, while Katterjåkk is an open site with a high degree of frozen precipitation. One of the gauges at each site is equipped with a wind shield. Parallel observations are conducted from November 2016 through May 2021. Regular observations are also conducted manually with modern gauges and with automatic gauges at the sites.

The wind shield effects (larger observed precipitation sums due to the inclusion of a wind shield) for the sheltered (Norrköping) and the open (Katterjåkk) sites are 7% and 16% for snow and 2% and 1% for rain, respectively.

The modern gauges generally collect more precipitation than the historical shielded gauges, the difference is 0–8% for rain and almost up to 50% for snow. However, these differences can, in part, be ascribed to micrometeorologal conditions at the sites.

The differences between observation methods are larger for snow and sleet than for rain. There are also larger differences in the open site than in the sheltered site.

The most closely placed modern gauge relative to the historical gauges (automatic gauge in Norrköping, manual gauge in Katterjåkk) gives the most similar precipitation sums, suggesting that micrometeorology is more important than the observation method.

The undercatch due to lacking wind shields in historical observations can probably not explain more than 20% of the increased observed precipitation in the late 19th and early 20th century.

The question of potential influence on climatological precipitation series due to the transition from historical to modern observation methods remains unconcluded.

Key-words: pecipitation, observations, climate, meteorology, windshield

1. Introduction

The strengthening of the hydrological cycle following the ongoing climate change implies increases in precipitation at mid to high latitudes such as in Sweden. Based on observations from a national network, *Schimanke et al.* (2022) reports a long-term increase of Swedish precipitation starting in the late 19th century. Specifically, from the period 1961–1990 to the period 1991–2020, mean annual precipitation has increased by 8% with considerable seasonal and regional variations. Climate simulations suggest continued future increases in precipitation intensity and total amount in Sweden (*Kjellström el al.,* 2018; *Lind et al.,* 2022). To put future projected precipitation changes into a historical perspective and to assess impacts of changes in precipitation including extremes, long accurate observational time series are key. The homogeneity of long observational time series must be considered as "homogeneous time series data are essential to analyze climate variability and change" (*Venema et al.*, 2020).

Precipitation has been observed regularly over a network of stations in Sweden since the late 19th century, as described below. These observations indicate low amounts of precipitation in the period 1880–1930; similar periods with relatively dry climate are also reported for other European regions (*Metzger* and *Jacob-Rousseau*, 2020; *Haslinger et al.,* 2019; *van der Schrier et al.*, 2007; *Kendon et al.,* 2022). However, long-time observations of river flow do not support the magnitude of a dry anomaly in Sweden suggested by the precipitation observations (*Lindström*, 2002). The discrepancy between observations of precipitation and river flow may be related to changes in evaporation or other environmental factors changing conditions for runoff. Also, it cannot be excluded that errors in precipitation observations (such as neglection of small precipitation amounts) may play a role.

Traditionally, precipitation has been collected in gauges for which the height of the water column has been measured (*Mill*, 1901). This method is still in practice today (*WMO*, 2021). Early automated precipitation observations include the siphoned rainfall recorder (*Rácz*, 2021), in which the water column height of the collected precipitation is recorded on tape. Modern automatic gauges based on the collection principle usually weighs the collected precipitation rather than measure the water column height (*Førland et al.*, 1996). Other automatic methods include the tipping-bucket-type gauge, in which small precipitation sums are counted and summed up, as well as optical methods (*WMO*, 2021).

A particular problem with precipitation observations relates to undercatch, which is most pronounced in winter, as solid precipitation is more strongly influenced (*Førland et al.*, 1996). The efficiency of the gauges to collect precipitation depends on their design but also on ambient conditions. In general, too little precipitation is sampled due to wind and/or evaporative loss, hence the term undercatch. Methods for correcting observed precipitation have been developed using constant, often monthly, correction factors (*Legates* and *Wilmott*,

1990). It has, however, been pointed out that such simple monthly factors may differ between different years, and that factors derived on large national/regional scales may not be appropriate on the local scale. For example, *Stisen et al.* (2012) promoted the idea of time-space varying correction factors for Denmark. Consequently, dynamic methods involving different correction factors considering synoptic weather conditions have been put forward (e.g., *Ehsani* and *Behrangi*, 2022). By applying a dynamic correction method on 4 000 rain gauges in the Baltic Sea region, *Rubel* and *Hantel* (2001) derived correction factors having maximum in February (observed precipitation to be multiplied by 1.25–1.50) and minimum in August (1.02–1.05). It is obvious that changes in observation equipment may impact the undercatch and the need for correction factors, thereby adding one dimension to the homogenization issue.

Potential inhomogeneities at Swedish weather stations include the introduction of wind shields and changes of observation gauges for precipitation observations starting in the late 19th century. These changes in instrumentation implies that it is not clear whether the large increase of precipitation sums observed in Sweden is real or partly an artefact of inhomogeneous observations caused by changing instruments and thereby different degree of undercatch.

To address the potential role of measurement equipment in the historical changes in observed precipitation in Sweden, the performance of historical precipitation gauges relative to modern ones is evaluated. Pairs of historical precipitation gauges are reconstructed (see *Fig. 1*) and installed at two climatologically dissimilar weather observation sites (see *Fig. 2*). One gauge of each pair is equipped with a wind shield. The goals of the study are to:

1. Estimate the *wind shield effect*, i.e., larger observed precipitation sums due to the inclusion of a wind shield, of the precipitation observations with a historical precipitation gauge;
2. Estimate the difference of the precipitation observations with historical gauges and modern gauges (both automatic and manual);
3. Estimate the differences (1–2) in snowy and rainy conditions,
4. Examine how the differences (1–2) vary with air temperature and (mean and gust) wind speed,
5. Estimate the wind shield effect for sub-zero and super-zero temperatures and examine the difference between shielded and unshielded observations for specific months;
6. If possible, estimate the effect of evaporation in the historical observations;
7. Estimate the network-wide undercatch due to lack of wind shields in historical observations; and
8. Determine if it is possible to conclude from the results of the study, whether the transition from the historical to the modern observations method could constitute homogeneity breaks in the observational time series.

Fig. 1. The four precipitation gauges included in this study, the historical unshielded gauge (top left), the historical shielded gauge (top right), the modern manually operated SMHI-gauge (bottom left), and the GEONOR automatic gauge (bottom right).

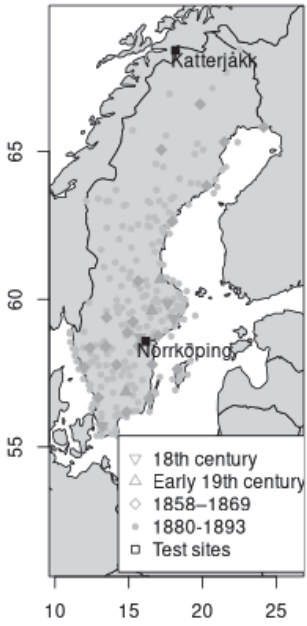

Fig. 2. Map of Sweden with the geographical positions of the test sites and the historical weather observation stations marked out, the symbols refer to the initial date of the stations.

A central question is if correction factors could be derived for the historical measurements. Note that the object of this study is to increase the homogeneity of the historical precipitation observation time series, not an effort to recreate true precipitation. Therefore, no full correction method, including aerodynamic, evaporation, and wetting correction factor for the different gauges, is considered.

2. The history of precipitation observations in Sweden

Regular precipitation observations in Sweden started in the mid-18th century at the astronomic observatories in Uppsala (1723), Lund (1748), and Stockholm (1786). In the digital archives there is also a short precipitation series (1730–1741) from a rural site (Risinge) in Östergötland. In the early 19th century, observations were also conducted at five additional locations (in the cities of Växjö, Strängnäs, Västerås, Gävle, and in a rural site in northern Hälsingland which is not yet digitally available), and in 1858–1860 a small network of about 20 additional meteorological station was set up on the initiative of the Royal Swedish Academy of Sciences (*Eriksson*, 1983). These first stations were unevenly distributed around the country with Jokkmokk being the northernmost station (66.6 °N) and Lund the southernmost (55.7 °N), see *Fig. 2*.

The precipitation measurements were mainly conducted by the collection of precipitation in zinc gauges with a mouth of 1 206.5 cm^2 (*Alexandersson*, 2002) corresponding to 1 Swedish square foot (*Hamberg*, 1911). Following the establishment of "Meteorologiska centralanstalten" (MCA), a precursor of the Swedish Meteorological and Hydrological Institute (SMHI), a gauge with a 1 000 cm^2 mouth was introduced in 1873 as an adaptation to the metric system. This gauge is reconstructed under the current study and is henceforth referred to as the "unshielded gauge", see *Fig. 1.* In 1878, a network of more than 300 precipitation observation stations were set up with the aid of the agricultural organization Kungliga Hushållningssällskapen (*Hamberg*, 1881). From around 1880 precipitation observations conducted at lighthouses where taken over by "Nautisk-meteorologiska byrån" (the Nautical Meteorological Bureau, which later became a part of the precursor of SMHI). The observation method was identical to that of MCA (*Nautisk-meteorlogiska byrån*, N.D.)

In the period from 1893 to 1935, cone shaped Nipher wind shields were introduced to the vast majority of precipitations gauges. The 1 000 cm^2 mouth zinc gauge with wind shield is henceforth referred to as the "shielded gauge", see *Fig. 1*. However, exactly when the first wind shields were installed and when the entire network of precipitation gauges was equipped with wind shields is unknown, due to insufficient documentation. In 1930, most of the precipitation stations had a wind shield (*Alexandersson*, 2003). In the mid 20th century, the 1 000 cm^2 mouth gauges were successively replaced with gauges with a mouth of 200 cm^2. This size of gauges is currently used at SMHI's manual observation

stations. In the 1960s, the zinc gauge was replaced by a light metal gauge (henceforth "SMHI-gauge", see *Fig. 1*), which is easier to handle and not as sensitive to frost weathering as the zinc gauge. Potential losses both due to spillage and leakages were thus restricted (*Eriksson*, 1983). The current SMHI-gauges have a Nipher wind shield.

Automatic observations are currently conducted with a GEONOR instrument (henceforth "automatic gauge", see *Fig.1.*), equipped with an Alter wind shield. Presently, SMHI operates more than 600 precipitation observation stations, out of which 120 are automatic.

A summary of the types of precipitation gauges historically used in the Swedish observation network is listed in *Table 1.*

Table 1. List of rain gauges used in the Swedish observation network

Approximate time of appearance	Area of mouth/cm^2	Material	Wind shield	Type
1723	1 206.5	Zinc	–	Manual
1873	1 000	Zinc	–	Manual[1]
1893	1 000	Zinc	Nipher	Manual[2]
~1950	200	Zinc	Nipher	Manual
~1960	200	Aluminum alloy	Nipher	Manual[3]
1995	200	Aluminum alloy	Alter	Automatic[4]

[1] "Unshielded gauge" ; [2] "Shielded gauge"; [3] "SMHI-gauge"; [4] "Automatic gauge"

3. Previous studies of Swedish precipitation measurement methods

The arguably largest source of error in precipitation measurements is the turbulence around the mouth of the gauge (*Alexandersson*, 2003). *Hamberg* (1911) cited field studies in the years 1890–1895, where the loss in measurements without a wind shield from May through October was found to be on average 12% compared to a pit-gauge. For strong winds the average loss was evaluated to be up to 34%. The difference between gauges with and without wind shield at 1.5 m height was up to 6%, even up to 20% for strong winds. From November through April, 10–35% more precipitation was measured with the shielded gauge compared to the unshielded one, in very windy conditions differences were 60–70%.

In a field study in Särna in 1907–1910 (*Hamberg*, 1911), a gauge with a wind shield on average collected 11% more precipitation than a gauge without a wind shield. The largest departure was found for winter (DJF), when the shielded gauge collected 35% more than the unshielded gauge. The corresponding departure in summer (JJA) was 3%. Winter precipitation being mainly in the form of snow is mentioned as possibly contributing to this seasonal difference.

Hamberg (1881, 1911) speculates that a correction for the annual precipitation for a windswept station with considerably long winter should be about 20%. For summer months the corrections should not exceed 10%, but for winter months a correction of up to 100% could be required.

Bergsten (1954) studied the difference in observed precipitation between the periods 1901–1930 and 1921–1950 for two sets of stations; stations that were equipped with a wind shield in both periods (homogeneous) and stations where the screen was introduced in the latter period (inhomogeneous). The wind shield was estimated to increase observed precipitation by 10–15% with some regional differences. The wind shield effect on the measurements in northern Sweden was less clear than in the south, a result *Bergsten* (1954) considered to be counter-intuitive.

Eriksson (1983) studied the observational time series 1931–1980 and argued that 1951–1980 probably is more homogeneous than 1931–1960 due to the more complete use of wind shields, however did not give any quantitative estimate.

Eriksson et al. (1989) estimated a wind related error in precipitation measurements of 2–15% for rain and 5–50% for snow. *Eriksson et al.* does not explicitly state whether these estimates refer to observations with or without wind shield, however, the standard method of precipitation observations at the time included wind shield. *Alexandersson* (2002) estimated an increase in measured precipitation of 5–10% following the introduction of wind shields.

Fredriksson and *Ståhl* (1994) conducted parallel measurements at the former observation site of SMHI's headquarter (located a couple of hundred meter southwest of the current observation site)"with three different automatic precipitation gauges alongside the regular manual precipitation measurements from October 1993 to March 1994 as a part of the preparation for the transfer to automatic measurements in the autumn of 1995 (*Alexandersson*, 2000). The automatic gauges generally recorded less precipitation than the manual measurements, with largest monthly departures of about 15%. The GEONOR gauge, currently used at SMHI weather observation stations (here referred to as the "automatic gauge"), delivered results closest to the manual measurements with an average departure of about 5% over the six months.

In their report from the extensive intercomparison study of Nordic precipitation gauges at the Jokioinen Observatory, *Førland et al.* (1996) cited a number of studies on the ratio between precipitation measured in shielded and unshielded gauges. Ratios are listed for rain (1.00–1.09), snow (1.21–1.75), and mixed (1.08–1.26). From the data of the Jokioinen observatory it could be

concluded, that the shielded SMHI-gauge caught 68.6% of the weight of the snow caught by the reference double-fenced gauge and 95.6% of the weight of the rain.

Alexandersson (2000) found, by comparing all simultaneously active automatic and manual stations in Sweden, that the automatic gauges observe on average 16% less precipitation than the corresponding manual measurements. The difference is largest wintertime when the automatic gauges observe 22% less precipitation than the manual measurements. The corresponding value for summer is 12%. The difference between manual and automatic measurements at the sites, where these were conducted in parallel, was found to vary considerably between individual stations, but the difference between manual and automatic measurements was also found to be smaller when the whole network of stations was considered. *Alexandersson* (2000) argues that difference in wind exposure probably is the main factor of the discrepancy.

Alexandersson (2003) used a correction factor for the SMHI-gauge between 1.5% and 12% for rain and between 4% and 36% for snow depending on how windswept the station is. The stations were divided into seven wind classes. Correction factors are for example applied in the estimation of true precipitation used in the gridded climate data product PTHBV (*Johansson* and *Chen*, 2003).

While the effect of the introduction of the wind shield and the automation has been object of the above mentioned studies, the potential inhomogeneity due to the shift to the smaller SMHI-gauge has thus far not been studied.

4. Climatology and description of the measurement sites

For the current project, two observation sites were selected: Norrköping and Katterjåkk, see *Fig. 2.* The climatology of these sites are briefly described below.

4.1. Norrköping

Norrköping lies at the end of Bråviken bay in the northeastern part of the region of Östergötland. The weather station is located at the SMHI headquarters about 2 km southwest of the city center, see *Fig. 3.* The area is slightly hilly with mostly lower buildings. The historical gauges were placed inside the fenced area of the official automatic station. The SMHI office buildings are found 60–100 m to the south. Additionally, there are some trees around the site. Unofficial manual measurements were conducted just outside the observations site.

Fig. 3. Map of a part of Norrköping with the observation site marked with a red/dark grey dot. The marked location is approximate. 1:10 000. (*Lantmäteriet*, 2023)

The weather stations in Norrköping (station number 86340) is considered to have a wind class 3 of 7, with the general criteria: "Quite well shielded site, where there can be a minor opening towards a larger field or lake. Well shielded site if it is situated in a generally windswept region". The corresponding wind correction is 3.5% for rain and 8.5% for snow (*Alexandersson*, 2003).

The mean annual observed precipitation (without corrections) in Norrköping (1991–2020) is 536 mm. The driest month is March (27 mm), the wettest month is July (65 mm), see *Fig. 4.* The average daily maximum temperature in July is 23 °C, the average daily minimum temperature in January is −4 °C. In the period for which observations of precipitation form is available (between 2000 and 2010), frozen precipitation (snow, hail, graupel, ice needles) was reported at least once for all months from October (about 3% of the precipitation occasions were reported as frozen) through April (13%). About 60% of the precipitation occasions in February was reported as frozen precipitation.

Preliminary calculations of the average monthly maximum snow depth (1981–2010) in Norrköping show that the deepest average maximum snow depth is in February with 21 cm, see *Fig. 5.* In this period, a measurable snow cover on the 15th each month was more common than not from December through March.

The dominant wind direction in Norrköping over the last twenty years (2004–2023) was west-southwest, and the annual mean wind speed was 2.2 ms^{-1}. The windiest season was winter (DJF) with at mean wind speed of 2.5 ms^{-1}, the least windy season was summer (JJA) with a mean wind speed of 2.0 ms^{-1}.

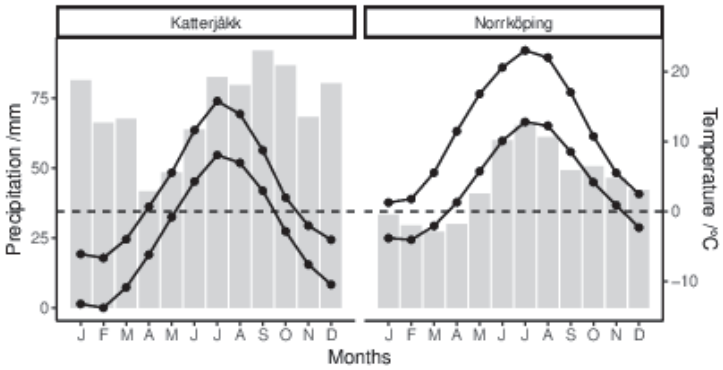

Fig. 4. Average monthly precipitation (bars), daily maximum and minimum temperatures (black lines) 1991–2020.

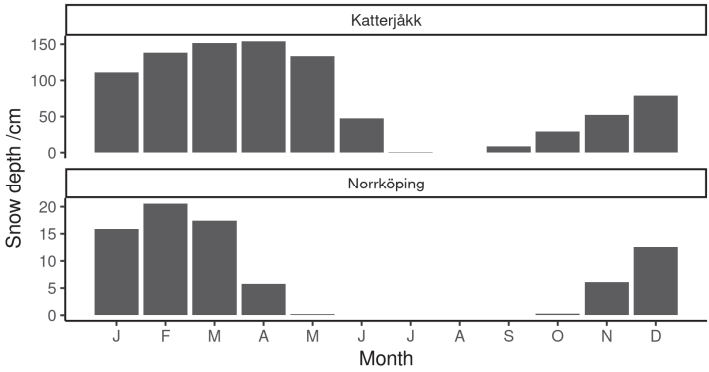

Fig. 5. Average maximum monthly snow depth (1981–2010) in Norrköping and Katterjåkk.

4.2. Katterjåkk

Katterjåkk is situated in the mountainous region in the northwestern part of the province of Lappland in northern Sweden. Within a radius of 10 km, the mountain peaks reach up to 1 100 m above the station height. The weather station lies on a southern hillside, east of a ravine where the Katterjåkk creek runs, see *Fig. 6*. In Katterjåkk, there was both an automatic (station number 18850) and a manual (station number 18820) weather observation station, separated by about 50 m with the automatic station to the south of the manual station. The mast for wind measurements is placed on a small hill 40 m further to the south of the automatic

station. The automatic station lies in a slight depression, while the site of the manual station is rather plain and is therefore quite windswept. An office building offers some shelter in the sector southeast to south-southwest and a small birch grove in the sector north to north-northeast. The historical gauges were placed close to the regular precipitation gauge of the manual observation site.

Fig. 6. Map of Katterjåkk with the observation site marked with a red/darkgrey dot, the automatic station is marked with a green/light grey dot. The marked locations are approximate. 1:10 000. (*Lantmäteriet*, 2023)

The weather stations in Katterjåkk is considered to have a wind class 5 of 7, with the general criteria "Open site with only partial protection from buildings or trees, sites on a hill or hillside in the inland". The corresponding wind correction is 6% for rain and 17% for snow (*Alexandersson*, 2003).

The average annual observed precipitation (without corrections) in Katterjåkk (1991–2020) is 859 mm. The driest month is April (42 mm), the wettest month is September (94 mm), see *Fig. 4*. The average daily maximum temperature in July is 16 °C, the average daily minimum temperature in February is −14 °C. Between 1991 and 2020, the highest share of precipitation occasions was reported as frozen in February (94%). The lowest share occurred in July (1%).

Preliminary calculations of the average monthly maximum snow depth (1981–2010) in Katterjåkk show that the deepest average monthly maximum

snow depth is in April with 154 cm, see *Fig. 5.* In at least fifteen of these thirty years, there was a measurable snow cover on the 15th of the month from October through May.

The dominant wind direction in Katterjåkk over the last twenty years (2004–2023) was west-northwest, and the mean wind speed was 3.3 ms^{-1}. The windiest season was spring (MAM) with at mean wind of speed of 3.8 ms^{-1}, the least windy season was summer (JJA) with a mean wind speed of 3.0 ms^{-1}.

5. Methods

5.1. Measurements

Parallel daily precipitation observations were conducted with the newly produced historical 1 000 cm^2-mouth gauge (referred to as historical gauges) with and without the wind shield (shielded and unshielded gauge, respectively) in Norrköping and Katterjåkk from November 2016 through May 2021. The mouth of the gauges was about 1.5 m over the ground in Norrköping, which is common practice (*WMO*, 2021). The gauges in Katterjåkk were placed slightly higher, about 2.3 m, in anticipation of large snow depths in Katterjåkk. In Norrköping, the observations were conducted every day approximately at 08:00 local time, in Katterjåkk at 07:00. The water in the gauge was poured into a 1 liter glass container, which was weighted. Snow was melted in room temperature for about one hour before measuring. Two pairs of gauges were used for each of the observation sites (with and without wind shield) to make sure that one pair of gauges was always open for precipitation, even when the measurements were ongoing or snow was being melted. In the seasons when precipitation mainly falls as rain, a funnel was installed in the mouth of the gauge to limit loss due to evaporation. Since snow would block the mouth of the funnel, the funnel was removed under the colder seasons when there is chance for snow and the loss due to evaporation is substantially smaller. All forms of precipitation (rain, snow, hail, graupel) were measured along with condensed water from fog, frost, and dew.

Occasionally, especially over weekends, the gauges were not emptied daily, which means that some values in the series correspond to accumulated precipitation over longer time periods than the ideal 24 h. For frequency of different accumulation times, see *Fig. 7.*

Especially in Katterjåkk, snow cover can change the local wind environment around the gauge, as the snow cover shift the effective height of the precipitation observations and the roughness of the surrounding terrain. The observed snow cover over the test period is described in *Fig. 8.* The deepest observed snow depth in Katterjåkk was 229 cm, in the end of March 2020.

Air temperature and wind speeds were observed at the official automatic weather stations. Precipitation values are available at 15-minute resolution, while 2 m air temperatures and wind speeds are available at hourly resolution.

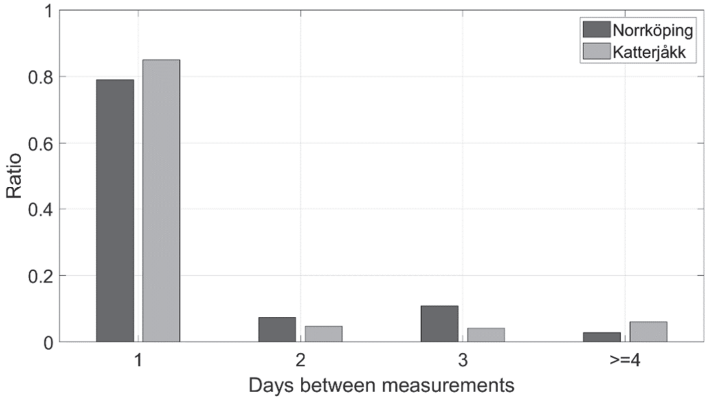

Fig. 7. The frequency of different accumulation times for the measurements with the historical gauges.

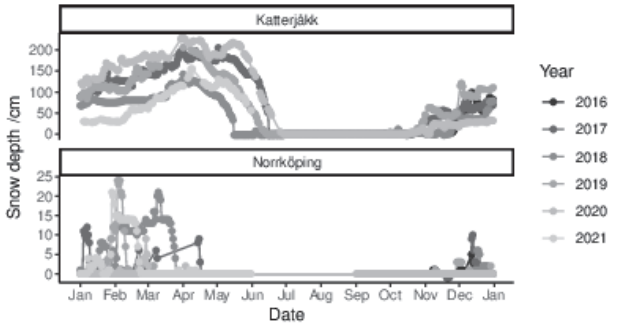

Fig. 8. Observed snow depth in Norrköping and Katterjåkk during the test period.

5.2. Calculations

Precipitation of three types (rain, sleet, and snow) observed in Norrköping and Katterjåkk with the automatic gauge (a), manual SMHI-gauge (m), jointly referred to as modern gauges, and with the unshielded (u) historical gauge are compared with corresponding observations with the shielded (s) historical gauge. Ordinary least squares regression, forced through the origin, is applied. Regression slopes for method i (β_{is}), with shielded gauge data as target variables, are obtained. Mean absolute error (MAE) between the precipitation observed, e.g., with the SMHI-gauge and the respective output of the linear regression models are calculated:

$$\mathrm{MAE}_i = \Sigma\ \mathrm{abs}(x_i - [x_s \times \beta_{is} + \alpha_{is}]) / N, \quad (1)$$

where x_i is the observed value with method i (s refers to the observational method with the shielded historical gauge), α is the intercept, and N is the number of observations. The MAE is thus a metric of how well the linear regression generally reproduces the individual observed values. Note that in order to convert these regression slopes to correction factors to make observations with method i homogeneous with method j (a_{ij}) at least one of the three methods, regression slopes must be inverted as homogenization of historical time series either seeks to recreate the conditions of the earliest (e.g., *Moberg et al.*, 2002) or, as it is most common, the latest observation (*Venema*, 2020). Thus, for most applications the correction factors to make unshielded historical gauge observations homogeneous with shielded historical gauge observations are identical to the corresponding regression slope ($a_{us} = \beta_{us}$), while the correction factors to make shielded historical gauge observations homogeneous with modern methods observations are the inverse of the corresponding regression slopes obtained here ($a_{sm} = \beta_{ms}^{-1}$, $a_{sa} = \beta_{as}^{-1}$).

The *wind shield effect* is defined here as the deviation from the regression slope ($\beta_{us} - 1$). A positive wind shield effect indicates that larger sums are observed with the wind shield. Since precipitation types for historical observations are not easily accessible, the wind shield effect is also calculated for sub-zero and super-zerotemperatures, where temperature thus is a proxy for precipitation types.

For the irregular measurements with accumulation times more than one day, sums for the corresponding observations of the modern gauges were used.

For the Katterjåkk series, the classification of precipitation type is gathered from information in the observers notes. For Norrköping it is instead deduced from the automatic weather station categorization of present weather. This is due to missing information of precipitation type in the observes notes in Norrköping.

To evaluate the sensitivity of the undercatch due to lacking wind shield on wind speed and temperature, series of ratios between precipitation observed with the unshielded gauges and other methods are calculated and compared with calculated averages of air temperature, mean wind speed (10-minute), and wind gust speed for the accumulation time.

For occasions when the gauges were not emptied daily, the ratio between total daily sums for the period from the automatic gauge and the accumulated precipitation in the historical gauge was calculated and binned according to the number of days of accumulation. Differences between the two were taken as a measure of evaporative loss.

For all calculations, only precipitation sums equal to or larger than 1 mm are used.

To estimate the undercatch due to lacking wind shields in historical observations, all digitally available daily precipitation observations prior to the year with the first installed wind shield at the Swedish weather observation

stations (1893) are studied. Only precipitation observations where concurrent mean daily temperature data are available are considered. The precipitation data are multiplied by the wind shield effect correction factor a_{us} according to whether the corresponding mean daily temperature was sub-zero (a^-) or super-zero (a^+). The ratio of the corrected and uncorrected sums is calculated. From the study correction factors for wind classes 3 (a_3) and 5 (a_5) can be deduced. As a raw and conservative estimate, precipitation is corrected according to the stations wind class (*Alexandersson*, 2003). Stations with wind class 1 are not corrected ($a^-_1 = a^+_1 = 1$). Stations with wind class 3 are corrected according to the correction factors that can be deduced from the Norrköping test series (a^-_3, a^+_3). Stations with wind class 5 to 7 are corrected according to the correction factors that can be deduced from the Katterjåkk test series (a^-_5, a^+_5). Stations with wind class 2 are corrected with the averages of corrections factors 1 and 3 ($a_2 = [a_1 + a_3] / 2$), stations with wind class 4 are corrected with the averages of corrections factors 3 and 5 ($a_4 = [a_3 + a_5] / 2$). Stations that were closed prior to *Alexandersson's* work, and therefore, do not have a windclass ascribed to them are treated as class 3 stations, since class 3 stations have the median correction factor.

The precipitation time series prior to the installation of the first wind shield (as those used in the analysis described above), are each compared with corresponding observations from the same station in an equally long period starting in 1930, where most precipitation station were equipped with a wind shield (*Alexandersson*, 2003). The dates are matched such that only data where the same day of year is available both in the late and the early period are considered. The total difference in accumulated precipitation between the early and late periods are 16%.

The results are also compared with the mean difference between the first consecutive standard normal period (*WMO*, 2017) of SMHI's climate indicator annual precipitation (*SMHI*, 2023, *Sturm*, 2024) 1881–1910, and first standard normal period 1931–1960, where wind shields were legio. The mean annual precipitation for the entire network increased by 8% from the period 1881–1910 to 1931–1960 according to this estimate.

6. Results

6.1. Norrköping

The wind shield effect for the historical gauges in Norrköping is about 7% for snow and 2% for rain, see *Table 2.* The rain observation results, for which the MAE between the regression model output and the observed values is smallest of all the regression models presented in this study, are shown as an example in *Fig. 9.* The MAE for all precipitation types is 0.06 mm. The wind shield effect for sub-zero and super-zero temperatures is 2% and 9%, respectively.

Table 2. Regression slope (β) and mean absolute error (MAE) for linear regression models for precipitation observed in Norrköping with the unshielded historical, modern (SMHI), and automatic gauges, respectively, all with the precipitation observed with the shielded historical gauge as the target variables

Precipitation types	Without wind screen		SMHI		Automatic	
	β	MAE/mm	β	MAE /mm	β	MAE /mm
All	1.02	0.06	0.96	0.94	1.00	0.39
Rain	1.02	0.04	0.95	0.91	1.00	0.36
Sleet	1.01	0.07	0.95	1.00	0.99	0.74
Snow	1.07	0.08	0.98	1.03	1.01	0.35

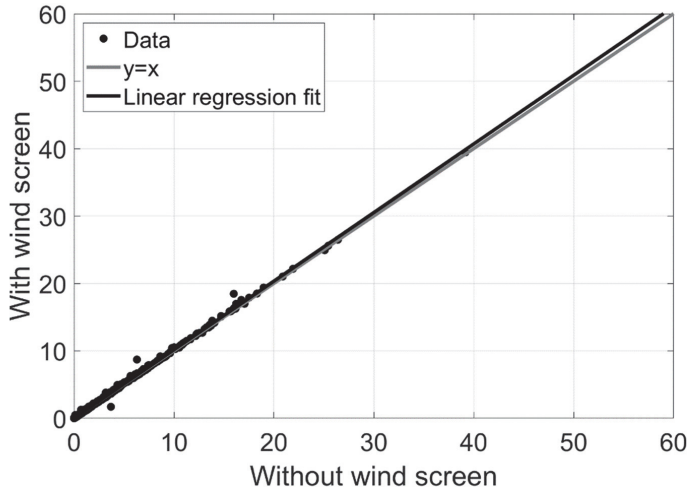

Fig. 9. Linear regression (black line) for daily precipitation sums observed in Norrköping with the shielded historical gauge with precipitation sums observed with the unshielded historical gauge as the explanatory values, the 1:1 relationship is depicted as a grey line.

The automatic gauge collects on average similar sums as the shielded gauge. The uncertainty is on average 0.4 mm, though higher for sleet (0.7 mm). The SMHI-gauge collects on average 4% more precipitation than the shielded gauge with an uncertainty of 0.9 mm. The snow observations are closer than rain and sleet between the SMHI-gauge and the shielded gauge, however, the uncertainty of the linear model is somewhat larger for snow observations than for rain and sleet.

Wind speed and temperature was not found to correlate significantly with the difference of precipitation sums between the methods. For example, for the ratio of the measurements with the unshielded gauge and the automatic gauge, the correlation with air temperature was $\rho = 0.19$, with mean wind speed $\rho = -0.10$, and with maximum wind gust speeds $\rho = -0.07$ (not shown).

There is a significant variation in the amount of mean precipitation between different months between the historical gauges, see *Fig. 10.* In winter and spring (December–May), the shielded gauge collects 6% more precipitation as a median, which is larger than the median (2%) for the summer and autumn months (June–November).

No clear signal of evaporation could be concluded from the study of observations with longer accumulation times (not shown).

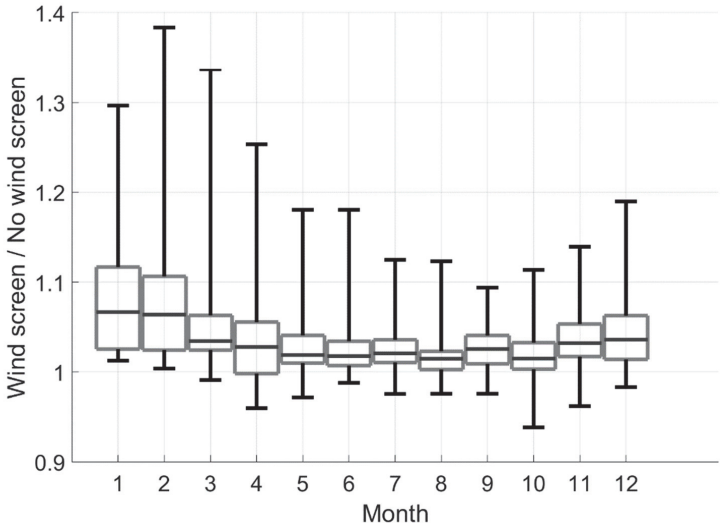

Fig. 10. Ratio of daily precipitation sums observed in Norrköping with the shielded and unshielded gauges for specific months. Horizontal black lines indicate the median, the boxes covers the 25- and 75-percentiles, the whiskers spans over the entire range.

6.2. Katterjåkk

The wind shield effect of the historical gauges in Katterjåkk is on average 11%, see *Table 3.* The effect is larger for snow (16%) than for rain (1%). The larger wind shield effect for snow is also reflected in the MAE, which is 0.4 mm for

snow and 0.08 mm for rain. The wind shield effect for sub-zero and super-zero temperatures is 4% and 15%, respectively.

Table 3. Regression slope (β) and mean absolute error (MAE) for linear regression models for precipitation observed in Katterjåkk with the unshielded historical, modern (SMHI), and automatic gauges, respectively, all with the precipitation observed with the shielded historical gauge as the target variables

	Without wind screen		SMHI		Automatic	
Precipitation types	β	**MAE /mm**	β	**MAE /mm**	β	**MAE /mm**
All	1.11	0.47	0.88	0.75	0.66	1.84
Rain	1.01	0.08	0.98	0.19	0.92	1.36
Sleet	1.08	0.59	0.88	0.71	0.64	3.87
Snow	1.16	0.42	0.74	0.98	0.51	1.29

The SMHI-gauge and the automatic gauge collect on average 12% and 34% larger sums than the shielded gauge. Again, the departures are larger for snow (26% and 49% larger sums, respectively) than for rain (2% and 8%, respectively). The uncertainty of the regression model is larger for the automatic gauge measurements (1.8 mm) than for the SMHI-gauge (0.8 mm). The results of the sleet measurements with the automatic gauge, for which the MAE is largest of all the regression models presented in *Tables 2.* and *3,* is shown as an example in *Fig. 11*.

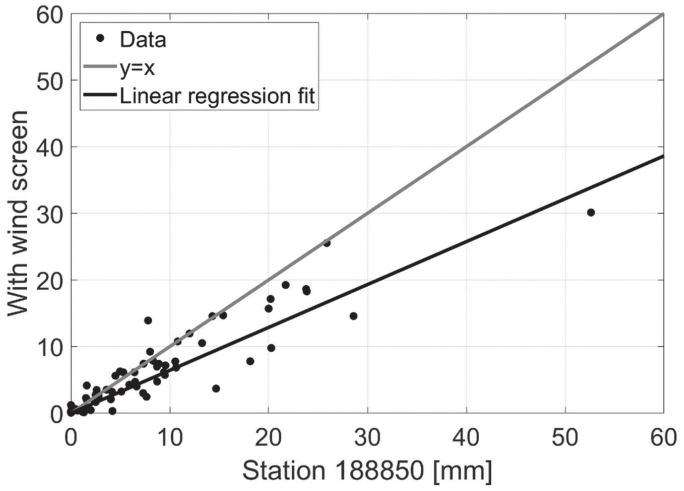

Fig. 11. Linear regression (black line) for daily sleet observed in Katterjåkk with the shielded historical gauge with sleet observed by the automatic gauge as the explanatory values, the 1:1 relationship is depicted as a grey line.

The difference between observations with the unshielded gauge and SMHI-gauge does not significantly depend on air temperature, mean wind speed, or wind gust speed.

There is no clear month to month signal of the ratio of the historical gauge observations, see *Fig. 12*. In winter and spring (December–May), the shielded gauge collects 43% larger sums than the unshielded gauge as a median, in summer and autumn (June–November) this number is 11%.

No clear signal of evaporation could be concluded from the study of observations with longer accumulation times (not shown).

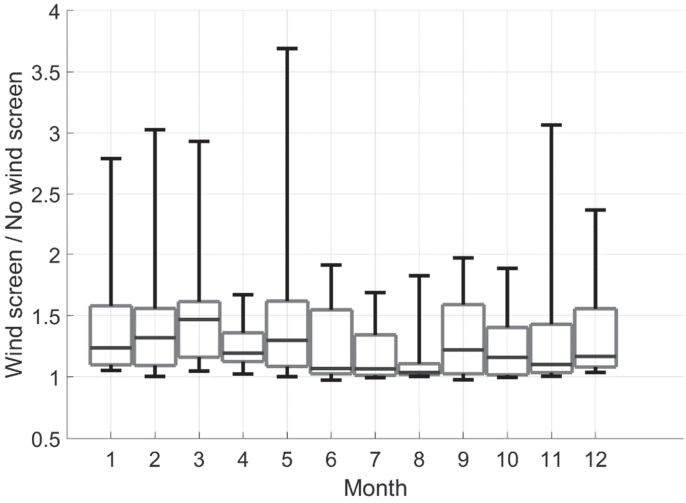

Fig. 12. Ratio of daily precipitation sums observed in Katterjåkk with the shielded and unshielded gauges for specific months. Horizontal black lines indicate the median, the boxes covers the 25- and 75-percentiles, the whiskers span over the entire range.

6.3. Evaluation of undercatch of historical observations

The earliest digitally available daily precipitation observations are from 1836 (Uppsala). In total, 49 weather stations have concurrent daily precipitation and mean temperature data in the period 1836–1893. More than 400 000 observations were included which corresponds to on average 23 years of data per station.

Precipitation observed during days with sub-zero temperatures (28% of the studied days) and super-zero temperatures (72%) were multiplied with correction factors according to the stations' windclass, see *Table 4*. In total, the corrected precipitation was 3% larger than the uncorrected precipitation. The difference was largest in winter (6%) and smallest in summer (2%). In spring the difference was 4%, in autumn 3%.

Table 4. Correction factors used to estimate the undercatch of historical precipitation observations according to the stations' windclass (*Alexandersson*, 2003). Sub-zero (-) and super-zero (+) temperatures are used as a proxy for precipitation form

Wind class	Formula	a^-	a^+	Number of historic stations*	Modern station**
1	a_1	1	1	1	4%
2	$a_2 = [a_1 + a_3]/2$	1.045	1.01	8	24%
3	a_3	1.09	1.02	14	35%
4	$a_4 = [a_3 + a_5]/2$	1.12	1.03	10	24%
5	a_5	1.15	1.04	3	9%
6	$a_6 = a_5$	1.15	1.04	2	3%
7	$a_7 = a_5$	1.15	1.04	0	0.5%
Not defined	$a_{ND} = a_3$	1.09	1.02	12	

* Stations with digitally available concurrent daily precipitation and temperature observations prior to 1893

** Share of stations listed in *Alexandersson* (2003)

7. Discussion

For the measurements in Norrköping, the wind shield effects of the historical gauges are on the low end of previous estimates of the wind shield effect (*Hamberg*, 1911; *Bergsten*, 1954; *Eriksson et al.*, 1989). For the measurements in Katterjåkk, the wind shield effect corresponds well to the value discussed by *Hamberg* (1911).

In general, snow gives more diverse observations between methods than rain, which is consistent with previous results. There are larger discrepancies between the parallel observations in Katterjåkk compared to Norrköping. This may partly be explained by the longer distance between the official automatic station and the location of the historical measurements. The more variable snow depth, and thereby, aerodynamic conditions around the site may also play a role.

In Katterjåkk, the observations with the historical gauges are better correlated with the modern manual SMHI-gauge observations than the automatic observations. In Norrköping, observations with the historical gauges resulted in observations closer to those of the automatic gauges. Micrometeorology (i.e., proximity in the location of two parallel observations) thus appears to be more important than the observation method, a similar conclusion was previously drawn by *Alexandersson* (2000).

The MAE of the linear regression models for "sleet" is higher than for snow and rain, probably partly due to the fewer observations and partly due to the more diverse nature of the precipitation types classed as "sleet".

The amplitude and the variability of the ratio between shielded and unshielded observations is larger in winter than in summer, probably due to the larger contributions of frozen precipitation. This pattern is not as clear for the Katterjåkk observations. The lag between the seasonal cycles of snow depth, and the share of frozen precipitation could perhaps explain the weak signal.

No estimate of loss due to evaporation could be deduced from the results. The study was not primarily designed to estimate evaporation loss, and the rather simple method employed proved insufficient. More detailed analysis of precise timing of precipitation and dewpoint deficits in the longer accumulation periods is suggested for a future study.

The estimated undercatch from lacking wind shields in historical observations (1836–1893) is smaller than the network-wide difference of precipitation between periods before 1893 and after 1930, as described above, and that of the two standard normal periods in the climate indicator (1881–1910 and 1931–1960). The undercatch should be considered to be a rough estimate, as estimates of wind shield effects are only obtained for Norrköping (windclass 3) and Katterjåkk (windclass 5) which can be converted to correction factors. Correction factors for stations with other wind classes can only be approximated. It is also not known, how representative these wind shield effects are for other stations within same wind class. The Katterjåkk wind shield effect for snow is for example afflicted by relatively large uncertainty. However, since most stations have a windclass between 2 and 4, the Norrköping wind shield effects have relatively small uncertainties and compares well with literature values, the estimate is still useful. It is also not straightforward to make an estimate of the difference in precipitation before and after the installation of wind shields as early observations are sparse. The climate indicator is produced with the EOF method, where the total precipitation of the entire network over the period from 1880 is estimated by combining the spatial signal of a period of complete coverage with the temporal signal of the available observations. The undercatch due to missing wind shields might therefore be indirectly compensated for to some extent in this product.

On the question whether the historical transition from the 1 000 cm^2-mouth gauges to the modern gauges has influenced the climatological precipitation series, the results are somewhat ambiguous. The test series in Norrköping show no or small deviations between the shielded historical gauge and the neighboring

modern gauge (automatic), while the Katterjåkk test series show quite large deviations between the modern and historical observations, and the linear regression models are also afflicted with large uncertainties.

8. Conclusion

The wind shield effect, i.e., larger observed precipitation sums due to the inclusion of a wind shield, is larger for the open site (Katterjåkk) than for the quite well shielded site (Norrköping), and larger for snow than for rain. The wind shield effect was found to be 7% for Norrköping and 16% for Katterjåkk for snow compared to 1% and 2% for rain, respectively.

The undercatch of the shielded historical gauges compared to the modern gauges is also larger for snow (up to 50%) than for rain (0–8%). There are larger differences between the methods in Katterjåkk than in Norrköping. This is probably partly due to the considerable differences in local terrain between the test site and the automatic weather station, partly due to the more windswept and more snowy conditions in Katterjåkk.

The mean average error (MAE) of linear regression models (i.e., how suitable it is to apply correction factors derived from simple linear models to the data) are smallest between the historical gauges, especially for the Norrköping series. The uncertainties are larger for snow and sleet than for rain. The most closely placed modern gauge relative to the historical gauges (automatic gauge in Norrköping, manual gauge in Katterjåkk) gives the most similar precipitation sums, suggesting that micrometeorology is more important than the observation method.

Wind speeds observed at the respective automatic weather station show no simple relationship on the undercatch of the historical gauges.

The wind shield effect is larger and varies more in the winter months than in the summer months, especially for the Norrköping observations. For the Katterjåkk observations, the month-to-month variations of the wind shield effect are difficult to interpret.

The estimated network-wide undercatch due to missing wind shields in historical observation is smaller than the total difference in precipitation between periods without and with wind shields. The study indicates that the installation of wind shields in the late 19th century and early 20th century is probably not the main contribution to the increasing trend in precipitation in this period.

From the results of the study, it cannot be concluded that the transition from historical to modern observations method have had an important influence on the observational time series.

Acknowledgements: The authors would like to thank all our co-workers who invested their time and effort in the manual precipitation measurements. Invaluable insights, advice, and support were offered by Thomas Carlund, Erik Engström, Lennart Wern, and Sverker Hellström at SMHI. The authors would also like to thank Gunnar Larsson for his help with the blueprints of the historical gauges. Furthermore,

the authors would like to thank Tomas Johansson for the permission to use his daily manual precipitation observations at SMHI headquarters and Sandra Andersson for the work of digitization and organization of the data. A special thanks goes to Anna Zetterlund, the observer in Katterjåkk for her indispensable work with precipitation observation, both regular and those being part of the current project.

References

Alexandersson, H. 2000: Manuell och automatisk nederbördsmätning. *Väder och vatten 10*, 18–19. (In Sweden)

Alexandersson, H., 2002: Temperature and precipitation in Sweden 1860–2001. *Meterorologi 104*. SMHI, Norrköping, Sweden. (In Sweden)

Alexandersson, H., 2003: Korrektion av nederbörd enligtenkel klimatologisk metodik. *Meteorologi 111*. SMHI, Norrköping, Sweden. (In Sweden)

Bergsten, F., 1954: Nederbörden i Sverige, medelvärden 1921–1950. *Medelande från Sveriges Meteorologiska och Hydrologiska Institut. Serie C 5*. 3–8. (In Sweden)

Ehsani, M.R. and *Behrangi, A.*, 2022: A comparison of correction factors for the systematic gauge-measurement errors to improve the global land precipitation estimate. *J. Hydrol. 610*. 127884. https://doi.org/10.1016/j.jhydrol.2022.127884

Eriksson, B., 1983: Data concerning the precipitation climate of Sweden-Normal values for the period 1951–80. *Report 1983:28.* SMHI, Norrköping, Sweden.

Eriksson, B., Carlsson, B., and *Dahlström, B.*, 1989: Preliminär handledning för korrektion av nederbördsmängder — Vid manuell uppmätning med SMHI-nederbördsmätare. *Meteorologi 77*. SMHI, Norrköping, Sweden. (In Sweden)

Fredriksson, U. and *Ståhl, S.*, 1994: En jämförelse mellan automatiska och manuella fältmäningar av temperatur och nederbörd. *Meteorologi 86*. SMHI, Norrköping, Sweden. (In Sweden)

Førland, E.J., Allerup, P., Dahlström, B., Elomaa, E., Jönsson, T., Madsen, H., Perälä, J. Rissanen, P., Vedin, H., and *Vejen, F.*, 1996: Manual for operational correction of Nordic precipitation data. *DNMI-Reports 24(96)*. 66

Hamberg, H.E., 1881: Månadsöversikt af väderleken i Sverige. Meteorologiska Centralanstalten, Stockholm, Sweden. (In Sweden)

Hamberg, H.E., 1911: Nederbörden i Sverige 1860–1910. *Meteorologiska iakttagelser i Sverige 53*. 11–15. (In Sweden)

Haslinger, K., Hofstätter, M., Kroisleitner, C., Schöner, W., Laaha, G., Holawe, F., and *Blöschl, G.*, 2019: Disentangling drivers of meteorological droughts in the European Greater Alpine Region during the last two centuries. *J. Geophys. Res.: Atmospheres 124*. 12404–12425. https://doi.org/10.1029/2018JD029527

Johansson, B. and *Chen, D.*, 2003: The influence of wind and topography on precipitation distribution in Sweden: Statistical analysis and modelling. *International J. Climatol: 23,* 1523–1535. https://doi.org/10.1002/joc.951

Kendon, M., McCarthy, M., Jevrejeva, S., Matthews, A., Sparks, T., Garforth, J., and *Kennedy, J.*, 2022: State of the UK Climate 2021. *Int. J. Climatol.42 (S1),* 1–8. https://doi.org/10.1002/joc.7787

Kjellström, E., Nikulin, G., Strandberg, G., Christensen, O.B, Jacob, D., Keuler, K., Lenderink, G., van Meijgaard, E., Schär, C., Somot, S. et al., 2018: European climate change at global mean temperature increases of 1.5 and 2 C above pre-industrial conditions as simulated by the EURO-CORDEX regional climate models. *Earth Syst. Dynam. 9,* 459–478. https://doi.org/10.5194/esd-9-459-2018

Lantmäteriet, 2023: *Min karta,* available at https://www.lantmateriet.se/sv/kartor/vara-karttjanster/min-karta/ accessed: *2023-09-15*. Lantmäteriet (Land Survey authority), Gävle, Sweden.

Legates, D.R. and *Willmott, C.J.*, 1990: Mean seasonal and spatial variability in gauge-corrected, global precipitation. *Int. J. Climatol. 10,* 111–127. https://doi.org/10.1002/joc.3370100202

Lind, P., Belušić, D., Médus, E., Dobler, A., Pedersen, R.A., Wang, F., Matte, D., Kjellström, E., Landgren, O., Lindsetdt, D., Christensen, O.B., and *Christensen, J.H.*, 2022: Climate change

information over Fenno-Scandinavia produced with a convection-permitting climate model. *Climate Dynam. 61*, 519–541. https://doi.org/10.1007/s00382-022-06589-3

Lindström G., 2002: Vattentillgång och höga flöden i Sverige under 1900-talet. *Hydrologi 18*. SMHI, Norrköping, Sweden. (In Sweden)

Metzger, A. and *Jacob-Rousseau, N.*, 2020: The 1857--1858 drought in Alsace: from water shortage to a socio-political extreme event. *Reg. Environ. Change 20*, 1–15. https://doi.org/10.1007/s10113-020-01632-7

Moberg, A., Bergström, H., Ruiz Krigsman, J., and *Svanered, O.*, 2002: Daily Air Temperature and Pressure Series for Stockholm (1756–1998). *Climatic Change 53*, 171–212. https://doi.org/10.1007/978-94-010-0371-1_7

Mill, H.R., 1901: The development of rainfall measurement in the last forty years. *British Rainfall 1900*. 23–45.

Nautisk-meteorlogisk byrån, N.D: *Instruktion för nederbördsobservationers utförande vid Svenska fyrstationer 7.* Nautiska Meteorologiska byrån, Stockholm, Sweden. (In Sweden)

Rácz T., 2021: On the correction of processed historical rainfall data of siphoned rainfall recorders. *Időjárás 125,* 513–519. https://doi.org/10.28974/idojaras.2021.3.9

van der Schrier, G., Efthymiadis, D., Briffa, K.R., and Jones, P.D., 2007: European Alpine moisture variability for 1800–2003. *Int. J. Climatol 27,* 415–427. https://doi.org/10.1002/joc.1411

Rubel, F., and *Hantel, M.*, 2001: BALTEX 1/6-degree daily precipitation climatology 1996–1998. *Meteorol. Atmosph. Phys. 77*, 155–166. https://doi.org/10.1007/s007030170024

Schimanke, S., Joelsson, M., Andersson, S., Carlund, T., Wern, L., Hellström, S. and *Kjellström, E.*, 2022: Observerad klimatförändring i Sverige 1860–2021. *Klimatologi 69*. SMHI, Norrköping, Sweden. (In Sweden)

Stisen, S., Højberg, A.L., Troldborg, L., Refsgaard, J.C., Christensen, B.S.B., Olsen, M., and *Henriksen, H.J.*, 2012: On the importance of appropriate precipitation gauge catch correction for hydrological modelling at mid to high latitudes. *Hydrol. Earth Syst. Sci. 16*, 4157–4176. https://doi.org/10.5194/hess-16-4157-2012

Sturm, C., 2024: Spatially aggregated climate indicatorsover Sweden (1860–2020), Part 2: Precipitation. EGUspere, 25 April 2024, 1–38. https://doi.org/10.5194/egusphere-2024-940

SMHI, 2023: *Swedish Meteorological and Hydrological Institute*: *Climate indicator* — Precipitation, available at https://www.smhi.se/en/climate/climate-indicators/climate-indicators-precipitation-1.91462 accessed: 2023-09-20. Swedish Meteorological and Hydrological Institute, Norrköping, Sweden.

Venema, V., Trewin, B., Wang, X.L., Szentimrey, T., Lakatos, M., Aguilar, E., Auer, I., Guijarro, J., Menne, M., Oria, C., Louamba, W.S.R.L. and *Rasul, G.*, 2020: Guidelines on Homogenization, 2020 edition, WMO-no. 1245. WMO, Geneva.

WMO, 2017: World Meteorological Organization: WMO Guidelines on the Calculation of Climate Normals, 2017 ed. WMO-No-1203. WMO, Geneva.

WMO, 2021: World Meteorological Organization: WMO Guide to Instruments and Methods of Observation. Volume I: Measurement of Meteorological Variables, 2021 ed. WMO-No. 8. WMO, Geneva.

DOI:10.28974/idojaras.2024.2.5

IDŐJÁRÁS

Quarterly Journal of the HungaroMet Hungarian Meteorological Service
Vol. 128, No. 2, April – June, 2024, pp. 219–235

Development of new version MASHv4.01 for homogenization of standard deviation

Tamás Szentimrey

Varimax Limited Partnership, Budapest, Hungary

Author E-mail: szentimrey.t@gmail.com

(Manuscript received in final form October 31, 2023)

Abstract— The earlier versions of our method MASH (Multiple Analysis of Series for Homogenization; *Szentimrey*) were developed for homogenization of the daily and monthly data series in the mean, i.e., the first order moment. The software MASH was developed as an interactive automatic, artificial intelligence (AI) system that simulates the human intelligence and mimics the human analysis on the basis of advanced mathematics. This year we finished the new version MASHv4.01 that is able to homogenize also the standard deviation, i.e., the second order moment. The problem of standard deviation is related to the monthly and daily data series homogenization.

Key-words: climate data series, homogenization, mathematical formulation, normal distribution, adjustment of standard deviation, AI system, MASH, MISH

1. Introduction

In essence, the theme of homogenization can be divided into two subgroups, such as monthly and daily data series homogenization. These subjects are in strong connection with each other of course, for example the monthly results can be used for the homogenization of daily data. In the practice, the monthly series are homogenized in the mean only, while there exist some trials to homogenize the daily series also in higher order moments. These procedures are based on a popular assumption that is the adjustment of mean is sufficient for monthly series,

and the adjustment of higher order moments is necessary only in the case of daily data series. In general, it is tacitly assumed that the averaging is capable to filter out the inhomogeneity in the higher order moments. However, this assumption is false, since it can be proved if there is a common inhomogeneity in the standard deviation of daily data then we have the same inhomogeneity in the monthly data. Therefore, we developed a mathematical procedure for the homogenization of mean and standard deviation together. This developed procedure was incorporated into our new software version MASHv4.01 (Multiple Analysis of Series for Homogenization; *Szentimrey*, 2023b), which is based on the examination of different type of monthly series, and the monthly results are applied for the homogenization of daily series. We remark if the data are normally distributed (e.g., mean temperature) then the homogenization of mean and standard deviation is sufficient, since in case of normal distribution if the first two moments are homogenous then the higher order moments are also homogeneous. The most important novelty of this paper is the methodology for adjusting the mean and standard deviation together, as detailed in Sections 5.3 and 5.4. However, first we need to review the mathematical, methodological background.

As for the MASH as an artificial intelligence system, it is not just a "buzzword", as MASH has been developed along these lines for many years. To illustrate this, here is a quote from the proceedings of the 4th Homogenization Seminar (*Szentimrey*, 2004):

"Programmed Statistical Procedure (Software: MASHv2.03)

EXAMPLE

Let us assume that there is a difficult stochastic problem.

In case of having relatively few statistical information:

– an intelligent human is possibly able to solve the problem, but it is time-consuming,
– the solution of the problem cannot be programmed.

In case of increasing the amount of statistical information:

– one is unable to discuss and evaluate all the information,
– but then the solution of the problem can be programmed (as in chess expert systems).

AIM, REQUIREMENT

– Development of mathematical methodology in order to increase the amount of statistical information.
– Development of algorithms for optimal using of both the statistical and the metadata information."

In essence, the Deep Blue chess expert system, which defeated Garry Kasparov in 1997, motivated the development of MASH.

In our conception, the meteorological questions and topics cannot be treated separately. Therefore, we present a block diagram (*Fig. 1*) to illustrate the possible

connection between various important meteorological topics. The software MASH and MISH (Meteorological Interpolation based on Surface Homogenized Data Basis; *Szentimrey* and *Bihari*, 2014) were developed by us. These software were applied also in the CARPATCLIM project (*Szentimrey et al.*, 2012a,b; *Lakatos et al.*, 2013). The paper of *Izsák et al.* (2022) presents another application to create a representative database for Hungary.

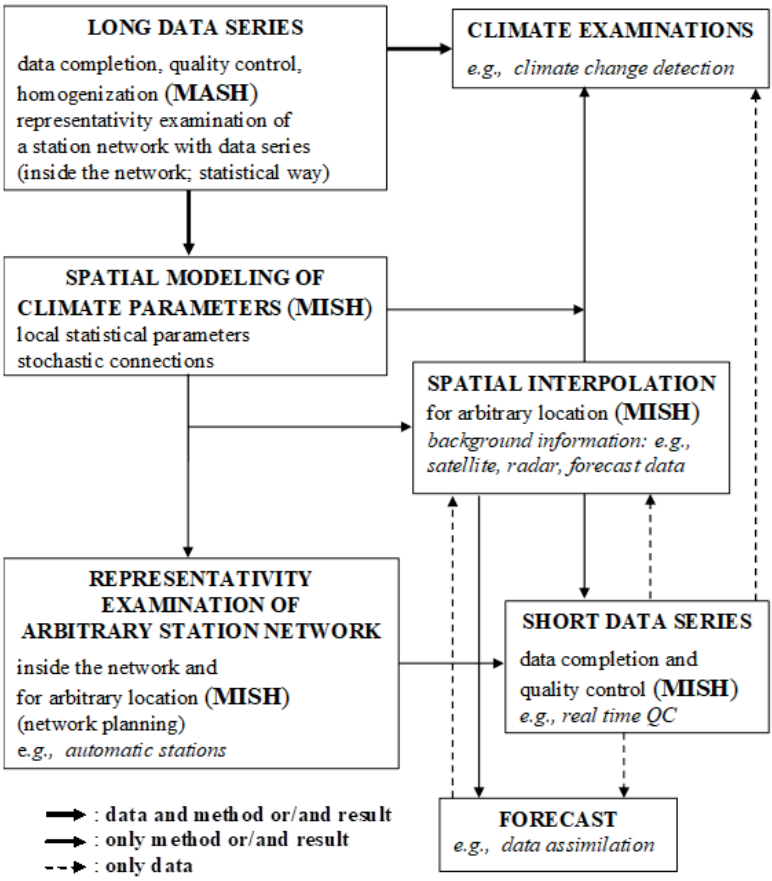

Fig. 1. Block diagram for the possible connection, between various basic meteorological topics and systems.

Finally, last but not least, in Section 7 we reflect to some incorrect sentences about MASH from a book.

2. Mathematical formulation of climate data homogenization

Unfortunately, the exact theoretical, mathematical formulation of the problem of homogenization is neglected at the meteorological studies in general. Therefore, we try to formulate this problem in accordance with the mathematical conventions. First we emphasize that the homogenization is a distribution problem and not a regression one (*Szentimrey*, 2013).

2.1. General mathematical formulation

Notation

Let us assume we have daily or monthly climate data series:
$Y_1(t)$ $(t = 1,2,..,n)$: candidate time series of the new observing system.
$Y_2(t)$ $(t = 1,2,..,n)$: candidate time series of the old observing system.
$1 \le T < n$: changepoint, series $Y_2(t)$ $(t = 1,2,..,T)$ can be used before and series $Y_1(t)$ $(t = T+1,..,n)$ can be used after the changepoint.

The appropriate theoretical cumulative distribution functions (CDF) are:

$$F_{1,t}(y) = P(Y_1(t) < y) \ , \ \ F_{2,t}(y) = P(Y_2(t) < y) \quad y \in (-\infty, \infty) \ , t = 1,2,..,n$$

It is very important to remark that as a consequence of some natural changes - e.g. annual cycle, climate change - the series of distribution functions $F_{1,t}(y)$, $F_{2,t}(y)$ $(t = 1,2,..,n)$ may change in time! In the statistical climatology the climate change is equivalent with the changing probability of the meteorological events. The inhomogeneity of data series can be defined on the basis of the distribution functions.

Definition 1

The merged series $Y_2(t)$ $(t = 1,2,..,T)$, $Y_1(t)$ $(t = T+1,..,n)$ is inhomogeneous, if the identity of the distribution functions $F_{2,t}(y) \equiv F_{1,t}(y)$ $(t = 1,2,..,T)$ is not true.

Definition 2

The aim of the homogenization is the adjustment or correction of values $Y_2(t)$ $(t = 1,2,..,T)$ in order to have the adjusted values $Y_{1,2h}(t)$ $(t = 1,2,..,T)$ with the same distribution as the elements of series $Y_1(t)$ $(t = 1,2,..,T)$ have, i.e.:

$$\mathrm{P}\big(Y_{1,2h}(t) < y\big) = \mathrm{P}(Y_1(t) < y) = F_{1,t}(y) \quad y \in (-\infty, \infty), t = 1,2,..,T. \qquad (1)$$

This definition means the equality in distribution, i.e.: $Y_{1,2h}(t) \stackrel{d}{=} Y_1(t)$ $(t = 1,2,..,T)$. ("*d* over =", simply means that the two distribution functions are the same.)

Theorem 1

Let us assume about the random variables Y_1,Y_2 and their distribution functions $F_1(y)$,$F_2(y)$, that $P\left(Y_j \in (a_j, b_j)\right) = 1$ and $F_j(y)$ is a strictly increasing continuous function on the interval (a_j, b_j) $(j = 1,2)$. Then applying the transfer function $Y_{1,2h} = F_1^{-1}\left(F_2(Y_2)\right)$ we obtain that the variable $Y_{1,2h}$ has the same distribution as Y_1, i.e: $\mathrm{P}\left(Y_{1,2h} < y\right) = \mathrm{P}(Y_1 < y) = F_1(y)$.

Definition 3

Transfer function: $F_{1,t}^{-1}\left(F_{2,t}(y)\right)$ and quantile function: $F_{1,t}^{-1}(p)$.
Theoretical formulation of homogenization of $Y_2(t)$ $(t = 1,2,..,T)$:
$Y_{1,2h}(t) = F_{1,t}^{-1}\left(F_{2,t}(Y_2(t))\right)$, then $\mathrm{P}\left(Y_{1,2h}(t) < y\right) = F_{1,t}(y)$.

Remark

The basis of the Quantile Matching methods can be integrated into the general theory. However, these methods developed in practice mainly for daily data are very weak empiric methods.

2.2 Mathematical formulation for normal distribution

The homogenization problem is very complicated in the general case, however in the case of normal distribution, a much simpler mathematical formula can be obtained. We emphasize that the normal distribution is a special case, but it is a basic one in mathematical statistics as well as in the meteorology. For example, the normal distribution model can be accepted for temperature variables in general.

Theorem 2

Let us assume the elements of data series $Y_1(t)$, $Y_2(t)$ are normally distributed, that is,
$Y_1(t) \in N(E_1(t), D_1(t))$, $Y_2(t) \in N(E_2(t), D_2(t))$ $(t = 1,2,..,n)$,
where $\mathrm{E}(Y_1(t)) = E_1(t)$, $\mathrm{E}(Y_2(t)) = E_2(t)$ are the means or expected values and $\mathrm{D}(Y_1(t)) = D_1(t)$, $\mathrm{D}(Y_2(t)) = D_2(t)$ are the standard deviations.

Then the transfer formula of homogenization:

$$Y_{1,2h}(t) = F_{1,t}^{-1}\left(F_{2,t}(Y_2(t))\right) = \frac{D_1(t)}{D_2(t)}(Y_2(t) - E_2(t)) + E_1(t)(t = 1,2,..,T) \qquad (2)$$

In case of normal distribution, we have a much simpler transfer formula for adjustment than the general form $Y_{1,2h}(t) = F_{1,t}^{-1}\left(F_{2,t}(Y_2(t))\right)(t = 1,2,..,T)$. This simple linear formula means that, if the data series have normal distribution, it is sufficient to homogenize the means (*E*) and standard deviations (*D*) only that is equivalent with the homogenization of the first two moments. We emphasize that the normal distribution is a basic model in the mathematical statistics as well as in the meteorology, and there is no "tail distribution" problem (*Szentimrey*, 2023a) for this important distribution according to the *Theorem 2*! For normal distribution, if the means and standard deviations are homogenous then the higher order moments are also homogeneous, and there is not any inhomogeneity in the tails of the distributions.

3. Relation of daily and monthly data homogenization

The monthly and daily data series homogenization are in strong connection with each other of course, for example the monthly results can be used for the homogenization of daily data.
If we have daily data series, the general way of homogenization is

- calculation of monthly series,
- homogenization of monthly series taking advantage of the larger signal to noise ratio,
- homogenization of daily series using the detected monthly inhomogeneities.

So we have the question: how can we use the valuable information of detected monthly inhomogeneities for the daily data homogenization?

4. Methodology for homogenization of monthly series

This section is an overview of some various theoretical aspects of monthly series homogenization (*Szentimrey*, 1999, 2008, 2021, 2023a,b; *Venema et al.*, 2012). The aim of these homogenization procedures is to detect the inhomogeneities of monthly series and to adjust the series. In connection with such homogenization methods, we have to give solutions for the following mathematical problems: relative models, statistical spatiotemporal modeling of the series, methodology for comparison of series, breakpoint (changepoint), and outlier detection, methodology for adjustment of series, quality control procedures, missing data completion, usage of metadata, relation of daily and

monthly homogenization, manual versus automatic methods, evaluation of methods (theoretical, benchmark validation). The following Sections 4.1–4.2 are related to the Chapter 5 of the WMO Guidelines on Homogenization (*WMO*, 2020).

4.1. General structure of the relative spatiotemporal models

Relative methods can be applied if there are more station data series given, which can be compared mutually. In this case, the statistical spatiotemporal modeling of the series is a basic question. The adequate comparison, breakpoint detection, and adjustment procedures depend on the chosen statistical model. Depending on the climate elements, additive or multiplicative models are applied.

4.1.1. The additive spatiotemporal model

This model is based on the normal distribution (Section 2.2) and it can be used if the data series are quasi normally distributed (e.g., temperature). For this model we assume inhomogeneity of mean (E), i.e., expected value.

In case of relative methods, a general form of additive model for more monthly series belonging to the same month in a small climate region can be written as follows (*WMO*, 2020):

$$X_j(t) = \mu(t) + E_j + IH_j(t) + \varepsilon_j(t) \quad (j = 1,2,\dots,N\ ;\ t = 1,2,\dots.,n)\,, \qquad (3)$$

where $\mu(t)$ is the common and unknown climate change signal, E_j are the spatial expected values, $IH_j(t)$ are the inhomogeneity signals, and $\varepsilon_j(t)$ are normal white noise series.

The type of inhomogeneity$IH(t)$ is in general a step-like function with unknown breakpoints T and artificial shifts $IH(T) - IH(T+1) \neq 0$. The normal distributed vector variables $\boldsymbol{\varepsilon}(t) = [\varepsilon_1(t),..,\varepsilon_N(t)]^T \in N(\mathbf{0},\mathbf{C})(t = 1,\dots,n)$ are totally independent in time. The spatial covariance matrix $\mathbf{C}$ describes the spatial structure of the series, which is important for comparison of series.

4.1.2. The multiplicative spatiotemporal model

If the data series are quasi lognormal distributed (e.g., precipitation) then the multiplicative model can be used. According to this model, the monthly series belonging to the same month in a small climate region can be written as follows:

$$X_j(t) = \mu(t) \cdot E_j \cdot IH_j(t) \cdot exp\big(\varepsilon_j(t)\big)\ \ (j = 1,2,\dots,N\ ;\ t = 1,2,\dots.,n)\,. \qquad (4)$$

This multiplicative model can be transformed into the additive one by certain logarithmic procedure, where the little values near zero are increased slightly before logarithmization. Therefore, the homogenization methodology

(Section 4.2) developed for additive model can be used with some modification also for the multiplicative model.

4.2. Methodological questions for additive spatiotemporal model

4.2.1. Methodology for comparison of series

The problem of comparison of series is related to the following questions: reference series creation, difference series constitution, multiple comparisons of series, etc. This topic is very important for detection as well as for adjustment, because the efficient series comparison can increase both the significance and the power. The development of efficient comparison methods can be based on the examination of the spatial covariance structure of data series. The examined series $X_j(t)$ have to be taken as candidate and reference series alike, furthermore, the homogeneity of the reference series is not assumed!

4.2.2. Methodology for breakpoint (changepoint) detection

One of the basic tasks of the homogenization is the examination of the difference series in order to detect the breakpoints and to attribute the appropriate ones for the candidate series.

The more sophisticated multiple breakpoints detection procedures were developed for joint detection of the breakpoints. There may be different principles of the detection methods that are classical ways in the mathematical statistics. Multiple breakpoints detection procedures for difference series are as follows.

a) Bayesian approach (model selection, segmentation), penalized likelihood methods:
   PRODIGE (*Caussinus* and *Mestre*, 2004), HOMER (*Mestre et al.*, 2013), ACMANT (Adapted Caussinus-Mestre Algorithm for Networks of Temperature series; *Domonkos*, 2011).
b) Multiple breakpoints detection based on test of hypothesis and confidence intervals for the breakpoints, that make possible, automatic use of metadata: MASH (*Szentimrey*, 1999, 2023b).

4.2.3. Methodology for adjustment of series

Beside the detection, another basic task of the homogenization is the adjustment of series. Calculation of the adjustment factors can be based on the examination of difference series for estimation of shifts at the detected breakpoints. In general, the methods use point estimation for the shifts at the detected breakpoints.

There are methods that use the standard least squares technique after breakpoint detection procedure for joint estimation of the shifts of all the examined series, for example the methods PRODIGE, HOMER, ACMANT. Probably the generalized least squares estimation technique based on spatial

covariance matrix would be more efficient, and it would be equivalent with the maximum likelihood estimation for the shifts in the case of normal distribution.

Another way is that the calculation of the adjustment factors is based on some confidence intervals given for the shifts at the detected breakpoints, as in the method MASH. The confidence intervals given for the breakpoints and shifts make the automatic use of metadata possible.

5. Methodology for homogenization of daily series

The basic question is what would be the appropriate, exact methodology for the daily data homogenization. According to Sections 3 and 4, how can we use the valuable information of detected monthly inhomogeneities for the daily data homogenization (*Szentimrey*, 2008, 2013, 2017, 2021, 2023a,b)? How can we use the methodology developed for monthly series?

5.1. A popular procedure for daily data, e.g., the variable correction methods

The typical steps of the procedure are as follows.

1. Calculation of monthly series from daily series.
2. Homogenization of monthly series:
   Breakpoints detection, adjustment in the first order moment (mean (*E*)).
   Assumption: homogeneity of higher order moments (e.g., standard deviation (*D*)).
3. Homogenization of daily series:
   A trial to homogenize also the higher order moments.
   (Quantile matching (*Wang* and *Feng,* 2013), spline methods (*Mestre et al.*, 2011))

The used monthly information are only the detected breakpoints.

However, the following questions are arising at this procedure:

– Is it an adequate model that we have inhomogeneity in higher moments only at daily series but not at monthly ones? Can this model be accepted according to the probability theory? No, it can be proved, if there is a common inhomogeneity in the standard deviation (*D*) of daily data, we may have the same inhomogeneity in monthly data.
– Why are the monthly adjustment factors not used for daily homogenization? It seems to lose some valuable information obtained during the monthly homogenization.

5.2. Problem of inhomogeneity of the standard deviation

According to the former assumption, which is popular in practice, the adjustment in mean (*E*) is sufficient for monthly and annual series, and the adjustment of higher order moments is necessary only in the case of daily data series. In general, it is tacitly assumed that the averaging is capable to filter out the inhomogeneities in the higher order moments. However, this assumption is false, it can be proved, if there is a common inhomogeneity in the standard deviation (*D*) of daily data, we may have the same inhomogeneity in monthly data.

Theorem 3

Let us assume $Y(t)$ $(t = 1,..,30)$ are daily data and the monthly mean is $\bar{Y} = \frac{1}{30}\sum_{t=1}^{30} Y(t)$.

The monthly variable for examination of the inhomogeneity of standard deviation (*D*) is

$$S = \sqrt{\frac{1}{2\cdot 29}\sum_{t=2}^{30}(Y(t) - Y(t-1))^2}\ . \tag{5}$$

Let us introduce some inhomogeneity of the mean (*E*) and the standard deviation (*D*) for the daily data by a linear function:

$Y_{ih}(t) = \alpha \cdot \big(Y(t) - \mathrm{E}(Y(t))\big) + \mathrm{E}(Y(t)) + \beta \qquad (t = 1,..,30).$

Then the expected values and the standard deviations are:

$\mathrm{E}(Y_{ih}(t)) = \mathrm{E}(Y(t)) + \beta\ ,\ \mathrm{D}(Y_{ih}(t)) = \alpha \cdot \mathrm{D}(Y(t)) \quad (t = 1,..,30).$

The appropriate monthly variables are:

$\bar{Y}_{ih} = \frac{1}{30}\sum_{t=1}^{30} Y_{ih}(t), \qquad S_{ih} = \sqrt{\frac{1}{2\cdot 29}\sum_{t=2}^{30}(Y_{ih}(t) - Y_{ih}(t-1))^2}.$

i) Then the monthly mean is also inhomogeneous in mean (*E*) and standard deviation (*D*) with the same measure like the daily values:
$\mathrm{E}(\bar{Y}_{ih}) = \mathrm{E}(\bar{Y}) + \beta$ and $\mathrm{D}(\bar{Y}_{ih}) = \alpha \cdot \mathrm{D}(\bar{Y})$.

ii) Moreover, variables S, S_{ih} can be used to estimate the inhomogeneity α of the standard deviation (*D*): $\mathrm{E}(S_{ih}) = \alpha \cdot \mathrm{E}(S)$

5.3. The alternative procedure for daily and monthly data developed in MASH

We suggest an alternative procedure to homogenize both the daily and the monthly series.
The steps of the procedure in case of quasi normal distribution (e.g., temperature) are as follows.
First we examine both the monthly mean series $\bar{Y}(t)$ for the inhomogeneity of expected values (E) and the monthly series $S(t)$ derived to *Theorem 3* for the inhomogeneity of standard deviations (D). The proper inhomogeneity characteristics are the difference of the expected values and the ratio of the standard deviations. Therefore, we apply different models for these parameters.

1. Homogenization of monthly series $S(t)$, $\bar{Y}(t)$.
   Homogenization of series $S(t)$ by the multiplicative model (4.1.2): breakpoints detection, estimation of inhomogeneity of standard deviation (D).
   Adjustment of standard deviation of series $\bar{Y}(t)$ is detailed in Section 5.4.
   Homogenization of adjusted series $\bar{Y}(t)$ by additive model (4.1.1): breakpoints detection, estimation of the inhomogeneity of mean (E). It is detailed in Section 5.4.
   Assumption: after homogenization of E, D, there is no inhomogeneity in the higher order (>2) moments of adjusted series $\bar{Y}(t)$. This assumption is always right in case of normal distribution according to *Theorem 2*.
2. Homogenization of daily series.
   Homogenization of mean (E) and standard deviation (D) on the basis of the monthly results. The used monthly information are the breakpoints and the monthly adjustments of the mean (E) and standard deviation (D). The adjustment is based on the transfer formula (Eq (2)) considering *Theorem 3*. If the daily data are normally distributed then after homogenization of E, D there is no inhomogeneity in the higher order moments according to *Theorem 2*.

5.4. Adjustment of monthly mean series, daily series, transfer formula

The adjustment of monthly mean series $Y_2(t)$ in mean (E) and standard deviation (D) is based on the transfer formula according to Eq. (2), i.e.:

$$Y_{1,2h}(t) = \frac{D_1(t)}{D_2(t)}(Y_2(t) - E_2(t)) + E_1(t) \quad (t = 1,2,..,T)\,. \tag{6}$$

5.4.1. Adjustment of $Y_2(t)$ in standard deviation (D)

The theoretical formula is $Y_{1,2hD}(t) = \frac{D_1(t)}{D_2(t)}(Y_2(t) - E_2(t)) + E_2(t)$ $(t = 1,2,..,T)$ but $E_2(t)$ $(t = 1,2,..,T)$ are unknown.
Therefore, the applied formula is $Y_{1,2hD}(t) = \frac{D_1(t)}{D_2(t)}(Y_2(t) - \bar{E}_2) + \bar{E}_2$,
where $\bar{E}_2$ is the mean value of $E_2(t)$ $(t = 1,2,..,T)$. $\bar{E}_2$ can be estimated by mean $\bar{Y}_2$.
Inhomogeneity of standard deviation $IH_D(t) = \frac{D_2(t)}{D_1(t)}$ can be estimated by homogenizing the monthly standard deviation series $S(t)$ using the multiplicative model.
The adjustment of $Y_2(t)$ is $Y_{1,2hD}(t) = \frac{Y_2(t)}{IH_D(t)} - IH_{D,E}(t)$,
where $IH_{D,E}(t) = \left(\frac{D_1(t)}{D_2(t)} - 1\right)\bar{E}_2$.

5.4.2. Adjustment of $Y_{1,2hD}(t)$ in mean (E)

According to Eq. (6), the inhomogeneity of $Y_{1,2hD}(t)$ in mean is $IH_{E,D}(t) = \mathrm{E}\left(Y_{1,2hD}(t)\right) - E_1(t)$, and it can be estimated by homogenizing the monthly mean series $Y_{1,2hD}(t)$ using additive model.
$IH_{E,D}(t) = \left(\frac{D_1(t)}{D_2(t)} - 1\right)(E_2(t) - \bar{E}_2) + E_2(t) - E_1(t)$.

5.4.3. Summary of the adjustment of $Y_2(t)$ and the daily data series

The adjustment of $Y_2(t)$ in mean (*E*) and standard deviation (*D*) can be written in the following linear function form:
$Y_{1,2h}(t) = \frac{Y_2(t)}{IH_D(t)} - IH_E(t)$, where $IH_E(t) = IH_{D,E}(t) + IH_{E,D}(t)$.
For homogenization of daily data series in mean (*E*) and standard deviation (*D*) we also use this linear function form, in accordance with the *Theorem 3.* In this case the estimated inhomogeneity values $IH_D(t)$, $IH_E(t)$ are smoothed, as it was developed in MASH for homogenization of daily data (*Szentimrey*, 2008, 2013).

6. Summary of software MASH

6.1. General comments

The new version MASHv4.01 (Multiple Analysis of Series for Homogenization; *Szentimrey* 1999, 2004, 2008, 2013, 2017, 2021, 2023a,b,c) has been developed

for homogenization of daily and monthly series. The most important novelty of this version is the homogenization in standard deviation (*D*) beside the mean (*E*), see Sections 5.3, 5.4. The basic concept of the MASH system is first to homogenize the monthly series derived from the daily series, and then to homogenize the daily series based on the detected monthly inhomogeneities. The procedures depend on the distribution of climate elements, and additive or multiplicative models can be used.

6.1.1. Quasi normal distribution (e.g., temperature)

Beside the monthly mean series, another type of monthly series are also derived to estimate the inhomogeneity of standard deviation (*D*). These latter series can be homogenized by the multiplicative model (4.1.2), and the monthly mean series can be adjusted with the estimated inhomogeneity in standard deviation (*D*). The adjusted monthly mean series can be homogenized in mean (*E*) by the additive model (4.1.1).

6.1.2. Quasi lognormal distribution (e.g., precipitation)

Monthly mean or sum series can be homogenized by the multiplicative model (4.1.2).
The multiplicative model can be transformed into the additive one (4.1.1) by certain logarithmic procedures.

6.2. The most important features of the MASH system

Homogenization of monthly series:

- Relative homogeneity test procedure.
- Step by step iteration procedure: the role of series (candidate, reference) changes step by step in the course of the procedure.
- Interactive automatic, artificial intelligence (AI) system (see Section 6.3).
- Additive or multiplicative model can be used depending on the distribution.
- Including automatic quality control and missing data completion.
- Providing the homogeneity of the seasonal and annual series as well.
- Metadata (probable dates of breakpoints) can be used automatically.
- The homogenization results and the metadata can be verified.

Homogenization of daily series:

- Based on the detected monthly inhomogeneities (*E, D*).
- Including automatic quality control and missing data completion for daily data.

The elder version of MISH and MASH software can be downloaded from:
http://www.met.hu/en/omsz/rendezvenyek/homogenization_and_interpolation/software/
We plan to share the new version MASHv4.01 this year (2023).

6.3. Some verification results for homogenization in mean (E) and standard deviation (D)

The aim of MASH is not the full automation, and we also are sceptical in such an aspect. Our intention was to develop a flexible, interactive automatic, artificial intelligence (AI) system that simulates the human intelligence and mimics the human analysis on the basis of advanced mathematics. The mechanic, labor-intensive sub-procedures are fully automated, moreover, the operating process can be controlled simply, and the accidental mistakes can be corrected interactively. The basic idea of this concept is controlling the results via the verification tables generated automatically during the automatic procedures (*Szentimrey*, 2004, 2023b). Interactive decisions also can be made based on the analysis of the verification tables.

Some examples for verification tables related to the inhomogeneities are presented in *Fig. 2.* In the example, 15 Hungarian July mean temperature series (1901–2015) were homogenized by MASH in mean (*E*) and standard deviation (*D*). The estimated inhomogeneities can be characterized by the following statistics.

i) For mean (*E*, additive model):
$IHE = \frac{1}{n}\sum_{t=1}^{n}|IHE(t)|$, where $E_{ih}(t) = E(t) + IHE(t) \quad (t = 1,\dots,n)$, and $E_{ih}(t)$, $E(t)$ are the means before and after homogenization.

ii) For standard deviation (*D*, multiplicative model):
$IHD = \frac{100}{n}\sum_{t=1}^{n}|IHD(t) - 1|$, where $D_{ih}(t) = D(t) \cdot IHD(t)$ $(t = 1,\dots,n)$, and $D_{ih}(t)$, $D(t)$ are the standard deviations before and after homogenization.

These *IHE* and *IHD* statistics can be seen in *Fig. 2.*

Estimated Inhomogeneities for Mean (E) (°C)

Series	IHE	Series	IHE	Series	IHE
3	0.80	8	0.55	15	0.53
7	0.52	12	0.48	10	0.48
14	0.31	6	0.31	5	0.29
11	0.24	1	0.23	4	0.14
9	0.13	2	0.09	13	0.08

AVERAGE: 0.35

Estimated Inhomogeneities for St. Deviation (D) (%)

Series	IHD	Series	IHD	Series	IHD
8	8.05	9	7.98	4	6.73
12	4.88	7	4.08	11	3.59
6	3.33	2	2.43	15	2.22
5	2.16	13	2.02	10	1.70
1	1.57	14	1.34	3	0.54

AVERAGE: 3.51

Fig. 2. Characterization of inhomogeneities for mean (E) and standard deviation (D).

7. Incorrect sentences about MASH from a book

During the last 11th Seminar for Homogenization, I was obliged to make some comments to the following book of Elsevier:
P. Domonkos, R. Tóth and *L. Nyitrai*, 2022: "Climate observations: data quality control and time series homogenization" (*Domonkos et al.*, 2022).
My comments published in the seminar proceedings (*Szentimrey*, 2023c) were as follows.
"The last sentence is on page 200 is: "MASHv3 is better than MASHv4." Sorry, but it is an absolutely misleading untrue statement! Publication of the book was in 2022 while publication of MASHv4 was later in 2023. The authors could not know MASHv4!
In Section (c) "Novelties in MASHv4", on page 200 is:"… the proposed algorithm easily detects false breaks of the standard deviation around the breakpoints for the means. It is because the empirical standard deviation is elevated for periods including shifts in the means." It is also an incorrect statement! We do not use the empirical standard deviation at all!
There is a funny personal note about me as the creator of MASH on page 198:
"The creator often chose unique mathematical solutions differing both from the traditional tools of climate data homogenization and from those suggested by other statisticians." Yes, because I am a mathematician!
Conclusion: The credibility of the content of this book is doubtful for me!"
After the seminar, in the same proceedings, Peter Domonkos responded to my objections and he accepted them (*Domonkos*, 2023).

References

Caussinus, H. and *Mestre, O.,* 2004: Detection and correction of artificial shifts in climate series. *Appl. Statist. 53*, Part 3, 405–425.

Domonkos, P., 2011: Adapted Caussinus-Mestre algorithm for networks of temperature series (ACMANT). *Int. J. Geosci. 2*, 293–309. https://doi.org/10.4236/ijg.2011.23032

Domonkos, P., Tóth, R. and *Nyitrai, L*. 2022: Climate observations: Data quality control and time series homogenization. Elsevier.
https://www.elsevier.com/books/climate-observations/domonkos/978-0-323-90487-2

Domonkos, P., 2023: Response to Tamás Szentimrey regarding the presentation of MASHV4 in "Climate observations" by Domonkos, P., Tóth, R., and Nyitrai, L., Proceedings of the 11th Seminar for Homogenization and Quality Control in Climatological Databases and 6th Conference on Spatial Interpolation Techniques in Climatology and Meteorology (Ed. *Lakatos M, Puskás M*, *Szentimrey T*), Budapest, Hungary, 2023, WCDMP-No. 87, 14.
https://library.wmo.int/idurl/4/68452

Izsák, B., Szentimrey, T., Lakatos, M., Pongrácz, R., and *Szentes, O*., 2022: Creation of a representative climatological database for Hungary from 1870 to 2020. *Időjárás 126*, 1–26.
https://doi.org.10.28974/idojaras.2022.1.1

Lakatos, M., Szentimrey, T., Bihari, Z., and *Szalai, S.,* 2013: Creation of a homogenized climate database for the Carpathian region by applying the MASH procedure and the preliminary analysis of the data. *Időjárás 117*. 143–158.

Mestre, O. et al., 2011: SPLIDHOM: A method for homogenization of daily temperature observations. *J. Appl. Meteorol. Climatol.* 50, 2343–2358. https://doi.org/10.1175/2011JAMC2641.1

Mestre, O. et al., 2013: HOMER: A homogenization software – Methods and applications. *Időjárás 117*, 47–67.

Szentimrey, T., 1999: Multiple Analysis of Series for Homogenization (MASH), Proceedings of the Second Seminar for Homogenization of Surface Climatological Data, Budapest, Hungary; WMO, WCDMP-No. 41, 27–46.

Szentimrey, T., 2004: Multiple Analysis of Series for Homogenization (MASH); Verification procedure for homogenized time series, Proceedings of the Fourth Seminar for Homogenization and Quality Control in Climatological Databases, Budapest, Hungary; WMO, WCDMP-No. 56, 193–201.

Szentimrey, T., 2008: Development of MASH homogenization procedure for daily data. Proceedings of the Fifth Seminar for Homogenization and Quality Control in Climatological Databases, Budapest, 2006, WCDMP-No. 71, WMO/TD-NO. 1493, 123–130.

Szentimrey, T. et al., 2012a: Final report on quality control and data homogenization measures applied per country, including QC protocols and measures to determine the achieved increase in data quality. Carpatclim Project, Deliverable D1.12.
http://www.carpatclim-eu.org/docs/deliverables/D1_12.pdf

Szentimrey T. et al., 2012b: Final report on the creation of national gridded datasets, per country. Carpatclim Project, Deliverable D2.9. http://www.carpatclim-eu.org/docs/deliverables/D2_9.pdf

Szentimrey, T., 2013: Theoretical questions of daily data homogenization, *Időjárás 117*. 113–122.

Szentimrey, T. and *Bihari, Z.,* 2014: Manual of interpolation software MISHv1.03, Hungarian Meteorological Service.

Szentimrey, T., 2017: Some theoretical questions and development of MASH for homogenization of standard deviation, Proceedings of the 9th Seminar for Homogenization and Quality Control in Climatological Databases and 4th Conference on Spatial Interpolation Techniques in Climatology and Meteorology (Eds. *Szentimrey T, Lakatos M, Hoffmann L*), Budapest, Hungary, 2017, WCDMP-No. 85, 63–73.

Szentimrey, T., 2021: Mathematical questions of homogenization and summary of MASH, Proceedings of the 10th Seminar for Homogenization and Quality Control in Climatological Databases and 5th Conference on Spatial Interpolation Techniques in Climatology and Meteorology (Eds. *Lakatos M, Hoffmann L, Kircsi A, Szentimrey T*), Budapest, Hungary, 2020, WCDMP-No. 86, pp. 4-17

Szentimrey, T., 2023a: Overview of mathematical background of homogenization, summary of method MASH and comments on benchmark validation. *Int. J. Climatol.43*, 6314–6329.
https://doi.org/10.1002/joc.8207

Szentimrey, T., 2023b: Manual of homogenization software MASHv4.01, Varimax Limited Partnership
Szentimrey, T., 2023c: Development of new version MASHV4.01 for homogenization of standard deviation (extended abstract), Proceedings of the 11th Seminar for Homogenization and Quality Control in Climatological Databases and 6th Conference on Spatial Interpolation Techniques in Climatology and Meteorology (Eds. Lakatos M, Puskás M, Szentimrey T), Budapest, Hungary, 2023, WCDMP-No. 87. 8–13. https://library.wmo.int/idurl/4/68452
Venema et al., 2012: Benchmarking monthly homogenization algorithms. *Climate Past 8*, 89–115.
Wang, X.L. and *Y. Feng,* 2013: RHtestsV4 User Manual, Climate Data and Analysis Section – Environment and Climate Change Canada. Published online July 2013. https://github.com/ECCC-CDAS.
WMO, 2020: World Meteorological Organization Guidelines on Homogenization, WMO-No. 1245.

DOI:10.28974/idojaras.2024.2.6

IDŐJÁRÁS

Quarterly Journal of the HungaroMet Hungarian Meteorological Service
Vol. 128, No. 2, April – June, 2024, pp. 237–249

Spatiotemporal imputation of missing rainfall values to establish climate normals

Brian O'Sullivan* and **Gabrielle Kelly**

Department of Mathematics and Statistics,
University College Dublin
UCD Earth Institute

**Corresponding author E-mail: brian.osullivan3@ucdconnect.ie*

(Manuscript received in final form January 23, 2024)

Abstract— Spatial kriging interpolation has been a widely popular geostatistical method for decades, and it is commonly used to predict both gridded and missing climatic variables. Climate data is typically monitored across a variety of timescales, from daily measurements to thirty-year periods, known as long-term averages (LTAs). LTAs can be constructed from daily, monthly, or annual measurements so long as any missing values in the data are infilled first. Although spatial kriging is an available method for the prediction of missing data, it is limited to a single moment in time for each imputation. Not only can missing values only be predicted with observations measured at the same instance in time, but the entire imputation process must be repeated up to the number of timesteps in which missing data is present. This study investigates the imputation performance of spatiotemporal regression kriging, an extension of spatial regression kriging which simultaneously accounts for data across both space and time. Hence, missing data is predicted using observations from other points in time, and only a single imputation process is required for the entire data set.

Spatiotemporal regression kriging has been evaluated against a variety of geostatistical methods, including spatial kriging, for the imputation of monthly rainfall totals for the Republic of Ireland. Across all tests, the spatiotemporal methods presented have outperformed any purely spatial methods considered. Furthermore, three different regression methods were considered when de-trending the data before interpolation. Of those tested, generalized least squares (GLS) was shown to provide the best results, followed by elastic-net regularization when GLS proved computationally unavailable. Finally, the data set has been infilled using the best performing imputation method, and precipitation LTAs are presented for the Republic of Ireland from 1981–2010.

Key-words: spatiotemporal kriging, rainfall, long-term averages, missing data, imputation, kriging, Ireland, elastic-net

1. Introduction

Climate normals or LTAs are the standard measure by which the climate is described, providing the average climatic conditions experienced by a region over a thirty-year period. A thorough understanding of precipitation is crucial to numerous endeavours in Ireland, ranging from agriculture to flood risk management (*Charlton et al.,* 2006; *Naughton et al.,* 2017). During the measuring period, missing data entries commonly arise for rain gauge stations. There are various potential causes for this, such as stations being opened, closed, or moved, malfunctioning equipment, or insufficient observations taken by the station monitor. Missingness present in the data set must first be addressed before continuing with any climatological or hydrological research, including the production of LTAs. This creates the need for robust and sophisticated methods which impute missing entries as accurately as possible in order to minimize bias caused by missingness in future analysis. In this study, the performance of spatiotemporal regression kriging is explored for the purpose of imputing missing monthly precipitation totals. Elastic-net regularization (*Zou* and *Hastie,* 2005) is also investigated as a potential model to de-trend the data for regression kriging.

Kriging is a popular geostatistical method for predicting variables of interest over a spatial field. Developed originally by *Matheron* (1963), it is widely applied in a variety of fields such as environmental science, mining, and remote sensing (*Tavares et al.,* 2008; *Mondal et al.,* 2017). The method interpolates values as weighted averages of observations from nearby stations, where weights are calculated according to the estimated variance between sample stations and the target point. Numerous extensions of kriging have been explored, and popular examples include universal kriging, cokriging, and Bayesian kriging (*Handcock and Stein,* 1993; *Myers,* 1982). Universal kriging is a particularly widespread method that includes a regression of the target variable against auxiliary variables present in the data (elevation, latitude, longitude, etc.). As kriging assumes a second order stationarity across the field, it is necessary to remove any trends initially present in the data. Hence, the popularity of universal kriging when kriging interpolation is employed with climate data. Small variations to universal kriging exist, namely, regression kriging and kriging with external drift. These three methods differ slightly in their implementation, but are all generally the same technique. Regression kriging divides the approach into a two-step process, where trends in the data are first removed by regression and the remaining residuals are interpolated by ordinary kriging. The regression method achieved by universal kriging is known as generalized least squares (GLS), and this approach is theoretically optimal for a linear estimator. However, the modular approach of regression kriging allows one to consider alternative regression methods such as elastic-net regularization or principle component regression (*Zou* and *Hastie,* 2005; *Jolliffe,* 1982).

Originally proposed as a purely spatial method, kriging has been extended to spatiotemporal contexts. Known as spatiotemporal kriging, the distance between points across a temporal field is considered alongside spatial distance, such that interpolation can be achieved using a data set not bound to a single point in time (*Montero et al.,* 2015). This approach lends itself particularly well to imputation, as missing observations can have nearby temporal neighbors either before or after the target point which are observed from the same station. Additionally, the entire data set can be imputed at once, removing the need to undergo a separate kriging procedure for each time step. Spatiotemporal kriging requires the production of more sophisticated spatiotemporal covariance models (*Gräler et al.,* 2016), but otherwise it is formulated similarly to spatial kriging. Spatiotemporal kriging has been applied successfully in many contexts. For example, *Hengl* (2012) predicted daily temperatures through spatiotemporal regression kriging with a sum-metric variogram model. The remainder of this study is reported as follows: First, a short overview of the data is provided. Then, the methodology behind both elastic-net regularization and spatiotemporal regression kriging is outlined. The results comprise of the imputation performance of all considered methods, followed by a brief discussion. All research has been implemented using the *R* programming language (*R Core Team,* 2021), with a particular emphasis on the `glmnet` (*Friedman et al.,* 2010) and `gstat` (*Gräler et al.,* 2016) packages.

2. Methods

The island of Ireland has a temperate oceanic climate with an abundance of rainfall throughout the year (*Lennon,* 2015). Precipitation is monitored by Met Éireann, the Irish meteorological service, using over 1100 rain gauge stations located around the country. The considered data set consists of monthly precipitation totals from 474 stations over a thirty-year monitoring period of 1981–2010. At least 50% of data-entries from these stations are recorded as non-missing. Additionally, the data set has been considered at different levels of completeness, i.e., only considering stations with at least 70% (365 stations), 50% (474 stations), or 30% (679 stations) of their entries recorded non-missing, respectively. The rain gauge distribution of the monitoring network at station completeness cutoffs of 100%, 70%, and 30% are displayed in *Fig. 1*.

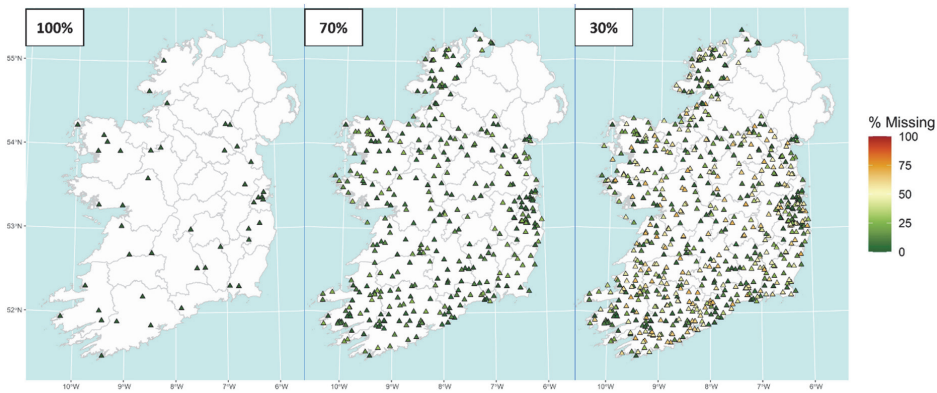

Fig. 1. Met Éireann precipitation monitoring network for the Republic of Ireland from 1981–2010. The network is presented at different completeness cutoffs (100%, 70%, and 30%, respectively).

Typically, when geospatial climate data is interpolated, any trend present in the data is removed. This is a necessity for regression kriging as the ordinary kriging step assumes a second-order stationarity with no external trend or "drift". Drift is described as the continuous change of the underlying target variable. It is modeled as a function of available predictor variables, e.g., longitude, latitude, elevation, etc., and how changes in these variables correspond with changes in the target. For linear effects, this function is simply expressed as the well-known linear model: $y = X\beta + \epsilon$. Removing drift is a fairly straightforward task, and can be done in a variety of ways. Ordinary least squares (OLS) is an elementary option, where regression parameters are determined according to the estimator: $\hat{\beta} = (X^T X)^{-1} X^T y$. However, OLS relies on the assumption that the underlying model residuals are independent and uncorrelated. Upon inspection of the variogram of residuals after regression is conducted (*Fig. 2*), this is clearly not the case. Alternatively, GLS accounts for auto-correlation between residuals by including the variance-covariance matrix of the residuals, C, in the estimator: $\hat{\beta} = (X^T C^{-1} X)^{-1} X^T C^{-1} y$. In combination with kriging, GLS gives the best linear unbiased estimator (BLUP). Besides these two unbiased regression techniques, a third method known as elastic-net regularization has also been considered.

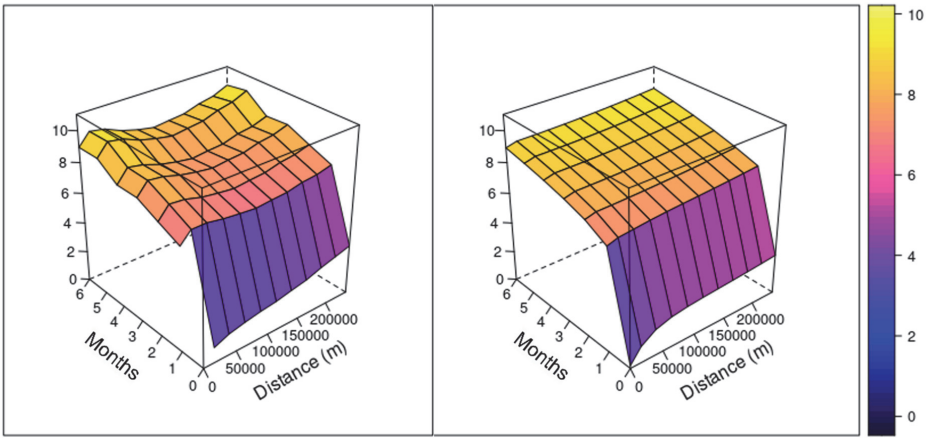

Fig. 2. Left: Empirical spatiotemporal variogram of residuals. Right: Fitted sum-metric variogram model consisting of spatial, temporal, and spatiotemporal Matérn structures.

Developed by *Zou* and *Hastie* (2005), elastic-net regularization is a technique designed to address high-dimensionality and/or highly correlated variables in a regression context. The objective function of elastic-net differs from that of OLS by the addition of a regularization penalty, L, i.e.,

$$\min_{\beta_0,\beta}\left\{\frac{1}{N}\|y-\beta_0-X\beta\|^2+L\right\}. \quad (1)$$

The elastic-net penalty is in fact a convex sum of penalties from two other methods, lasso regression and ridge regression, $L_1=\lambda\|\beta\|_1$ and $L_2=\lambda\|\beta\|_2^2$, respectively. Both penalties are designed to shrink the regression coefficients, β, present in the standard linear model by constraining either the L_1-norm or L_2-norm of all β below a constant, i.e., $\|\beta\|_1=\sum_{i=1}^{p}|\beta_i|<c$ for lasso regression and $\|\beta\|_2^2=\sum_{i=1}^{p}\beta_i^2<c$ for ridge regression. The tuning parameter, λ, determines the degree of shrinkage that is applied to the regression parameters. It is normally preselected before regression or can be fit by 10-fold cross validation using the `cv.glmnet` function available in *R* package, `glmnet` (*Friedman et al.,* 2010). By considering a linear combination of both L_1 and L_2 penalties, the elastic-net penalty is expressed as follows:

$$L_{ENet}=\lambda\sum_{i=1}^{p}(\alpha\beta_i^2+(1-\alpha)|\beta_i|). \quad (2)$$

An additional parameter, $\alpha \in [1, 0]$, is introduced which describes how closely the elastic-net penalty is to lasso ($\alpha = 1$) or ridge ($\alpha = 0$) regression. Elastic-net boasts the advantages of feature selection (from lasso) and robustness in the presence of multicollinearity (from ridge). *Table 1* describes the covariates that were considered in every regression model implemented during this study. As normally distributed data is desirable when using regression prediction methods, a square-root transformation has also been applied to the initial data before imputation. This transformation is reversed at the last step in imputation and has shown to greatly improve the imputation results.

Kriging predicts values by a weighted average method, $\bar{Y} = \sum_{i=1}^{N} w_1 Y(x_i)$, where weights, w, are assigned to nearby observations according to their spatiotemporal relationship with the target. A Gaussian random field, Y, over the spatial and temporal domains, S and T, is assumed, and each value is observed at a distinct point in space and time. That is, $Y(s, t)$ is the total monthly precipitation measured by the station located at s for the month, t. The target variable is considered as a sum of deterministic components, $m(s, t)$, and random components, $\epsilon(s, t)$:

$$Y(s, t) = m(s, t) + \epsilon(s, t). \tag{3}$$

The central idea of kriging is the assumption that Y is second-order stationary so long as the deterministic component, $m(s, t)$, is constant. Here is why any drift present in the data must initially be removed before kriging. Once second-order stationarity is achieved, the covariance between any pair of observations does not depend on their positions, but only on the distance between them. This allows the introduction of the variogram which models the semivariance of point pairs, i.e., the dependence between them with respect to their separation:

$$\gamma(s_1, t_1, s_2, t_2) = \frac{1}{2} Var\{Y(s_1, t_1) - Y(s_2, t_2)\} = \gamma(h, u). \tag{4}$$

All data entries, $x = x(s, t)$, are separated both spatially, h, and temporally, u. The construction of γ is done over multiple steps. An empirical variogram is first created from the observed data, where all available point pairs are grouped into bins according to their separation. The average γ of each bin is calculated and plotted, upon which a parametric representation of γ is fitted to the empirical variogram using the limited-memory BFGS algorithm in `gstat` (L-BFGS). Generally, the parametric form of a purely spatial variogram is as follows:

$$\gamma(h) = \tau^2 + \sigma^2(1 - \rho(h)) \tag{5}$$

The correlation, $\rho(h)$, is a monotonic decreasing function where $\rho(0) = 1$ and $\rho(h) = 0$ as $h \to \infty$. Three parameters are needed to represent the variogram model – the nugget τ^2, the sill $\tau^2 + \sigma^2$, and the range ϕ (*Diggle* and *Giorgi,*

2019). For Matérn covariance models, an additional parameter must be considered, κ, which is known as the "shape".

With these parameters, various covariance models can be fit to the spatial empirical variogram. Popular models include the Spherical, Gaussian, Exponential, and Matérn models. A Matérn structure was used throughout this study and was found to provide the best imputation performance. Its structure contains a modified Bessel function of order, $\kappa(K_\kappa(h/\phi))$, and a Gamma function $\Gamma(\kappa)$. It is presented below:

$$\rho(h) = \{2^{\kappa-1}\Gamma(\kappa)\}^{-1}(h\phi^{-1})^{\kappa}K_\kappa(h\phi^{-1}). \quad (6)$$

A variety of covariance models are available for the spatiotemporal context (*Gräler et al.,* 2016). The sum-metric structure was applied by *Hengl et al.* (2012) for daily temperature data and has been found to be similarly suitable for this study. The sum-metric model consists of three components, a spatial variogram $\gamma_s(h)$, a temporal variogram $\gamma_t(u)$, and a joint variogram, $\gamma_{joint}(\sqrt{h^2 + (\chi \cdot u)^2})$:

$$\gamma(h,u) = \gamma_s(h) + \gamma_t(u) + \gamma_{joint}(\sqrt{h^2 + (\chi \cdot u)^2}). \quad (7)$$

Each component has been modeled using a Matérn correlation structure (Eqs. 5 and 6) with their own distinct fitted parameters (σ^2, τ^2, ϕ, and κ). The third term, γ_{joint}, also contains an anisotropy term, χ, allowing temporal separation to be scaled relative to an equivalent spatial distance. The anisotropy adds an additional parameter to the sum-metric model, bringing the number of parameters needed to be fit by L-BFGS to thirteen (four for each Matérn structure and χ). *Fig. 2* displays the fitted spatiotemporal variogram for the de-trended precipitation data. Notably, the dependency is observed to be much stronger spatially than temporally. As the data is expressed in monthly time steps, the weaker temporal dependency may be attributed to the long period of time between data entries.

Once a variogram of the residuals has been produced and fitted, prediction weights, w, can be calculated through the kriging system of equations. For ordinary kriging, the mean, $m(s,t)$, is assumed unknown, however, this can be relaxed by introducing the constraint that all weights add to one: $\sum_{i=1}^{M} w_i = 1$. The missing value at target point, $x_0 = x(s_0,t_0)$, is predicted by a weighted average of the $M = 700$ nearest observations over all space and time, x_i, $by\ \sum_{i=1}^{M} w_i Y(x_i)$. The ordinary kriging system of equations is given by Eq. (8), where $\gamma(x_i,x_j)_{M\times M}$ is an $M \times M$ matrix of the semivariances between all observed point pairs considered in the kriging system, and $\gamma(x_0,x_i)_{M\times 1}$ is a column vector of the semivariances between the target and the observed points:

$$\gamma(x_i, x_j)_{M\times M} w_{M\times 1} = \gamma(x_0, x_i)_{M\times 1} \qquad \sum_{i=1}^{N} w_i = 1 \qquad (8)$$

Inverse distance weighting (IDW) is a simple benchmark method which also predicts target points by weighted average. Instead of modeling a dependency structure like kriging however, an inverse spatial power law is assumed, and the corresponding weights are described as $w = h^{-2}$. The imputation performance of three methods have been evaluated: inverse distance weighting, spatial regression kriging, and spatiotemporal regression kriging. Any trend present in the data (*Table 1*) has been removed prior to interpolation for all methods. Furthermore, three trend removal procedures were considered for spatiotemporal kriging: OLS, elastic-net, and GLS. When implementing GLS, the variance-covariance matrix, C, is obtainable through the modeled theoretical variogram. This is ultimately achieved by an iterative process, where residuals are first obtained to produce the variogram, and regression is repeated using GLS and the now modeled dependency structure. Unfortunately for larger data sets, inversion of C proved computationally unattainable. Tests have been conducted on two data sets from 1981–2010: 474 stations across the Republic of Ireland and a smaller subset of 27 stations in Greater Dublin. Inclusion of the smaller data set allows GLS spatiotemporal kriging to be considered. The imputation of each method was evaluated under 10-fold cross-validation using three performance metrics: root mean squared error (RMSE), relative RMSE ($RMSE_R$), the RMSE normalized by the deviation of the observed data, and R^2, the percentage of variance explained between observed (y) and predicted values ($\hat{y}$):

$$RMSE = \sqrt{\frac{\sum_{i=1}^{N}(y_i - \hat{y}_i)^2}{N}}; \quad RMSE_R = \frac{RMSE}{\sigma}; \quad R^2 = 1 - \frac{\sum_i (y_i - \hat{y}_i)^2}{\sum_i (y_i - \bar{y}_i)^2}. \qquad (9)$$

Table 1. All covariates used when removing trends in precipitation data by regression.

Covariate	Description
east & east^2	Easting, Irish Grid TM75 (m/m^2)
north & north^2	Northing, Irish Grid TM75 (m/m^2)
east × north	Easting/Northing interaction (m^2)
points5 & points5^2	Mean elevation in 5 km radius around station (m/m^2)
exp25k	Ocean cover within 25 km radius of station (%)
t	Time of observation in months from January 1981 to December 2010 (i.e., $t \in (1, 360)$)

3. Results

Imputation performance is reported in *Table 2*. Across all three metrics (RMSE, $RMSE_R$, and R^2), it is clear that the inclusion of a temporal component in the imputation method greatly benefits the prediction accuracy for both large and small data sets. Moreover, this improvement is shown to be consistent throughout the year in *Fig. 3*, where the spatiotemporal methods tested provide a steady improvement for every month. With regards to the regression method applied, elastic-net has shown to slightly outperform OLS in both cases, although GLS expectedly produces the best results when available. Notably, the choice of regression method has a considerably lower impact on imputation accuracy when compared to the introduction of spatiotemporal approaches.

Table 2. 10-fold cross validation results for Republic of Ireland and Greater Dublin. For the 474 stations, ST-kriging with GLS was unavailable due to computational intractability

	Republic of Ireland (474 stations)			**Greater Dublin (27 stations)**		
Method	RMSE	$RMSE_R$	R^2	RMSE	$RMSE_R$	R^2
IDW	21.21mm	30.28%	0.909	15.69 mm	29.81%	0.911
Spatial Kriging	20.61mm	29.41%	0.914	18.13 mm	34.44%	0.884
ST-Kriging	17.47mm	24.94%	0.938	14.05 mm	26.70%	0.929
ST-Kriging ENET	17.42mm	24.86%	0.938	13.89 mm	26.39%	0.930
ST-Kriging GLS	-	-	-	13.80 mm	26.23%	0.931

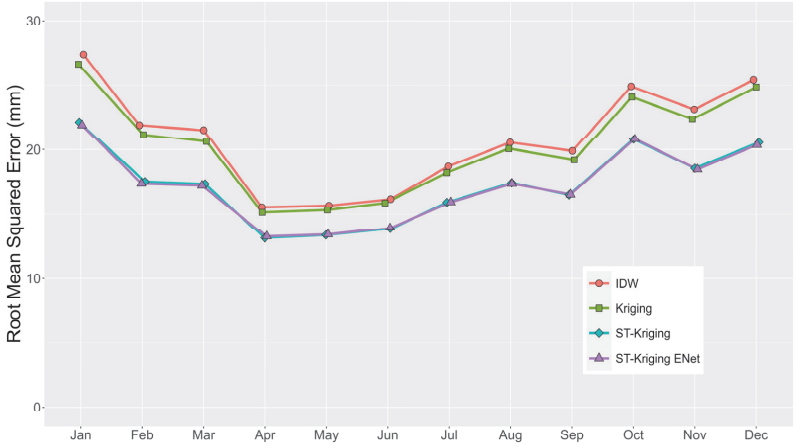

Fig. 3. Monthly RMSE calculated by 10-fold cross validation of the network with a completeness cutoff of 50%. Spatiotemporal methods are shown to consistently outperform throughout the year.

In addition to *Table 2*, further tests have been conducted where the data set comprises of increasingly incomplete stations. Three data sets have been tested where the included stations have a completeness of at least 70%, 50%, or 30%, respectively. The best performing method for large data sets, spatiotemporal kriging with elastic-net, was evaluated alongside these data sets to explore how the method performs against progressively sparser data. Results from *Table 3* demonstrate that the inclusion of less complete stations improves the overall RMSE. However, no improvement in $RMSE_R$ was observed between a cutoff completeness of 50% and 30%. $RMSE_R$ allows imputation performance to be compared across different data sets, a benefit which is unavailable to RMSE (*Hengl,* 2007). Thus the results indicate that the appropriate completeness cutoff to consider during imputation lies somewhere close to the range of 50% to 30%.

Table 3. 10-fold cross validation results according to different completeness cutoffs. Imputation is achieved by spatiotemporal kriging with elastic-net.

% Missing	No. Stations	RMSE (mm)	$RMSE_R$ (%)	R^2
70%	365	17.89	25.18	0.937
50%	474	17.42	24.86	0.938
30%	679	17.15	24.86	0.938

Once the data set is fully imputed, LTAs can finally be produced. *Fig. 4* demonstrates the monthly precipitation LTAs for the island of Ireland, created using the fully imputed data set with a 50% completeness cutoff. All missing data entries were first imputed by elastic-net spatiotemporal kriging, then monthly averages were calculated and interpolated on to a 1 km × 1 km grid. Notably from *Fig. 1*, no rain gauge stations were available for Northern Ireland in this study, and as such, the interpolated values are not expected to sufficiently represent the precipitation over this region. Overall, a mean monthly rainfall of mm is reported from 1981–2010, with an increase in rainfall observed in the west and southwest of the island, particularly during the winter months.

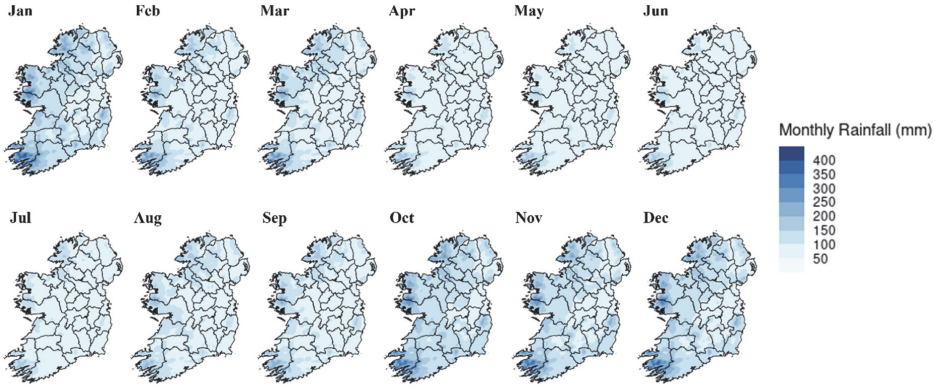

Fig. 4. Gridded long-term averages of monthly precipitation from 1981–2010 (1 km × 1 km).

4. Conclusion

A spatiotemporal regression kriging method has been demonstrated to show improved imputation capabilities when compared to its purely spatial counterpart. Furthermore, elastic-net regularization has shown to be a suitable regression method to remove any trend present in a climatic data set. Although GLS provides slightly better results, it is not always available when working with large data sets, which is typically the case in a spatiotemporal context. Given the achieved results, spatiotemporal kriging is presented as a viable option for the imputation of incomplete precipitation data sets. The small adjustment from OLS to elastic-net when removing trend may also be worthwhile, as improved imputation can be achieved for very little additional computational cost. For spatiotemporal kriging, however, it is noted that the increased computation is significant, even when GLS is not considered. The recorded computational time needed to impute for the 50% completeness cutoff 474 stations using spatial kriging was 29.29 seconds, far smaller than the 6.48 hours required for spatiotemporal kriging.

For future research, improving the computational viability of GLS is of utmost concern, potentially via a likelihood-based or Bayesian approach to model fitting. Additionally, the entire island of Ireland may be considered by including data from the Northern Ireland rainfall monitoring network managed by the United Kingdom Meteorological Office. This is generally standard procedure in other climatological research from Met Éireann (*Walsh,* 2016), and would allow for a more comprehensive overview of the complete island. Spatiotemporal kriging may also lend itself well in the imputation for other climatic variables such as temperature or wind speed. Evidently, the temporal dependency is much

stronger amongst such variables, a property that which would allow spatiotemporal kriging to yield substantial improvements. However, for Ireland, the observation coverage of rainfall is considerably higher than many other variables, and the lack of sufficient data may limit the capabilities of these more sophisticated imputation methods.

Acknowledgements: We wish to extend our sincere gratitude to Met Éireann for their invaluable provision of the monthly precipitation data for Ireland used throughout this study.
This work was conducted with the financial support of Science Foundation Ireland (SFI) under Grant Number SFI 18/CRT/6049.

References

Charlton, R., Fealy, R., Moore, S., Sweeney, J., and *Murphy, C.,* 2006: Assessing the Impact of Climate Change on Water Supply and Flood Hazard in Ireland Using Statistical Downscaling and Hydrological Modelling Techniques. *Climatic Change 74,* 475–491. https://doi.org/10.1007/s10584-006-0472-x

Diggle, P. and *Giorgi, E.,* 2019: *Model-based Geostatistics for Global Public Health: Methods and Applications.* Chapman and Hall/CRC, New York. 35–37. https://doi.org/10.1201/9781315188492

Friedman, J. H., Hastie, T., ***and*** *Tibshirani, R.,* 2010: Regularization Paths for Generalized Linear Models via Coordinate Descent. *J. Stat. Software 33,* 1–22. https://doi.org/10.18637/jss.v033.i01

Gräler, B., Pebesma, E., and *Heuvelink, G.,* 2016: Spatio-Temporal Interpolation using gstat. *The R Journal 8, 1,* 204–218. url: https://journal.r-project.org/archive/2016/RJ-2016-014/index.html

Handcock, M. S. and *Stein, M. L.,* 1993: A Bayesian Analysis of Kriging. *Technometrics 35,* 403–410. https://doi.org/10.2307/1270273

Hengl, T., 2007: A Practical Guide to Geostatistical Mapping of Environmental Variables. Office for Official Publications of the European Communities, Luxembourg, 118–119. https://publications.jrc.ec.europa.eu/repository/handle/JRC38153

Hengl, T., Heuvelink, G. B. M., Tadíc, M. P., and *Pebesma, E. J.,* 2012: Spatio-temporal prediction of daily temperatures using time-series of MODIS LST images. *Theor. Appl. Climatol. 107*, 265–277. https://doi.org/10.1007/s00704-011-0464-2

Jolliffe, I. T., 1982: A Note on the Use of Principal Components in Regression. *J. Roy. Stat. Soc. Series C: Appl. Stat. 31,* 300–303. https://doi.org/10.2307/2348005

Lennon, J. J., 2015: Potential impacts of climate change on agriculture and food safety within the island of Ireland. *Trends Food Sci. Technol. 44,* 1–10. https://doi.org/10.1016/j.tifs.2014.07.003

Matheron, G., 1963: Principles of geostatistics. *Econ. Geol. 58,* 1246–1266. https://doi.org/10.2113/gsecongeo.58.8.1246

Mondal, A., Khare, D., Kundu, S., Mondal, S., Mukherjee, S., and *Mukhopadhyay, A.,* 2017: Spatial soil organic carbon (SOC) prediction by regression kriging using remote sensing data. *The Egyptian J. Remote Sens. Space Sci. 20,* 61–70. https://doi.org/10.1016/j.ejrs.2016.06.004

Montero, J., Fernándes-Avilés, G., and *Mateu, J.,* 2015: Spatial and Spatio-Temporal Geostatistical Modeling and Kriging. Wiley, New York. 266–279. https://doi.org/10.1002/9781118762387

Myers, D.E., 1982: Matrix formulation of co-kriging. *Math. Geol. 14,* 249–257. https://doi.org/10.1007/BF01032887

Naughton, O., Johnston, P. M., and *Gill, L. W.,* 2017: Groundwater flood risk mapping and management: examples from a lowland karst catchment in Ireland. *J. Flood Risk Manage. 10,* 53–64. https://doi.org/10.1111/jfr3.12145

R Core Team, 2021: *R:* A Language and Environment for Statistical Computing. R Foundation for Statistical Computing, Vienna, Austria. https://www.R-project.org/

Tavares, M.T., Sousa, A.J., and *Abreu, M.M.,* 2008: Ordinary kriging and indicator kriging in the cartography of trace elements contamination in São Domingos mining site (Alentejo, Portugal). *J. Geochem. Explor. 98,* 43–56. https://doi.org/10.1016/j.gexplo.2007.10.002

Walsh, S., 2016: Long-term rainfall averages for Ireland, 1981–2010. 15, Climatological Note, Met Éireann. http://hdl.handle.net/2262/76135

Zou, H. and *Hastie, T.,* 2005: Regularization and Variable Selection via the Elastic Net. *J. Roy.Stat. Soc. Series B (Stat. Methodol.) 67,* 301–320. https://doi.org/10.1111/j.1467-9868.2005.00503.x

DOI:10.28974/idojaras.2024.2.7

IDŐJÁRÁS

Quarterly Journal of the HungaroMet Hungarian Meteorological Service
Vol. 128, No. 2, April – June, 2024, pp. 251–266

Annual and seasonal ANOVA and trend analysis of sub-daily temperature databases in Hungary

Zsófia Barna* and **Beatrix Izsák**

HungaroMet Hungarian Meteorological Service,
Kitaibel Pál Street 1, H-1024, Budapest, Hungary

**Corresponding author E-mail: zsofibarna0528@gmail.hu*

(Manuscript received in final form February 20, 2024)

Abstract— Commonly studying climate is gaining more and more space thanks to the expansion of the tools of statistical climatology and the development of the informatical background. Trend analyses of annual and seasonal mean temperature values clearly show that the Hungarian values are mostly in line with the global trend, and in some cases exceed it. Since a sufficient number of measurements are only available from the 1970s, we used hourly temperature values (03 UTC, 09 UTC, 15 UTC, 21 UTC) of the period 1971–2020 for station data series in Hungary for the trend analysis. In order to make the examined datasets sufficiently representative, we homogenized the station data series, filled in data gaps, and performed quality control using the MASH software. To ensure spatial representativeness, we interpolated the homogenized station data onto a dense, regular grid network with the MISH system. In addition, we used the ANOVA method to examine the expected values, standard deviations assigned to the hourly values, and we analyzed on maps how the values within the day changed in each region over 50 years.

Key-words: ANOVA, trend analysis, sub-daily temperature data, MASH software, MISH software, Hungary

1. Introduction

Climate change and its corresponding professional background knowledge have now become especially important. The examination of the past and present climate also plays an important role worldwide, especially with regard to investigations related to the process of climate change. In order to get an adequate picture of the detected changes, we can work with six-hourly temperature datasets. It is quite important that when modeling hourly values compared to daily data, we

had to determine the regression coefficients, since we cannot interpolate in the same way within a day, since the expected values differ for example at dawn and at noon, and it can also be seen that there is a strong stochastic relation between the daily and hourly values. The hourly values were homogenized, the missing data were filled in, and then the available values were interpolated into the points where no measurements were taken. The purpose of this research is to examine the database of four hourly values within a day to see how much they changed overall during the research period, i.e., between 1971–2020. We used linear trend analysis for this comparing the changes that took place by area between the databases. Moreover, we also examined the databases and their differences and similarities using the ANOVA methodology.

2. Data

Six-hourly UTC (03 UTC, 09 UTC, 15 UTC, 21 UTC) measurements were used for the analysis. First, we did a homogenization process by applying the MASH system (*Szentimrey,* 2017) in order to fill in all the data gaps, followed by interpolation. The interpolation method was done by MISH (*Szentimrey* and *Bihari,* 2007*,* 2014). In the case of 03 UTC 47, 09 UTC 49, 15 UTC 49, and 21 UTC 55 station data series were available for this study. After the homogenization we interpolated the homogenized station data series to 1233 grid points which corresponds to 0.1° resolution (*Fig. 1*). Then we chose a much more detailed 0.5' resolution grid for interpolation to produce the trend maps. Due to the large number of missing data, we had to leave the very incomplete stations during the homogenization (*Szentimrey et al.,* 2014a).

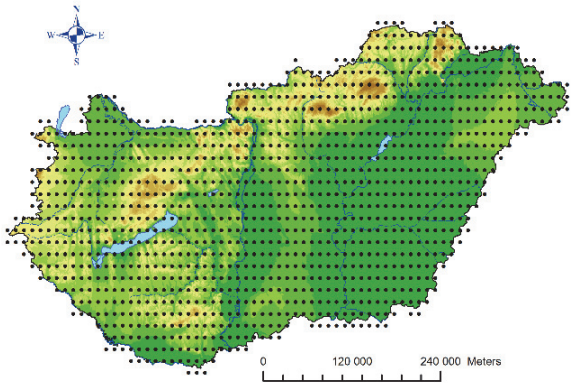

Fig. 1. The geographical location of the 1233 grid points in Hungary (EPSG:4326: WGS 84).

3. Interpolating sub-daily values with MISH, description of the methodology

Applying the MISH interpolation system compared to other methods used in climate research has a much smaller interpolation error in the interpolated data series, so its use is much more recommended for meteorological data compared to other interpolation methods (*Barna et al.,* 2023; *Izsák et al.,* 2023). This is due to the fact that in meteorology we cannot assume that there is no spatial trend, as the complex orography of the country means that different regions have different expected values.

Fig. 2 shows the montly difference of the six-hourly temperature values from the daily mean, and according to that we can declare that at 09 and 15 UTC the values are higher than the daily mean, furthermore, for 03 UTC and 21 UTC the daily mean value is higher than this two hourly value during the whole year. This can help in the decision when determining the regression parameters for interpolating the sub-daily hourly values (*Izsák,* 2023). Below we describe the metodology of interpolating hourly temperature values (*Szentimrey,* 2019).

Fig. 2. Monthly difference of the six-hourly temperature values from the daily mean values (°C).

The following interpolation formula (additive model) is applied for the daily mean temperature data (*Szentimrey et al.,* 2011, 2014b):

$$\hat{Z}(\boldsymbol{s}_0) = \sum_{i=1}^{M} \lambda_i \big(E(\boldsymbol{s}_0) - E(\boldsymbol{s}_i)\big) + \sum_{i=1}^{M} \lambda_i Z(\boldsymbol{s}_i)\,, \qquad (1)$$

where $Z(\boldsymbol{s}_0)$ (s: location) is a predictand, $Z(\boldsymbol{s}_i)$ $(i = 1,\dots,M)$ are predictors (observations), and the weighting factors $\sum_{i=1}^{M} \lambda_i = 1$ and λ_i $(i = 1,\dots,M)$ depend on the stochastic relations, while $E(\boldsymbol{s}_i)$ $(i = 0,\dots,M)$ are the daily spatial trend values (*Szentimrey,* 2019).

The optimal interpolation parameters λ_i $(i = 1,\dots,M)$ minimize the root-mean-square error, and these are known functions of the climate statistical parameters (*Szentimrey,* 2019*,* 2020).

Based on the daily interpolation formula, the following formula is applied to the $t = 03, 09, 15, 21$ UTC values, accepting the weighting factors:

$$\hat{Z}(\boldsymbol{s}_0, t) = \sum_{i=1}^{M} \lambda_i \big(E(\boldsymbol{s}_0, t) - E(\boldsymbol{s}_i, t)\big) + \sum_{i=1}^{M} \lambda_i Z(\boldsymbol{s}_i, t)\,, \quad (t = 03, 09, 15, 21) \tag{2}$$

where $E(\boldsymbol{s}_i, t)$ $(i = 0,\dots,M)$ represents the spatial trend values for the given times.

To model the $E(\boldsymbol{s}, t)$ $(t = 3{,}9{,}15{,}21)$ hourly spatial trend values, the following linear model was chosen:

$$E(\boldsymbol{s}, t) = \alpha(t) + \beta(t) \cdot E(\boldsymbol{s}) \qquad (t = 03, 09, 15, 21). \tag{3}$$

In this case, the interpolation formula for hourly values is given as follows:

$$\hat{Z}(\boldsymbol{s}_0, t) = \beta(t) \cdot \Big(\sum_{i=1}^{M} \lambda_i \big(E(\boldsymbol{s}_0) - E(\boldsymbol{s}_i)\big)\Big) + \sum_{i=1}^{M} \lambda_i Z(\boldsymbol{s}_i, t) \quad (t = 03, 09, 15, 21). \tag{4}$$

Thus, the modeled daily spatial trend values $E(\boldsymbol{s}_i)$ $(i = 0,\dots,M)$ and the estimated $\beta(t)$ $(t = 03, 09, 15, 21)$ hourly regression coefficients can be used to interpolate the hourly values (*Szentimrey*, 2019).

Looking at the average test statistics it is clear, that the correlation differs significantly from zero assumed in the null hypothesis. Moreover, these correlations allow us to conclude that there is a strong relationship between the daily and the six-hourly values. For example, if we choose a significance level of 0.05 considering a t-test statistic for a 50-year data series, the critical value for an individual station is 2.01. Summarizing the results of *Table 1*, the model for gridding of the daily values can be used to produce the gridded hourly values. According to *Table 1*, there is a large difference between the regression coefficients (β) related to measurements at 03 UTC, 09 UTC, 15 UTC, and 21 UTC. *Table 2* illustrates that hourly spatial trends can be well determined by linear regression on daily spatial trend (*Szentimrey,* 2019).

Table 1. Alpha and beta regression parameters for 12 months and for the 4 hourly values

	T03		T09		T15		T21	
	alpha	**beta**	**alpha**	**beta**	**alpha**	**beta**	**alpha**	**beta**
1	-1.34	0.91	-0.18	0.92	2.00	1.24	-0.48	1.01
2	-1.82	0.90	0.23	0.97	2.77	1.32	-0.60	0.95
3	-1.90	0.77	0.95	1.00	2.58	1.28	-0.74	0.94
4	-1.00	0.69	0.92	1.08	1.50	1.27	-0.01	0.86
5	0.34	0.66	0.73	1.07	-0.23	1.28	0.39	0.85
6	2.16	0.63	1.19	1.05	-0.75	1.27	0.24	0.87
7	2.34	0.63	0.31	1.09	-1.19	1.28	0.17	0.88
8	2.22	0.65	1.57	1.03	-1.89	1.35	-0.29	0.90
9	1.09	0.68	0.35	1.10	-2.01	1.43	-1.48	0.97
10	0.22	0.68	0.45	1.10	-0.72	1.47	-0.52	0.91
11	-0.59	0.80	0.69	0.97	0.64	1.35	-0.85	1.00
12	-0.73	0.95	-1.15	0.89	1.90	1.07	0.07	1.08

Table 2. Correlations (corr) and t-test statistics (tstat) for 12 months and for the 4 hourly values

	T03		T09		T15		T21	
	corr	**tstat**	**corr**	**tstat**	**corr**	**tstat**	**corr**	**tstat**
1	0.94	18.18	0.97	28.90	0.93	17.19	0.95	23.05
2	0.89	12.81	0.95	20.50	0.90	14.20	0.94	20.11
3	0.84	10.55	0.90	13.97	0.88	13.02	0.89	14.32
4	0.75	7.72	0.88	12.51	0.90	14.03	0.82	10.25
5	0.78	8.34	0.91	14.60	0.93	17.86	0.85	11.78
6	0.74	7.35	0.91	14.79	0.93	17.48	0.84	11.39
7	0.66	5.96	0.90	13.78	0.90	14.15	0.78	9.13
8	0.69	6.34	0.86	11.65	0.88	12.60	0.77	8.91
9	0.71	6.74	0.85	11.25	0.88	13.01	0.84	11.47
10	0.71	6.68	0.85	11.28	0.86	11.70	0.81	9.95
11	0.82	9.48	0.91	14.59	0.90	14.27	0.93	19.07
12	0.95	19.71	0.96	23.87	0.93	16.77	0.95	22.81

Next, we examined the data series using linear trend analysis and the ANOVA method for comparison of the hourly datasets to each other (*Szentimrey,* 1989). The applied methodology is the same as described for the analysis of the six-hourly databases (*Barna et al.,* 2021*,* 2022). In detailing the results using

ANOVA method, we present a comparison of the six-hourly datasets produced and examine the expected values and standard deviations for the extended area of Hungary. ANOVA methodology can also be used to examine the anomaly values. As a result it can be concluded that in the warmer years (1992, 2003, 2007) of the period under study (1971–2020), the anomaly relative to the mean is larger for 09 and 15 UTC than for 03 and 21 UTC. The highest positive anomaly values can be associated to the southern Great Plain areas, and the lowest (negative) values can be assigned to the extensive surroundings of our mountains and lakes.

4. Results

4.1. ANOVA

Turning to the results, *Fig. 3* illustrates the spatial expected values between 1971–2020 for the four hourly values, and *Fig. 4* represents the temporal expected values where the examination period is also 1971–2020. In accordance to our expectations, the 21 UTC values are below the average daily temperature values, but the 09 UTC values can already be related to the 18 UTC data series examined earlier *Barna et al.* (2021). The 15 UTC data clearly have the highest values among the shown data series. Looking at the spatial distribution of the values in Hungary, the central part of Transdanubia and the southern Great Plain region can be characterized by higher values in the morning, Similar spatial trend can be observed at 09 UTC, where higher values can be attributed to the southern areas of the country, particularly the Körös-Maros region (12–14 °C). Also for 15 UTC, lower values are obtained in the northern part of Hungary. The 21 UTC data series are lower values in the Northern Central Mountains and the Transdanubian Central Mountains, compared to the rest of the country.

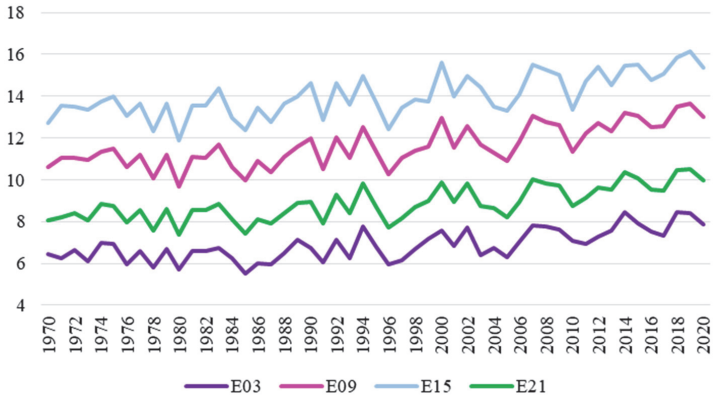

Fig. 3. Yearly spatial expected values for hourly values (03 UTC, 09 UTC, 15 UTC, 21 UTC) (1971–2020) (^{0}C).

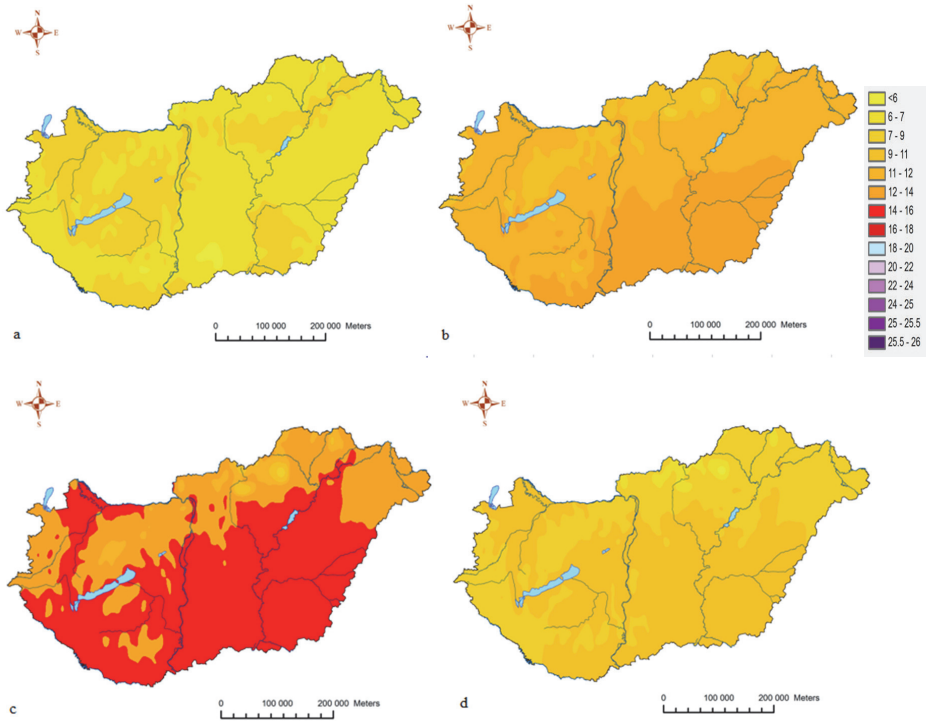

Fig. 4. Yearly temporal expected values for hourly values (03 UTC (a), 09 UTC (b), 15 UTC (c), 21 UTC (d)) (1971–2020) (ºC).

Examining the spatial distribution of the standard deviation values, it can be said that the 03 UTC database is the least variable, and the 15 UTC database is considered the most variable according to *Fig. 5*. Compared to the analyses for the main terminus measurements (*Barna et al.,* 2021), here we can already assign higher standard deviation values to the data series. Looking at the maps comparing temporal standard deviations, the 03 UTC case is the least variable (*Fig. 6*). *Fig. 6* shows that the southern regions of the country exibit the lowest standard deviation, with minimum values below 0.6. Compared to 09 UTC, higher standard deviations can be assigned to the central parts of the country. In case of the 15 UTC, two contiguous areas with standard deviation above 1.15 can be seen, which was not seen previously the border areas between Körös-Maros and the northwestern borderside of the country. The 21 UTC case also proves to be less variable with higher values in the southwestern part of the country.

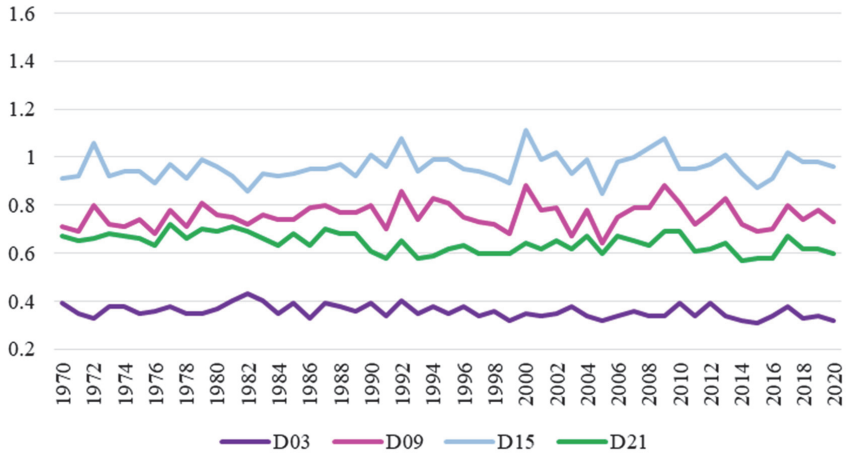

Fig. 5. Yearly spatial standard deviation values for hourly values (03 UTC, 09 UTC, 15 UTC, 21 UTC) (1971-2020) (^{0}C).

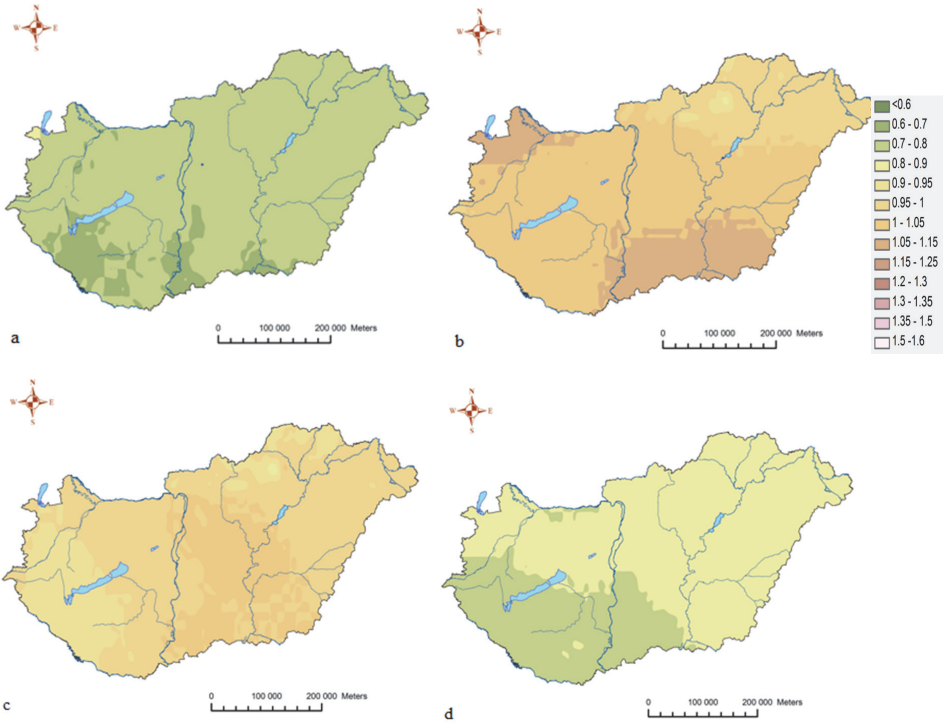

Fig. 6. Yearly temporal standard deviation values for hourly values (03 UTC (a), 09 UTC (b), 15 UTC (c), 21 UTC (d)) (1971–2020) (^{0}C).

All in all, the diagrams above show the spatial standard deviations and the maps show the average of the temporal standard deviations in the whole area of Hungary. If we examine the average temperature, the average of the variances over time is the largest (*Barna et al.,* 2021). The consequence is that since the temporal variance are higher (*Table 3*), longer data series are needed for each test. If the spatial variability were greater, many more station data series would be required to conduct the desired analyses. For example, when examining the 15 UTC data series based on *Fig. 6*, we need a much denser spatial coverage than the 03 UTC data, because the values are much more variable due to the greater spatial dispersion. On the other hand, if the variance in time is larger, a long sample is required for accurate estimates.

Table 3. Yearly Anova statistics

Yearly Anova statistics	**T03**	**T09**	**T15**	**T21**
Total mean	6.88	11.62	14.03	8.86
Total variance	0.66	1.50	1.94	1.06
Spatial variance of temporal means	0.11	0.55	0.89	0.40
Spatial mean of temporal variances	0.55	0.95	1.05	0.67
Temporal variance of spatial means	0.53	0.93	1.02	0.65
Temporal mean of spatial variances	0.13	0.58	0.92	0.41

4.2. Trend analysis

In this section, we present the results of the trend analysis which looks at how the data series changed over time. It is important that the trend maps show the change over the entire period, not the direction tangent. We examined the hourly data series on an annual and seasonal scales. We fitted linear trend to the data series. Annual changes are presented first (*Fig. 7*). We tested the estimated trend at the significance level of 0.1. With the exception of winter, we identified significant change for the entire area of Hungary. Regarding the 03 UTC trend values, an area characterized by values below 1.5 °C can be observed. In case of 09 UTC, values above 2.5 °C occur in the central parts of the country. Even the trends for the 15 UTC database, values above 2 °C indicated across the country, lower values can be seen in the northeastern areas of the country. However, the spatial distribution of the 21 UTC trend values shows a very diverse pattern. Values below 1.75 °C are typical in the southeastern areas of the country. Moving eastwards, higher and higher values are visible, in the central part of the country the trend values ranging from 1.75–2.25 °C. Besides in the northeastern part of the country, values between 2.25 and 2.5 °C appear.

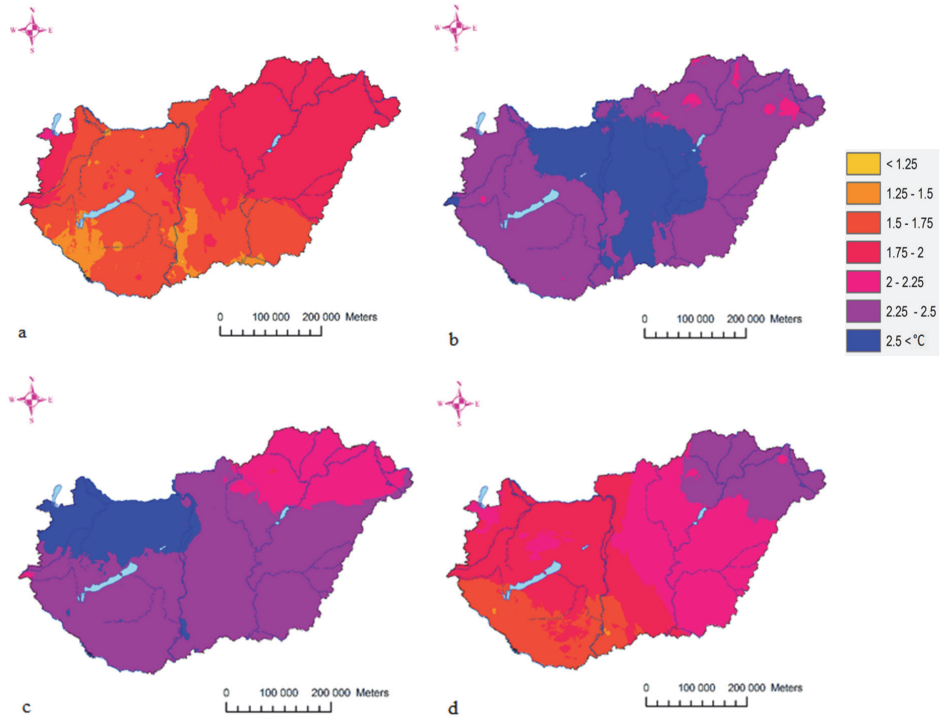

Fig. 7. The values of yearly change over the whole period (1971–2020), for hourly values (03 UTC (a), 09 UTC (b), 15 UTC (c), 21 UTC (d)), with linear trend estimation (ºC). The change is significant at the 0.1 significance level in the entire area of Hungary.

Let us have a look at how the spring trends are shaping up. Based on *Fig. 8* we can see that the spatial distribution of the 03 UTC trends has an area with the highest values appearing along the northwestern border. Apart from this, the trend values remain below 2 °C in the rest of the country. Values below 1 °C also appear in the extended area of the Danube and the Körös-Maros region. The largest area trends above 2.5 °C were obtained in the 09 UTC database. In addition, the southern Transdanubian region and the eastern area of the Great Plain can also be characterized by trends above 2 °C. A northwestern region can be characterized by values above 2.5 °C at 15 UTC. Going east these values decrease continuously, so in the areas south from the Danube and west from the Tisza, values above 2.25 °C appear and further east above 2 °C then above 1.75 °C. Examining the 21 UTC case it can be said, that the spatial distribution of the values can be best identified with the 18 UTC case examined in *Barna et al.* (2021). However, in terms of the order of magnitude of the values as a result of the trend analysis, this database is characterized by lower values. Trend values below 1 °C also appear in the southern areas of the country, and the highest values above 2 °C can be assigned to the northeastern area.

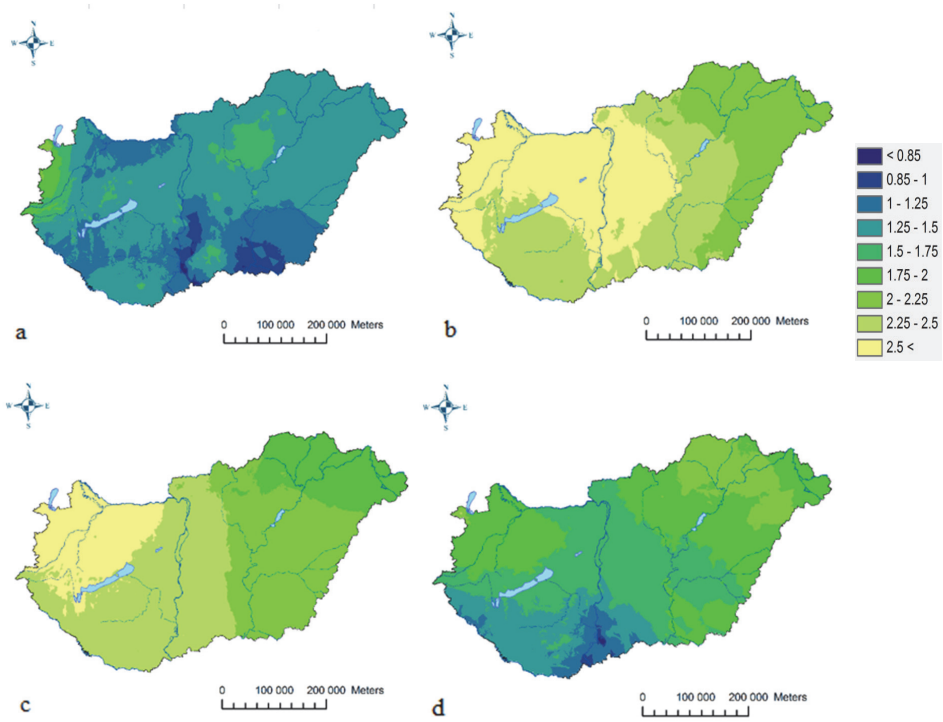

Fig. 8. The values of spring change over the whole period (1971-2020), for hourly values (03 UTC (a), 09 UTC (b), 15 UTC (c), 21 UTC (d)), with linear trend estimation (ºC). The change is significant at the 0.1 significance level in the entire area of Hungary.

Fig. 9 illustrates the results of the summer trend analysis. The lowest trend values can be assigned to the 03 UTC case. However, as we expect it, as they are summer tests, they are higher compared to the results of the other seasons and the 03 UTC database's annual results. The lowest values (<2.25 °C) appear in the Transdanubian areas and the Southern Great Plain region. Examining the trend values of 09 UTC, lower values appear in the southwestern and northeastern areas of the country compared to the central areas, but these are also above 3 °C. Comparing all the cases analyzed, it is clear that the highest values appear for 15 UTC. Along the northeastern border, where the lowest values also occurred, we can declare values above 3 °C. With the exception of this region temperature, values above 3.25 °C are typical throughout the country. For the 21 UTC dataset, the overall values are lower compared to the results of trend estimation for the 09 and 15 UTC data. The 21 UTC hourly trend values are the lowest along the southwestern border and continue to increase as we move towards the eastern half of the country. To the east from the Danube, except for the southern areas of the Danube-Tisza region, the typical estimated trends are already above 2.75 °C.

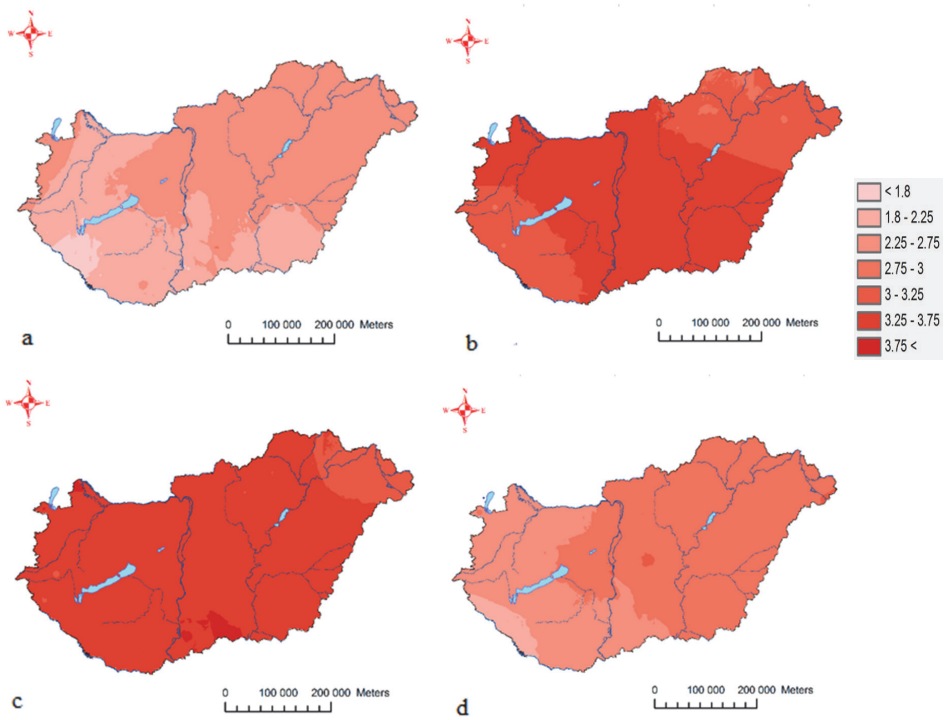

Fig. 9. The values of summer change over the whole period (1971-2020), for hourly values (03 UTC (a), 09 UTC (b), 15 UTC (c), 21 UTC (d)), with linear trend estimation (ºC). The change is significant at the 0.1 significance level in the entire area of Hungary.

Among the analyzed seasonal trends, autumn is illustrated by *Fig. 10*. In the case of the 03 UTC data, the highest values can be assigned to the region east from Tisza, and the lowest values obtained by linear trend estimation to the northern and southwestern areas of Transdanubia. Regarding the 09 UTC dataset, the Transdanubian region also shows lower values and even lower values can be highlighted in mountainous areas. When examining the 15 UTC database, the lowest trend values can be associated with the mountainous and southwestern areas, while the highest trend values can be located east from the line of the Tisza and in the extensive area of the capital city. Moreover, examining the entire area of Hungary, trend values above 2 °C appear in many places at 15 UTC data. Looking at the results for the 21 UTC database, we can see a similar tendency of the spatial distribution, i.e., the trend values obtained by fitting linear trend, continue to increase from west to east. Thus, lower values characterize the southwestern part of the country, and the greatest values appear in the northeastern part.

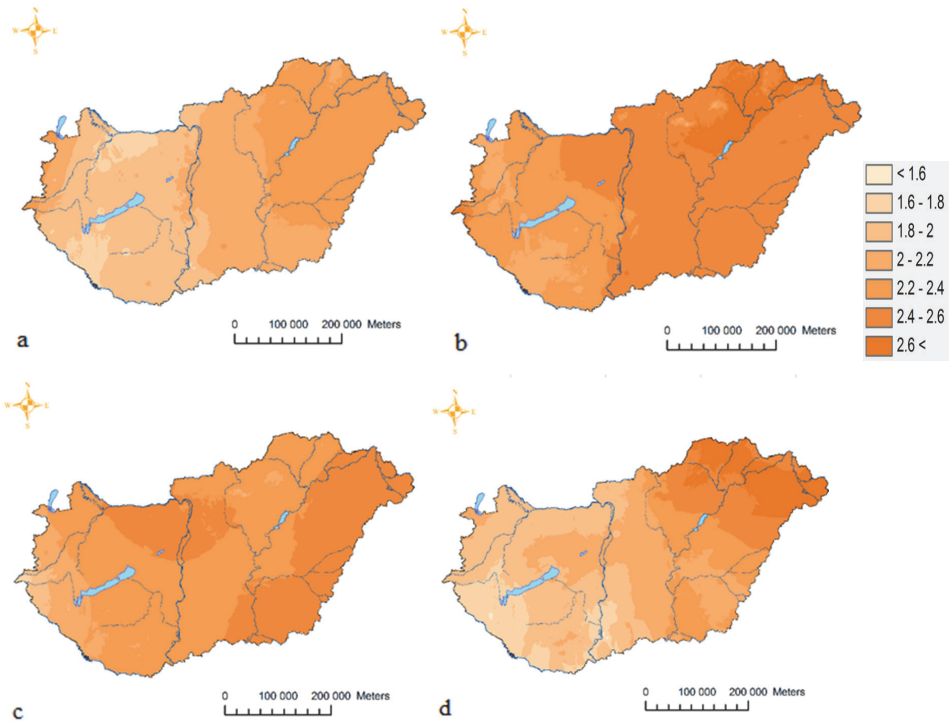

Fig. 10. The values of autumn change over the whole period (1971-2020), for hourly values (03 UTC (a), 09 UTC (b), 15 UTC (c), 21 UTC (d)), with linear trend estimation (ºC). The change is significant at the 0.1 significance level in the entire area of Hungary.

Finally, turning to the analysis of winter trends, the change occurring during the entire test period cannot be considered significant trend for all examined stations. There are 11 stations at 03 UTC, 32 stations at 09 UTC, 16 stations at 15 UTC, and 19 stations at 21 UTC with significant change. Taking the hourly databases one by one, in case of 03 UTC, lowest trends can be observed in the southwestern areas of the country. Compared to this, the 09 UTC tend values are already particularly high with values above 1.2 °C across the country. However, this is still considered low, compared to the results obtained with the other three seasonal trend analysis. Regarding 15 UTC, Hungary can be separated into two parts according to the estimated trend, since the lowest values appear in the northeastern areas. Moving westward the trend values gradually increase. According to this, the highest change appear reaching the western border areas, and this is the area where the stations with significant change are located. Based on the tests of significance of trends for the 21 UTC data, *Fig. 11* indicates that the northwestern and northeastern areas of the country show higher values compared to the central and southern areas.

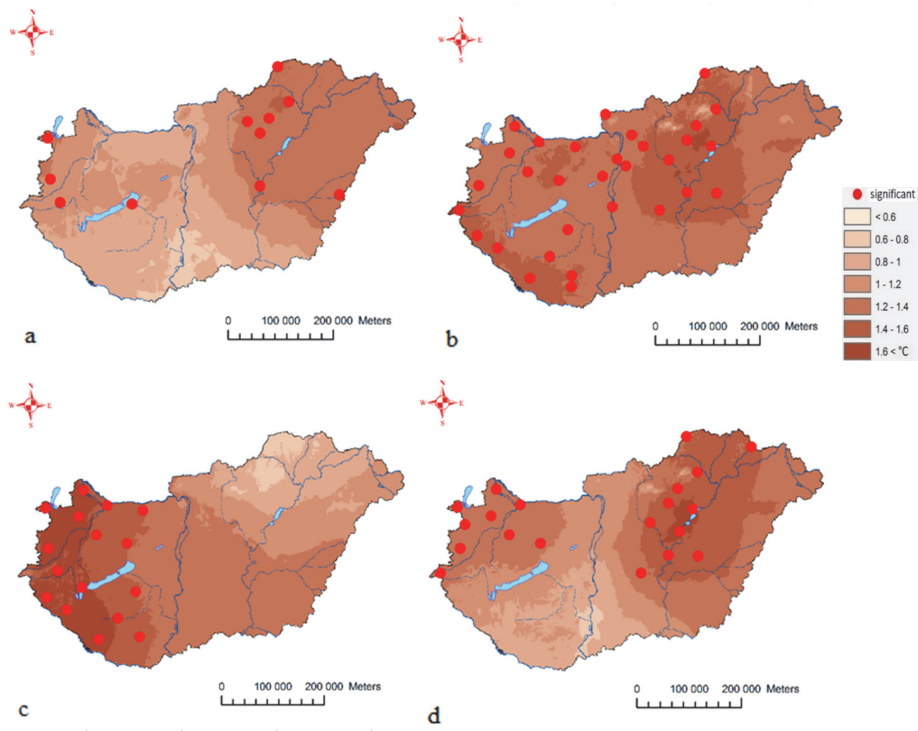

Fig. 11. The values of winter change over the whole period (1971-2020), for hourly values (03 UTC (a), 09 UTC (b), 15 UTC (c), 21 UTC (d)), with linear trend estimation (ºC). Red points indicate the place of significant change at 0.1 significance level.

For the comparison from other point of view of the seasonal trends to each other, *Table 4* consists of the minimum, maximum, and average trend values appear in the country for each six-hourly data. Minimums are the highest at 09 UTC, the only exception is in summer, when the value belonging to the 15 UTC dataset is the highest. The same distribution appears when examining the means. However, in winter, spring, and summer the maximums are the highest at 15 UTC, and in autumn values are the highest at 09 UTC.

Table 4. Seasonal trend values over the whole period (1971–2020) of the six-hourly values obtained by linear trend estimation. Minimum, mean and maximum values are given as spatial values.

03 UTC trend	**Min**	**Mean**	**Max**
Winter	0.52	1.10	1.46
Spring	0.60	1.33	2.28
Summer	1.47	2.29	2.93
Autumn	1.56	2.07	2.44
09 UTC trend	**Min**	**Mean**	**Max**
Winter	0.75	1.37	1.79
Spring	2.00	2.42	2.84
Summer	2.90	3.35	3.79
Autumn	1.97	2.43	2.89
15 UTC trend	**Min**	**Mean**	**Max**
Winter	0.63	1.27	1.92
Spring	1.75	2.29	2.97
Summer	2.95	3.49	3.95
Autumn	1.65	2.34	2.63
21 UTC trend	**Min**	**Mean**	**Max**
Winter	0.58	1.23	1.67
Spring	0.46	1.71	2.34
Summer	1.99	2.77	3.12
Autumn	1.43	2.13	2.77

5. Main conclusions

According to our analysis, we can highlight that the results of the ANOVA method indicate the differences between the hourly databases regarding the expected values and standard deviations. The presented maps and diagrams illustrate that the 15 UTC database has the highest expected values. Considering the standard deviations, the difference of the datasets is not particularly large, but the temporal and spatial variability of the 03 and 21 UTC databases and the 09 and 15 UTC databases can be separated from each other. As a result of the trend analysis, it can be seen that the 15 UTC database shows the highest trends, as expected. We can conclude that the estimated annual and seasonal linear trends

emerge in the 03 UTC and 21 UTC data series are similar, however, comparing the 09 UTC and 15 UTC trend values, the magnitude and spatial distribution of those differe too.

Acknowledgements: This paper was supported by the FFT FTA NP2022-II-8/2022 Sustainable Development and Technologies National Programme of the Hungarian Academy of Sciences and the RRF-2.3.1-21-2022-00014 National Multidisciplinary Laboratory for Climate Change.

References

Barna, Zs., Izsák, B., and *Pieczka, I.,* 2021: Trendvizsgálat: Óraértékek hazai hőmérsékleti trendje. In: 47. Meteorológiai Tudományos Nap, 2021. november 18. Globális éghajlati trendek, hazai kutatási kihívások. Országos Meteorológiai Szolgálat, Budapest. (In Hungarian) https://doi.org/10.21404/47.MTN.2021

Barna, Zs., Izsák, B., and *Pieczka, I.*, 2022: Trendvizsgálat: óraértékek hazai hőmérsékleti trendje. *Légkör 67*, 122–129. (In Hungarian) https://doi.org/10.56474/legkor.2022.3.1

Barna, Zs., Izsák, B., and *Pieczka, I.,* 2023: Comparison of interpolation methods of six-hourly temperature data series. Eleventh Seminar for Homogenization and Quality Control in Climatological Databases and Sixth Interpolation Conference Jointly organised with the Fourteenth EUMETNET Data Management Workshop, Budapest, Hungary, 9–11 May 2023, 62–70.

Izsák, B., Szentimrey, T., Bihari, Z., and *Barna, Zs.,* 2023: Development of observation based temperature dataset. Eleventh Seminar for Homogenization and Quality Control in Climatological Databases and Sixth Interpolation Conference Jointly organised with the Fourteenth EUMETNET Data Management Workshop, Budapest, Hungary, 9–11 May 2023, 51–56.

Izsák, B., 2023: Homogenization and interpolation of relative humidity hourly values with MASH and MISH software. *Int. J. Climatol 43*, 6285–6299. https://doi.org/10.1002/joc.8205

Szentimrey, T., 1989: A lineáris analitikus trendvizsgálat néhány elvi módszertani kérdése. *Időjárás 93*, 151–156. (In Hungarian)

Szentimrey, T., 2017: Manual of homogenization software MASHv3.03. Hungarian Meteorological Service.

Szentimrey T., 2019: Mathematical methodology and software for comparison of gridded datasets. Budapest, OMSZ tanulmány.

Szentimrey, T., 2020: Mathematical questions of spatial interpolation and summary of MISH. Tenth Seminar for Homogenization and Quality Control in Climatological Databases and Fifth Conference on Spatial Interpolation Techniques in Climatology and Meteorology, Budapest, 59–69.

Szentimrey, T. and *Bihari, Z*., 2007: Mathematical background of spatial interpolation, meteorological interpolation based on surface homogenized data bases MISH (Meteorological Interpolation based on Surface Homogenized Data Basis). Proceedings of the Conference on Spatial Interpolation in Climatology and Meteorology, 2004 Október 24–29, Budapest, 17–27.

Szentimrey, T. and *Bihari, Z.*, 2014: Manual of interpolation software MISHv1.03, Országos Meteorológiai Szolgálat.

Szentimrey, T., Bihari, Z., and *Lakatos, M.,* 2011: Mathematical, methodological questions concerning the spatial interpolation of climate elements. Proceedings of the Second Conference on Spatial Interpolation in Climatology and Meteorology, Budapest, Hungary, 2009. *Időjárás 115*, 1–11.

Szentimrey, T., Bihari, Z., and *Lakatos, M*., 2014a: Mathematical questions of homogenization and quality control. Eighth Seminar for Homogenization and Quality Control in Climatological Databases and Third Conference on Spatial Interpolation Techniques in Climatology and Meteorology, Budapest, 5–23.

Szentimrey, T., Bihari, Z., and *Lakatos, M.,* 2014b: Mathematical questions of spatial interpolation of climate variables. Eighth Seminar for Homogenization and Quality Control in Climatological Databases and Third Conference on Spatial Interpolation Techniques in Climatology and Meteorology, Budapest, 107–114.

DOI:10.28974/idojaras.2024.2.8

IDŐJÁRÁS

Quarterly Journal of the HungaroMet Hungarian Meteorological Service
Vol. 128, No. 2, April – June, 2024, pp. 267–286

Analysis of daily and hourly precipitation interpolation supplemented with radar background: Insights from case studies

Kinga Bokros*, **Beatrix Izsák,** and **Zita Bihari**

National Laboratory for Water Science and Water Safety,
HungaroMet Hungarian Meteorological Service,
Kitaibel Pál Street 1, H-1024, Budapest, Hungary

**Corresponding author E-mail: bokros.k@met.hu*

(Manuscript received in final form February 1, 2024)

Abstract— This study concerns the interpolation of daily and hourly precipitation data in regions where small but intense thunderstorms, such as supercells, have occurred, and which, due to their size, often evade conventional meteorological stations. Consequently, relying solely on these measurements for interpolation can introduce errors and yield incomplete representations. To mitigate these issues, this research incorporates radar background information. The study selects days marked by significant precipitation during summer season and employs the Meteorological Interpolation based on Surface Homogenized Data (MISH) method for interpolation, both with and without radar-derived background data. Furthermore, our research also investigates the adaptability of the MISH method in handling radar anomalies, which encompass errors, missing data, and spurious measurements resulting from unintended radar reflections. Additionally, it examines whether the precipitation measured by radar can be used for climatic purposes on its own (without traditional measurements). Statistical techniques are employed to assess the improvement in interpolation quality with the inclusion of radar data and to quantify the relationship between interpolations with and without supplementary radar information. The study underscores the critical role of combining measurement data and radar products in the interpolation framework. This approach has implications for societal and agricultural sectors and offers potential benefits for hazard forecasting accuracy.

Key-words: precipitation measurements, radar background data, interpolation, MISH method, thunderstorm, Hungary

1. Introduction

It is a common phenomenon that small but intense thunderstorms, particularly supercells, with significant precipitation passes among meteorological stations.

measurements and observations of the substantial daily precipitation accumulations, that may occur within relatively small geographic areas. Consequently, the interpolation based solely on these measurements will also be subject to errors and will not provide a complete, accurate picture. The mitigation of potential interpolation errors necessitates the incorporation of background information sources. Such sources may encompass data derived from satellite imagery, weather forecasts, or radar measurements. These auxiliary data play a critical role in refining the accuracy of precipitation interpolation processes, thereby enhancing our understanding of spatial and temporal precipitation patterns.

Different countries have developed different interpolation methods. The German approach to spatially interpolating hourly rainfall employs a multivariate geostatistical method known as kriging with external drift (KED). This method incorporates additional information from sources such as topography, daily rainfall data, and weather radar data to enhance the spatial representation of short-time-step rainfall. Through extensive investigations during various flood events, it was found that the type of semivariogram had a minimal impact on interpolation performance. Weather radar data proved particularly valuable for convective summer events, while daily rainfall data sufficed for stratiform winter events. This method also employs a multi-step interpolation procedure to improve the representation of fractional precipitation coverage, ultimately enabling more accurate hydrological modeling of floods (*Verworn* and *Haberlandt,* 2011). The Austrian approach to spatial precipitation interpolation involves two steps: deriving monthly climatological mean precipitation fields using kriging with external drift and topographic predictors, followed by calculating daily relative anomalies and multiplying them with the respective background fields, ensuring consistency with the climatology and minimizing systematic errors (*Hiebl* and *Frei,* 2023). The Ensemble-based Statistical Interpolation with Gaussian Anamorphosis (EnSI-GAP) is a spatial analysis method for hourly precipitation data which is used in Norway. It combines ensemble forecasts, radar-derived estimates, in situ observations, and citizen observations to synthesize precipitation information. EnSI-GAP assumes locally stationary and transformed Gaussian random fields, with gamma distribution as the marginal distribution at each point. It is designed to run in parallel, considering each hour independently, and can adapt to situations where the background ensemble does not represent the truth accurately, making it valuable for filling gaps in precipitation data and providing accurate estimates, particularly in observation-sparse regions (*Lussana et al*., 2021).

In our research to process the daily precipitation datasets, we employed the MISH (Meteorological Interpolation based on Surface Homogenized Data) method, as detailed in the work of *Szentimrey* and *Bihari* (2007, 2014). The interpolation procedure was executed for the entire geographic expanse of the

country, and it was conducted both with and without the incorporation of radar-derived background information.

We also made an effort to investigate how the MISH interpolation method handles radar-related anomalies, including errors, absent data, and spurious measurements arising from unintended radar signal reflections or echoes from non-target sources. To explore this matter, we conducted a comprehensive selection of days characterized by distinct scenarios: firstly, instances where radar measurements failed to detect precipitation over a substantial portion of the country, despite traditional precipitation measuring stations registering precipitation events. Secondly, we identified days featuring the occurrence of *second-trip echo radar errors*. Subsequently, we examined these datasets, which encompassed both measurements and radar-derived products, with the outcomes of the interpolation process. This comparative analysis underscores the critical importance of combining measurement data and radar products in the interpolation framework.

Finally, we sought the answer to whether radar-measured precipitation, beyond its role in the interpolation of daily and hourly data, could serve climatological purposes, specifically for conducting long-term analyses, such as those spanning the period from 2015 to 2022.

Our analytical approach centered on the utilization of statistical techniques to elucidate the extent to which the inclusion of radar-derived data as background information enhanced the quality of the interpolation. Furthermore, our investigation aimed to quantify the robustness of the relationship existing between the interpolations conducted with the integration of radar-derived background information and those performed without such supplementary data.

The occurrence of intense thunderstorm cells, which are frequently associated with substantial precipitation, can result in flash flooding, thereby engendering myriad adverse repercussions in societal and agricultural domains. Consequently, the judicious integration of radar-derived background information into the interpolation process assumes paramount importance. This approach offers substantial advantages within the realms of both society and agriculture, and it holds potential utility in enhancing the accuracy of hazard forecasting.

2. Data and methods

2.1. Precipitation measurements in Hungary

In our research, we harnessed two pivotal sources of meteorological data in Hungary: precipitation measurements and radar-derived data. The former Hungarian Meteorological Service (OMSZ), now HungaroMet operates a comprehensive network of 276 meteorological stations that continuously gather real-time data (shown in *Fig. 1* with dark blue dots). Additionally, HungaroMet collects daily precipitation data from 500 stations on a monthly basis (shown in

Fig. 1 with red dots). This extensive network, including 500 stations, was used to create a rich database interpolated to the entire country using a homogenization process (*Szentes et al.,* 2023) with the software MASH (*Szentimrey*, 1999; 2008; 2017; 2023). This means that for studies conducted before 2023, we created interpolated data using the homogenized daily records from the 500 stations. However, for our daily and hourly rainfall analyses in 2023, we only used data from 276 stations.

Furthermore, HungaroMet maintains a network of five radar stations across Hungary, located in Budapest, Pogányvár, Szentes, Napkor, and Hármashegy, as indicated by the yellow dots in *Fig. 1*. These radar stations cover the entire geographical expanse of the country within a 240-kilometer radius, employing ten different elevation angles in five-minute measurement cycles. For our investigation, we relied on daily and hourly radar-derived precipitation data.

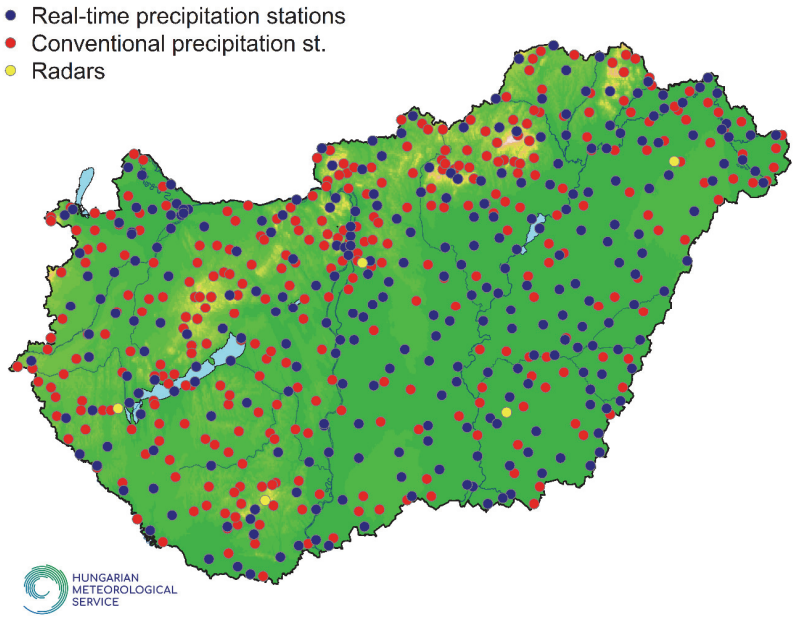

Fig. 1. Radar network (yellow), real-time (dark blue), and traditional precipitation measurement stations (red) of the HungaroMet.

During the process of day selection, our foremost consideration was to opt for days falling within the summer semester, given that this period is characterized by the occurrence of localized, intense rainfall-producing showers and thunderstorms. The three days chosen for this purpose are

- June 5, 2021,

- July 16, 2021,
- July 13, 2023.

In the case of the latter date, we conducted not only daily but hourly precipitation interpolation.

2.2. Methods and software

2.2.1. SOFTWARE MISHv1.03

The software version MISHv1.03 consists of two units that are the modeling and the interpolation systems. The interpolation system can be operated on the results of the modeling system. We summarize briefly the most important facts about these two units of the developed software (*Szentimrey* and *Bihari*, 2014).

Modeling subsystem for climate statistical (local and stochastic) parameters:

– Based on long homogenized data series and supplementary deterministic model variables. The model variables may be such as height, topography, distance from the sea, etc..
– Benchmark study, cross-validation test for interpolation error or representativity.
– High resolution grid (e.g., 0.5'×0.5'),

Interpolation subsystem:

– Additive (e.g. temperature) or multiplicative (e.g. precipitation) model and interpolation formula can be used depending on the climate elements.
– Daily, monthly, seasonal values and many years' means can be interpolated.
– Capability for application of supplementary background information (stochastic variables) e.g., satellite, radar, forecast data.
– Data series completion (missing value interpolation for daily or monthly station data).
– Interpolation, gridding of monthly or daily station data series for given predictand locations.

The MISH-MASH software can be downloaded from:
http://www.met.hu/en/omsz/rendezvenyek/homogenizationand_interpolation/software/

2.2.2. Multiplicative interpolation (precipitation) Mathematical model

Let us assume that
$Z(\boldsymbol{s}_0, t)$ is the predictand,
$Z(\boldsymbol{s}_i, t)$ $(i = 1, \ldots, M)$ are predictors (where $\boldsymbol{s}$ represents space and t represents time)

The linear or additive model is appropriate in case of normal probability distribution. However, in case of a quasi lognormal distribution (e.g., precipitation sum), we deduced a mixed additive multiplicative formula which is used also in our MISH system, and it can be written in the following form,

$$\hat{Z}(\boldsymbol{s}_0) = \vartheta \cdot \left(\prod_{q_i \cdot Z(\boldsymbol{s}_i) \geq \vartheta} \left(\frac{q_i \cdot Z(\boldsymbol{s}_i)}{\vartheta} \right)^{\lambda_i} \right) \cdot \left(\sum_{q_i \cdot Z(\boldsymbol{s}_i) \geq \vartheta} \lambda_i + \sum_{q_i \cdot Z(\boldsymbol{s}_i) < \vartheta} \lambda_i \cdot \left(\frac{q_i \cdot Z(\boldsymbol{s}_i)}{\vartheta} \right) \right) \quad (1)$$

where the interpolation parameters are $\vartheta > 0$, $q_i > 0, \lambda_i \geq 0$ $(i = 1, \ldots, M)$, and $\sum_{i=1}^{M} \lambda_i = 1$.

The interpolation parameters are related to the median: $\vartheta = m(\boldsymbol{s}_0), q_i = \frac{m(\boldsymbol{s}_0)}{m(\boldsymbol{s}_i)}$, where $m(\mathbf{s}_i)(i = 0, \ldots, M)$ are the spatial median values.

The optimum interpolation parameters are uniquely determined by the climate statistical parameters (local parameters, stochastic connections). Modeling of climate statistical parameters can be based on long data series and model variables.

Since the parameters q and ϑ are defined with the median, it is clear that the multiplication part of the interpolation formula itself dominates for precipitation amounts reaching the median, so the first part of the formula holds. If little or no precipitation is measured, the interpolation formula is limited to the additive part. Thus, the good properties of the quasi-multiplicative formula itself give us the ability to interpolate with the same modeled climate statistical parameters for each time of day or hour as for the daily values.

2.2.3. Interpolation with background information in MISH

The background information, such as forecast, satellite, and radar data can efficiently decrease interpolation errors. Let us assume that
$Z(\boldsymbol{s}_0, t)$: predictand,
$\hat{\boldsymbol{Z}}(\boldsymbol{s_0}, \boldsymbol{t})$: interpolated predictand without background information.
Moreover, background information on a dense grid is also given:
$\boldsymbol{B} = \{B(\boldsymbol{s}, t) \mid \boldsymbol{s} \in D\}$, where D is the space domain.
$\hat{Z}_B(\boldsymbol{s}_0, t)$: interpolated predictand with background information.

The linear regression model is given by:

$$\frac{Z(\boldsymbol{s},t)}{E(\boldsymbol{s})} = \beta_0(t) + \beta_1(t) \cdot \frac{B(\boldsymbol{s},t)}{E(\boldsymbol{s})} + \varepsilon(\boldsymbol{s}, t) \quad (2)$$

where $E(\boldsymbol{s})$ represents spatial trend and $\varepsilon(\boldsymbol{s}, t)$ is the noise term.

Estimation of parameters $\beta_0(t)$ and $\beta_1(t)$, as well as the correlation $R(t) = \text{corr}\left(\frac{Z(\boldsymbol{s},t)}{E(\boldsymbol{s})}, \frac{B(\boldsymbol{s},t)}{E(\boldsymbol{s})}\right)$, we rely on $Z(\boldsymbol{s}_i, t)$ and $B(\boldsymbol{s}_i, t)$ for $(i = 1, \ldots, M)$, along with a modeled spatial trend.

$$\hat{Z}_B(\boldsymbol{s}_0, t) = \hat{Z}(\boldsymbol{s}_0, t) + \beta_1(t) \cdot \left(B(\boldsymbol{s}_0, t) - \hat{B}(\boldsymbol{s}_0, t)\right) \quad (3)$$

where

$\hat{Z}(\boldsymbol{s}_0, t) = F_M(Z(\boldsymbol{s}_1, t), \ldots, Z(\boldsymbol{s}_M, t); q_1, .., q_M, \lambda_1, .., \lambda_M)$,
i.e., the interpolation without background information,
$\hat{B}(\boldsymbol{s}_0, t) = F_M(B(\boldsymbol{s}_1, t), \ldots, B(\boldsymbol{s}_M, t); q_1, .., q_M, \lambda_1, .., \lambda_M)$
i.e., the same interpolation formula for the background information,
and $\beta_1(t)$ is the estimated regression coefficient.

Remark:

– If $R(t) = 0$ then $\hat{Z}_B(\boldsymbol{s}_0, t) = \hat{Z}(\boldsymbol{s}_0, t)$.

That is, the background information is so bad that we do not use it at all.

– If $B(\boldsymbol{s}_i, t) = Z(\boldsymbol{s}_i, t)$ $(i = 1, \ldots, M)$ then $R(t) = 1$ and $\hat{Z}_B(\boldsymbol{s}_0, t) = B(\boldsymbol{s}_0, t)$.

That is, the measurements are the same as the radar information, in which case the radar information will also be the value of $\hat{Z}_B(\boldsymbol{s}_0, t)$ at the points where no measurements are taken.

3. Results

3.1. June 5, 2021

On June 5, 2021, a precipitation zone traversed the country, accompanied by showers, thunderstorms, and sporadic hail in some areas. The highest daily precipitation amounts were observed in the southwestern region of the country, with measurements of 19.3 and 19.8 mm recorded at Nagykanizsa and Letenye stations. At Becsehely station, 39 mm of precipitation was reported. The result of interpolation without background information is shown in *Fig. 2*, which displays a maximum precipitation amount of 35.3 mm in the southwestern region, while lesser amounts of precipitation occurred in the north and northeastern parts of the country.

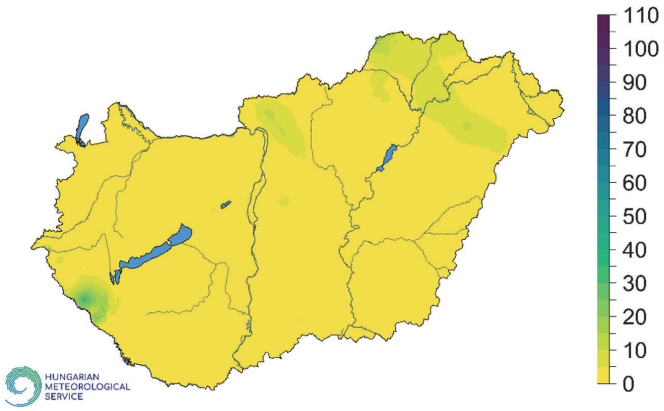

Fig. 2. Interpolation of 24-hour total precipitation [mm] on June 5, 2021, without background information (using 500 measurements).

Fig. 3 illustrates the 24-hour radar rainfall amount, which was used as background information during the interpolation process. Evidently, it is observable that a significantly higher 24-hour precipitation total appears in the southwest, in contrast to *Fig. 2*, where the absence of this pronounced precipitation maximum suggests that the most intense and substantial precipitation from the thunderstorm cell bypassed the surface precipitation monitoring stations, but was nevertheless detected by the radar.

In addition to the prominent values in the southwest, *Fig. 3* also reveals a band of 15–20 mm equivalent precipitation in the western regions of the country and the Transdanubian region, which does not appear among the measurements.

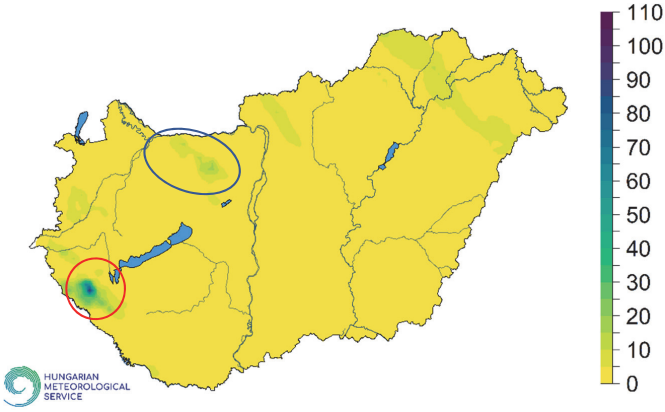

Fig. 3. 24-hour radar precipitation amount [mm] (June 5, 2021).

While interpolation without the radar background information indicate 35–39 mm of maximum precipitation within 24 hours, the incorporation of radar background information into the MISH interpolation revealed a precipitation total of 106.9 mm in the southwestern region (*Fig. 4*).

A strong relationship was observed between the observations and the background information, with a high correlation coefficient of R = 0.889. Furthermore, with the inclusion of background information in the interpolation, higher precipitation amounts were also observed in the northern Transdanubian region. It is apparent that while 0–5 mm of precipitation is depicted in the northern Transdanubian region without background information, the utilization of radar data results in daily precipitation totals of 5–30 mm.

For lesser amounts of precipitation that fell over a larger area, the two interpolation products exhibited greater agreement (in northern and northeastern Hungary), yielding values ranging between 5–15 mm in both cases.

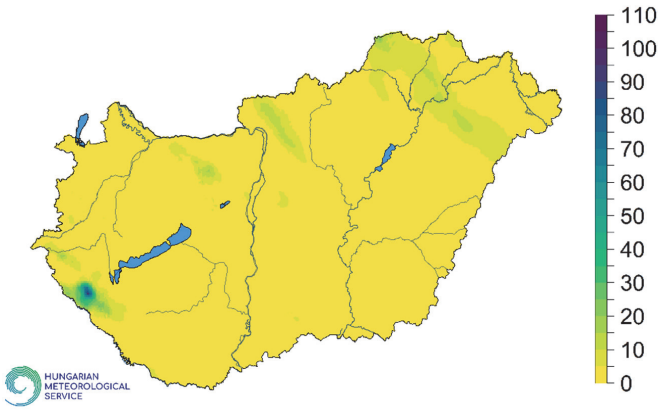

Fig. 4. 24-hour interpolated precipitation amount [mm] on June 5, 2021, with radar background information (using 500 measurements).

3.2. Flash flood in Kunfehértó (July 16, 2021)

On July 16, 2021, meteorological conditions in Hungary were significantly impacted by a cold front at elevated altitudes, leading to the occurrence of inclement weather characterized by rainfall and storms across various regions of the country. The most substantial levels of precipitation were observed in several areas, including southern Transdanubia, the Southern Great Plain, the region situated between the Danube and Tisza rivers, and Pest County. Furthermore, notable thunderstorms with associated copious rainfall were witnessed in the

Szatmár Plain and Bodrogköz regions located in the eastern part of the country. The meteorological measurements indicated that the highest daily precipitation total was recorded at Báta station, amounting to 49.2 mm. An interpolation conducted without the incorporation of background information suggested an even greater maximum daily precipitation total just a few kilometers from Báta, specifically in the village of Dávod, where it reached 65.02 mm (refer to *Fig. 5*).

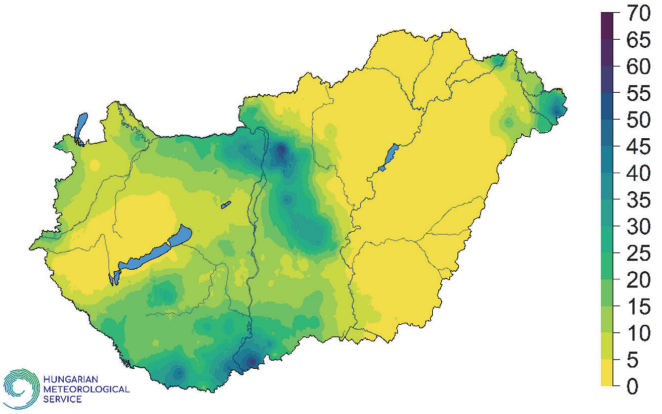

Fig. 5. Interpolation of 24-hour total precipitation [mm] on July 16, 2021, without background information (using 500 measurements).

The three figures displaying 24-hour rainfall totals, as depicted in *Figs. 5–7*, exhibit remarkable similarity. They collectively reveal a pronounced correlation of 0.918 between the observed data and the radar background information. All three figures consistently depict higher levels of precipitation in the southern and northern regions of Hungary. However, it is noteworthy that the radar failed to capture the elevated precipitation values observed in the Szatmár Plain and Bodrogköz regions (refer to *Fig. 6*), where the recorded 24-hour precipitation levels ranged from 5 to 15 mm. In contrast, the interpolation without the use of radar background information (*Fig. 5*) suggested the presence of approximately 60 mm of precipitation within a smaller area, particularly reflecting 57.2 mm of rainfall over a 24-hour period at Gacsály station on July 16, 2021.

Another significant discrepancy arises from the fact that the radar database exclusively registered the occurrence of 60 mm of rainfall within an hour and a half, which led to a flash flood in Kunfehértó, while this event remained unrecorded by the primary meteorological stations. Consequently, when conducting interpolation without radar background information, only an estimated 15–20 mm of precipitation is indicated in the proximity of Kunfehértó. All of this also points to the importance of integrating radar data into rainfall interpolation.

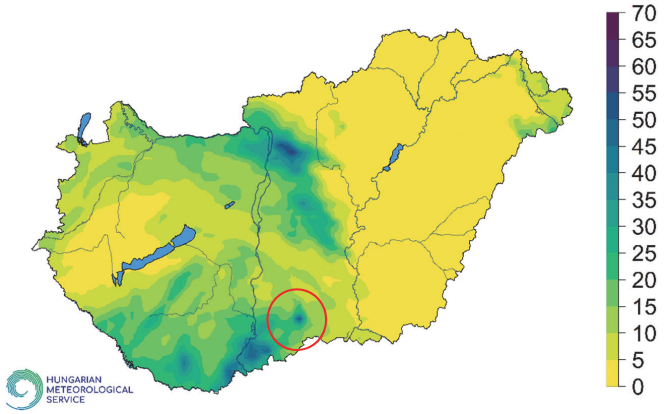

Fig. 6. 24-hour radar precipitation amount (July 16, 2021).

The results obtained through interpolation employing radar background information are presented in *Fig. 7*. This representation elucidates the higher daily precipitation totals observed in eastern Hungary, as well as the significant precipitation event surpassing 60 mm, which was responsible for the flash flood incident in Kunfehértó over the 24-hour period.

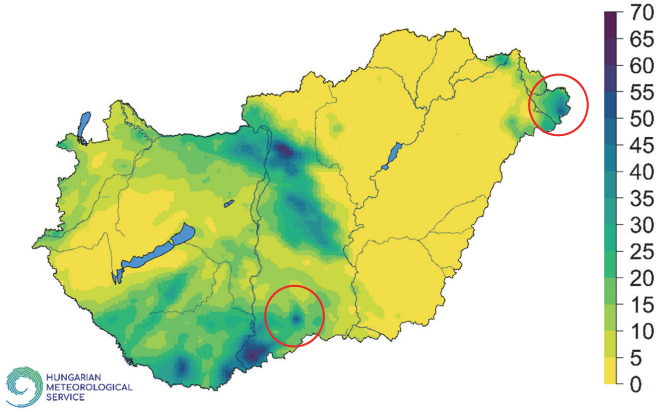

Fig. 7. 24-hour interpolated precipitation amount on July 16, 2021, with radar background information (using 500 measurements).

3.3. July 13, 2023

In the early hours of July 13, 2023, an advancing thunderstorm system, characterized by its northeasterly trajectory, precipitated copious rainfall and intense downpours across the entire country. Subsequently, this precipitation zone dissipated later in the afternoon, thereby ceasing its impact on the country.

On July 13, 2023, some irregularities occurred in precipitation measurement. Therefore, we are examining the day on an hourly basis. Comparing the results of the interpolated daily precipitation amount measured by precipitation gauges (*Fig. 8*) with the results of radar measurements (*Fig. 9*), it is evident that in a significant part of the country, including the Great Plain and the northern regions, there is little to no precipitation due to the temporary absence of radar measurements. Regarding the regional average, there is a difference of 2 mm between the two precipitation datasets, however in some areas (northern Hungary), a difference of 10–14 mm can be observed.

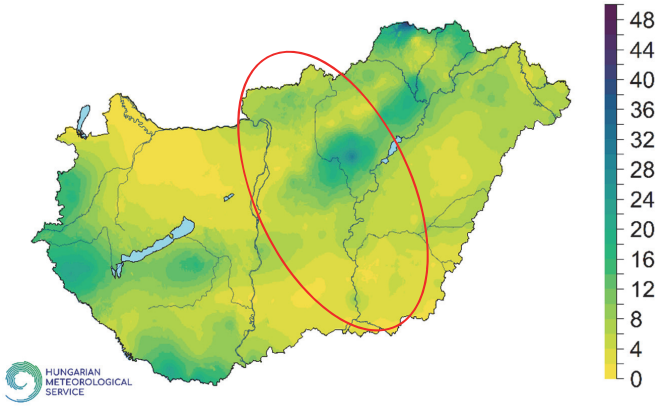

Fig. 8. Interpolation of 24-hour total precipitation [mm] on July 13, 2023, without background information (using 276 measurements).

The significant disparity between the interpolated dataset, which lacks radar background information (*Fig. 8*), and the radar measurements (*Fig. 9*) can be attributed to the smaller number of precipitation stations; additionally, the absence of radar measurements further exacerbates this difference. Consequently, the correlation coefficient that quantifies the association between these two datasets is notably diminished, standing at a modest value of **0.556**.

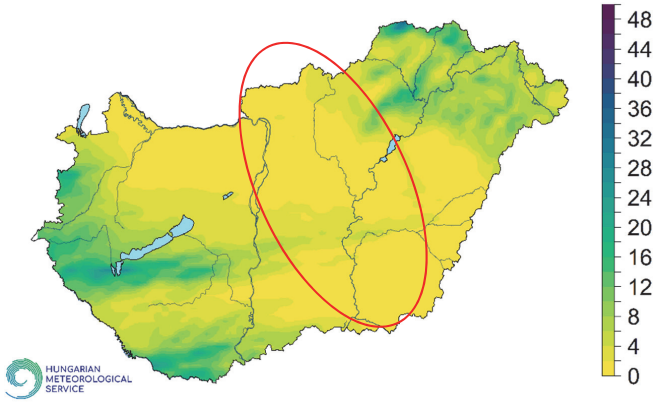

Fig. 9. 24-hour radar precipitation amount (July 13, 2023).

Subsequent to the incorporation of radar-derived background information in the interpolation process of precipitation measurements, the daily precipitation amount of 2–6 mm missing from the radar measurements also appeared in the central and southeastern parts of the country (*Fig. 10*).

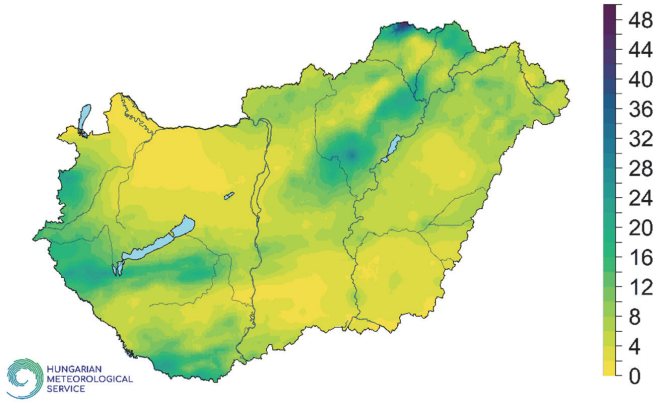

Fig. 10. 24-hour interpolated precipitation amount on July 13, 2023, with radar background information (using 276 measurements).

In addition to the temporary absence of radar measurements, there was also a rare occurrence of a so-called second-trip echo radar error when multiple reflections from an extremely intense thunderstorm cell in the area of Slovenia were observed on the radar images (*Fig. 11*).

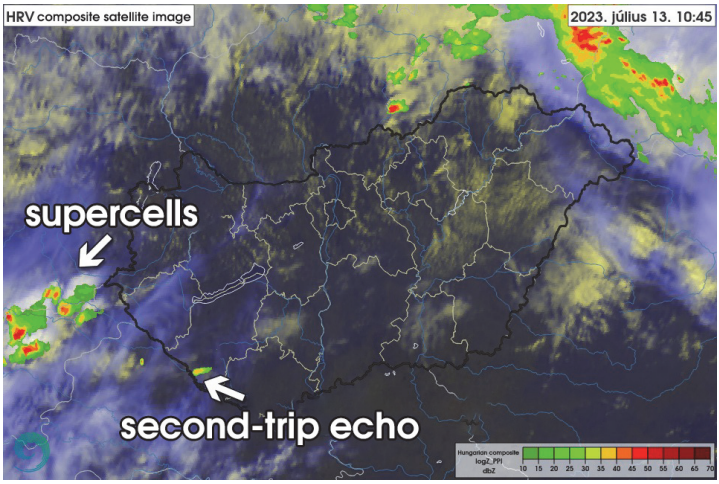

Fig. 11. Second-trip echo radar error caused by extremely high thunderstorms.

3.4. Hourly analysis

On July 13, 2023, an examination of the hourly precipitation amounts revealed that the amount of precipitation that fell in the Great Plain and the southeast, according to traditional measurements, which is missing from the 24-hour radar precipitation amount, could have fallen in the morning hours, around 7 UTC (*Fig. 12*).

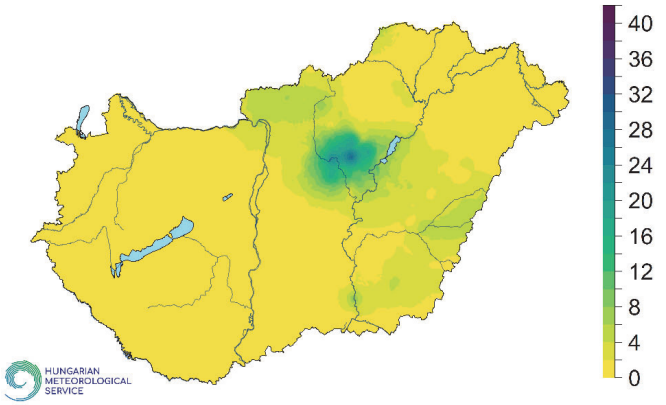

Fig. 12. Interpolation of hourly total precipitation [mm] on July 13, 2023, 7 UTC without background information (using 276 measurements).

Unexpectedly, the 7-hour cumulative radar precipitation data reveals the existence of a precipitation zone in central and southeastern Hungary (*Fig. 13*) that is absent in the corresponding 24-hour radar measurements (*Fig. 9)*.

We sought to identify the cause of the unexpected outcome, focusing on the likely disparities between corrected and uncorrected hourly precipitation sums. We assumed that while the corrected precipitation amount reflects the missing precipitation, this deficiency remains uncompleted in the uncorrected dataset. Consequently, we examined the uncorrected hourly radar sum. However, our initial hypothesis was not confirmed, as the investigation of uncorrected radar precipitation sums yielded similar results, wherein the precipitation deficit from the 24-hour total also manifested.

Notwithstanding this, using the MISH method, both hourly and daily interpolation effectively captures the precipitation amounts in question for the northern part of Hungary, as well as the central and southeastern parts of the country (*Fig. 10* and *Fig. 14).* The relationship which was observed between the hourly observations and the background information is really high despite the absent precipitation, the correlation coefficient is 0.91.

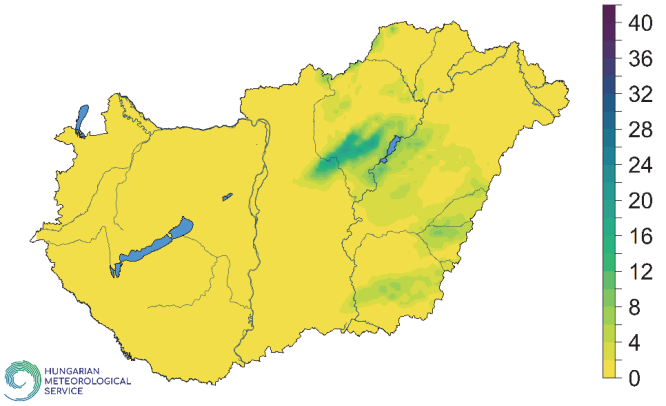

Fig. 13. Hourly radar precipitation on July 13, 2023, 7 UTC.

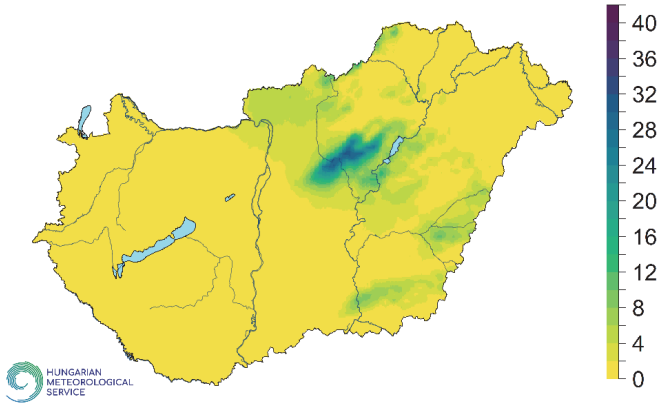

Fig. 14. Interpolation of hourly total precipitation [mm] on July 13, 2023, 7 UTC with background information (using 276 measurements).

The "second-trip echo" radar error signal that occurs around 10 UTC (*Fig. 11*) cannot be identified in the display of the 24-hour radar precipitation amount (*Fig. 9*), so it is worth examining the hourly precipitation at 10 UTC to make sure of the presence of a false precipitation signal.

Fig. 15 illustrates that inaccuracies stemming from deceptive reflections undergo filtration within the radar database, consequently precluding their incorporation in the display.

Fig. 15. Hourly radar precipitation [mm] on July 13, 2023, 10 UTC.

3.5. Correlation between measurements and radar information, monthly values

Through the presentation of case studies, it becomes evident that the integration of radar precipitation data holds considerable utility in the interpolation. Simultaneously, the inquiry arises regarding the suitability of radar-measured precipitation for climatological applications. To address this query, we aggregated monthly precipitation data obtained through radar measurements from the year 2015 (the commencement of available radar data) to 2022, subsequently conducting a comparative analysis with conventionally measured precipitation. Employing data encompassing homogenized precipitation records from 500 stations (*Szentes et al*., 2023) over the period 2015–2022, we applied the MISH interpolation technique to the monthly precipitation values.

For each month, we calculated the spatial average and calculated the correlation between the two datasets. The strongest linear relationship occurs in August, while February has the weakest correlation (*Fig. 16*).

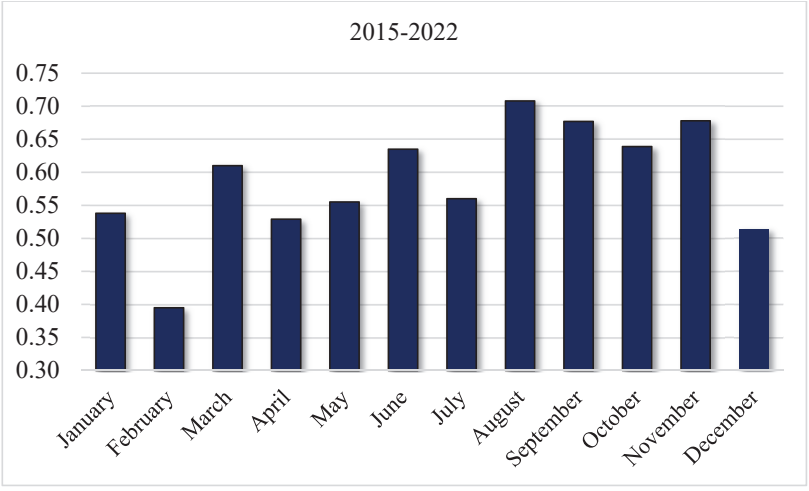

Fig. 16. Correlation between measurements and radar information, spatial average.

While radar-measured precipitation proves valuable in scenarios involving the passage of smaller, convective cells across the country, thus circumventing conventional meteorological stations, its suitability for climatological purposes is a subject of ongoing debate. *Fig. 17* shows the average precipitation amount in July averaged over the period 2015–2022. This observation implies that the radar data greatly underestimates the measured precipitation totals on July. There can be several reasons why radar measurements might underestimate monthly

precipitation amounts, especially when considered for climatological purposes. Some common factors include:

- Beam blockage: Radar beams are not perfectly straight, they follow the curvature of the Earth. Terrain features such as mountains or tall buildings can block the radar beam, leading to underestimation of precipitation in the shadowed areas.
- Attenuation: Raindrops can absorb and scatter radar signals, especially at higher frequencies.
- Z-R relationship: The radar reflects the intensity of precipitation, and this is converted to rainfall rates using a Z-R relationship (reflectivity to rainfall rate). However, the relationship can vary with temperature, type of precipitation, and other factors. If the chosen Z-R relationship is not appropriate for the conditions, it can lead to inaccuracies (*Krajewski et al*., 2010).

Our observation suggests that, currently, radar data is not a viable substitute for conventional measurements, thus rendering its utility limited in the context of climate-related applications. However, in cases where there is a strong correlation between radar information and measurements, they are definitely additional information compared to point measurements. In this article we also presented cases where radar information is an effective complement to measurements. Accurate precipitation estimates are needed for hazard warning, for insurance companies to settle claims, and of course for the public to justify the damage.

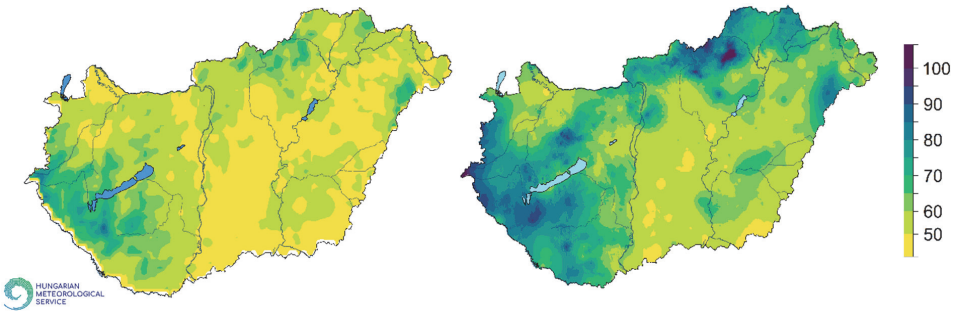

Fig. 17. Representation of July radar precipitation totals (left) and measurements (right) for the averaged period 2015–2022.

4. Conclusion

In conclusion, this study has demonstrated the significant impact of incorporating radar-derived background information in the interpolation of daily and hourly precipitation data, especially in regions prone to small but intense thunderstorms, such as supercells. The research focused on the MISH (Meteorological Interpolation based on Surface Homogenized Data) method and its adaptability in handling radar anomalies, including errors, missing data, and spurious measurements.

The results from the analysis of three specific days in Hungary highlight the critical role of radar data in improving the accuracy of precipitation interpolation. In cases where traditional meteorological stations failed to capture the most intense and substantial precipitation events, radar data filled the gaps, providing a more complete and accurate picture. The incorporation of radar background information resulted in higher daily precipitation totals, and the correlation between observed data and radar background information was consistently strong.

Furthermore, the study emphasizes the importance of integrating radar data into the interpolation process for hazard forecasting. Small but intense thunderstorms can lead to flash flooding and have adverse repercussions in societal and agricultural domains. Therefore, the combination of measurement data and radar products offers substantial advantages, enhancing accuracy in hazard forecasting and improving our understanding of spatial and temporal precipitation patterns.

Although in the long term (e.g., 2015-2022 average) radar precipitation amounts cannot be used for climate purposes, as they significantly underestimate the amount of measured precipitation, in instances where a robust correlation exists between radar-derived information and measured values, the former can provide supplementary insights compared to conventional measurements.

In future studies, it may be beneficial to improve the time resolution of the assessments. Instead of focusing solely on daily or hourly precipitation data, the inclusion of even shorter intervals, like 10- or 5-minute data, in precipitation interpolation along with radar information could be a valuable avenue for investigation.

Overall, this research underscores the critical role of radar-derived background information in precipitation interpolation, offering valuable insights for meteorological and hydrological applications, ultimately contributing to better decision-making in managing and mitigating the impacts of extreme weather events.

Acknowledgement: This paper was supported by the Sustainable Development and Technologies National Programme of the Hungarian Academy of Sciences (FFT NP FTA 2022-II-8/2022), the framework of the Széchenyi Plan Plus program with the support RRF-2.3.1-21-2022-00014 National Multidisciplinary Laboratory for Climate Change project, and the RRF-2.3.1-21-2022-00008 project. Additionally, we would like to express our sincere appreciation to *Gergő Simon* for his valuable contributions related to *Figure 11*, specifically in enhancing the representation of the *second-trip echo*.

References

Hiebl, J. and *Frei, C.,* 2023: Correction to: Daily precipitation grids for Austria since 1961 – development and evaluation of a spatial dataset for hydroclimatic monitoring and modelling. *Theor. Appl. Climatol. 151*, 951. https://doi.org/10.1007/s00704-022-04288-x

Krajewski, W.F., Villarini, G., and *Smith, J.A*., 2010: RADAR-Rainfall Uncertainties, *Bull. Amer. Meteorol. Soc. 91*, 87–94. https://doi.org/10.1175/2009BAMS2747.1

Lussana, C., Nipen, T.N., Seierstad, I.A., and *Elo, C.A,* 2021*:* Ensemble-based statistical interpolation with Gaussian anamorphosis for the spatial analysis of precipitation. *Nonlin. Process. Geophys. 28*, 61–91, https://doi.org/10.5194/npg-28-61-2021

Szentes, O., Lakatos, M., and *Pongrácz, R.,* 2023. New homogenized precipitation database for Hungary from 1901. *Int. J. Climatol. 43,* 4457–4471. https://doi.org/10.1002/joc.8097

Szentimrey T., 1999: Multiple Analysis of Series for Homogenization (MASH). In: Proceedings of the Second Seminar for Homogenization of Surface Climatological Data, Budapest, Hungary. WMO, WCDMP (41), 27–46.

Szentimrey T., 2008: Development of MASH homogenization procedure for daily data, Proceedings of the Fifth Seminar for Homogenization and Quality Control in Climatological Databases, Budapest, 2006; WCDMP-No. 71, WMO/TD (1493)

Szentimrey, T. and *Bihari, Z.,* 2007: Mathematical background of the spatial interpolation methods and the software MISH (Meteorological Interpolation based on Surface Homogenized Data Basis), Proceedings of the Conference on Spatial Interpolation in Climatology and Meteorology, Budapest, Hungary, 2004, COST Action 719, COST Office, 2007, 17–27.

Szentimrey, T. and *Bihari, Z.,* 2014: Manual of interpolation software MISHv1.03, Hungarian Meteorological Service

Szentimrey, T., 2017*:* Manual of homogenization software MASHv3.03. Hungarian Meteorological Service, 71.

Szentimrey, T., 2023: Overview of mathematical background of homogenization, summary of method MASH and comments on benchmark validation. *Int. J. Climatol*. 43, 6314–6329. https://doi.org/10.1002/joc.8207

Verworn, A. and *Haberlandt, U.,* 2011: Spatial interpolation of hourly rainfall – effect of additional information, variogram inference and storm properties. *Hydrol. Earth Syst. Sci. 15*, 569–584, https://doi.org/10.5194/hess-15-569-2011

INSTRUCTIONS TO AUTHORS OF *IDŐJÁRÁS*

The purpose of the journal is to publish papers in any field of meteorology and atmosphere related scientific areas. These may be

- research papers on new results of scientific investigations,
- critical review articles summarizing the current state of art of a certain topic,
- short contributions dealing with a particular question.

Some issues contain "News" and "Book review", therefore, such contributions are also welcome. The papers must be in American English and should be checked by a native speaker if necessary.

Authors are requested to send their manuscripts to

Editor-in Chief of IDŐJÁRÁS
P.O. Box 38, H-1525 Budapest, Hungary
E-mail: journal.idojaras@met.hu

including all illustrations. MS Word format is preferred in electronic submission. Papers will then be reviewed normally by two independent referees, who remain unidentified for the author(s). The Editor-in-Chief will inform the author(s) whether or not the paper is acceptable for publication, and what modifications, if any, are necessary.

Please, follow the order given below when typing manuscripts.

Title page should consist of the title, the name(s) of the author(s), their affiliation(s) including full postal and e-mail address(es). In case of more than one author, the corresponding author must be identified.

Abstract: should contain the purpose, the applied data and methods as well as the basic conclusion(s) of the paper.

Key-words: must be included (from 5 to 10) to help to classify the topic.

Text: has to be typed in single spacing on an A4 size paper using 14 pt Times New Roman font if possible. Use of S.I. units are expected, and the use of negative exponent is preferred to fractional sign. Mathematical formulae are expected to be as simple as possible and numbered in parentheses at the right margin.

All publications cited in the text should be presented in the *list of references*, arranged in alphabetical order. For an article: name(s) of author(s) in Italics, year, title of article, name of journal, volume, number (the latter two in Italics) and pages. E.g., *Nathan, K.K.,* 1986: A note on the relationship between photo-synthetically active radiation and cloud amount. *Időjárás 90,* 10–13. For a book: name(s) of author(s), year, title of the book (all in Italics except the year), publisher and place of publication. E.g., *Junge, C.E.,* 1963: *Air Chemistry and Radioactivity*. Academic Press, New York and London. Reference in the text should contain the name(s) of the author(s) in Italics and year of publication. E.g., in the case of one author: *Miller* (1989); in the case of two authors: *Gamov* and *Cleveland* (1973); and if there are more than two authors: *Smith et al.* (1990). If the name of the author cannot be fitted into the text: *(Miller,* 1989); etc. When referring papers published in the same year by the same author, letters a, b, c, etc. should follow the year of publication. DOI numbers of references should be provided if applicable.

Tables should be marked by Arabic numbers and printed in separate sheets with their numbers and legends given below them. Avoid too lengthy or complicated tables, or tables duplicating results given in other form in the manuscript (e.g., graphs). *Figures* should also be marked with Arabic numbers and printed in black and white or color (under special arrangement) in separate sheets with their numbers and captions given below them. JPG, TIF, GIF, BMP or PNG formats should be used for electronic artwork submission.

More information for authors is available: journal.idojaras@met.hu

Published by the HungaroMet Hungarian Meteorological Service

Budapest, Hungary

ISSN 0324-6329 (Print)

ISSN 2677-187X (Online)